The Differential Activation Of Downstream Unfolded Protein Response Pathways in Human Cell Lines

MATILDA RUVIMBO MASOSE

Matilda Ruvimbo Masose March 2016

The Differential Activation Of Downstream Unfolded Protein Response Pathways in Human Cell Lines

A Thesis Submitted for the degree of Master of Science

School of Biological and Biomedical Sciences

University of Durham

Supervisor: Dr Adam Benham

Abstract

HLA-B27 heavy chain misfolding has been linked to the pathogenesis of the chronic inflammatory disease Ankylosing Spondylitis. Ankylosing Spondylitis is a disease which primarily affects the axial skeleton but has also been shown to affect various other organs including the heart, lungs and eyes. However, there is limited evidence to show how HLA-B27 misfolding leads to differing responses in different cell types. This study sought to investigate the activation of common downstream pathways of the unfolded protein response in HT1080 and HeLa cells in response to tunicamycin in the hope of translating the data into an Ankylosing Spondylitis disease model. The pathways that were investigated were the autophagy, apoptosis and inflammatory signalling pathways.

It was found that in i) HT1080 cells, as a response to immediate induction of ER stress, endoplasmic reticulum membranes expanded to cope with stress but then employed different responses to cope with prolonged ER stress. ii) In both HeLa and HT1080 cells, autophagy was differentially activated, with HT1080 cells and HeLa cells activating autophagy pathways during early and late tunicamycin induced ER stress responses respectively. iii) HT1080 cells did not activate apoptosis during both early and late responses as opposed to HeLa cells, where apoptosis activation was seen in late ER stress responses. And finally iv) HT1080 and HeLa cells were found to have differential tyrosine kinase signalling in both early and late ER stress responses.

The observations that these different cell lines have differing coping mechanisms to ER stress may have implications in elucidating the pathogenesis of AS and in the development of more effective therapies.

Table of Contents

List of Figures and Tables

Abbreviations

APAF-1	Apoptotic protease-activating factor 1
AS	Ankylosing Spondylitis
ASK1	Apoptosis signal-regulating kinase 1
ATF4	Activating Transcription Factor 4
ATF6	Activation Transcription Factor 6
ATG12	Autophagy-related protein 12
ATG13	Autophagy-related protein 13
ATG16	Autophagy-related protein 16
ATG4B	Autophagy-related protein 4 homolog B
ATG7	Autophagy-related protein 7
BAK	Bcl2 homologous antagonist killer
BAX	Bcl2-Associated X protein
Bcl-2	B cell lymphoma 2
BIP	Binding Immunoglobulin Protein
CHIP	Carboxyl Terminus of Hsc70-Interacting Protein
CHOP	C/EBP-homologous protein
CNX	Calreticulin
CRT	Calnexin
DISC	Death Inducing Signal Complex
DTT	Dithiothreitol
EDEM	ER degradation-enhancing alpha-mannosidase-like protein
eIF2α	Eukaryotic Initiation factor a2 alpha
ER	Endoplasmic Reticulum
ERAD	Endoplasmic Reticulum Associated degradation
ERSE	Endoplasmic Reticulum Stress Response Element
FADD	FAS-associated death domain protein
FIP200	Focal adhesion kinase family interacting protein of 200 Kd
GADD34	Growth arrest and DNA damage-inducible protein 34
Gen	Genistein
GSK-3β	Glycogen synthase kinase 3 beta
GWAS	Gene Wide Association Study
HLA-B27	Human Leukocyte Antigen B27

IL- 23	Interleukin 23
IL- 6	Interleukin 6
IL-13	Interleukin 13
IL-17	Interleukin 17
IL-23R	Interleukin 23 Receptor
IL-4 I	Interleukin 4
IRE1	Inositol Requiring Enzyme 1
JAK	Janus Kinase
JNK	c-Jun N-terminal kinases
LC3B	Microtubule-associated protein 1A/1B light chain 3B
MHC	Major Compatibility Complex
mRNA	Messenger Ribonucleic Acid
NFkB	Nuclear factor NF-kappa-B p105 subunit
NE	Nuclear Envelope
OST	Oligosaccharyltransferase
PE	Phosphatidylethanolamine
PER	Peripheral Endoplasmic Reticulum
PERK	Protein kinase R (PKR)-like endoplasmic reticulum kinase
PtdIns	Phosphatidylinositol 4,5-bisphosphate
SDS-PAGE	Sodium Dodecyl Sulphate Gel Electrophoresis
SERCA	Sarcoplasmic/ER Calcium transport ATPase
STAT3	Signal transducer and activator of transcription 3
TNF	Tumour Necrosis Factor
TRAF2	TNF receptor-associated factor 2
Tun	Tunicamycin
ULK1	Serine/threonine-protein kinase
UPR	Unfolded Protein Response
XBP1	X-Box protein 1

Declaration

I declare that the material contained in this thesis is the result of my own work and has not been previously submitted for a higher degree.

Matilda Ruvimbo Masose

Acknowledgements

I would like to thank my supervisor Dr Adam Benham for his encouragement, support, advice and especially his patience throughout this project. I would also like to thank everyone in Laboratory 8 for their support and entertainment throughout my degree.

And finally I would like to thank my Mum, Alice and Dad, Maxwell for their patience and support throughout my studies.

1. General Introduction

1.1. The Endoplasmic Reticulum: Structure and Function

The endoplasmic reticulum (ER) was first described in 1902 by Emilio Veratti and can be described as a single continual membranous organelle (Westrate et. al. 2015). The ER can be divided into two domains: i) the nuclear envelope (NE) domain which surrounds the nucleus and ii) the peripheral domain which consists of interconnected tubules that span into the cytoplasm of cells (Voeltz et. al. 2002). The NE consists of a bilayer of two flat inner and outer membranes. As seen in figure 1.1, the NE's structure is maintained by proteins in the inner membrane which bind to chromatin, lamin, linker proteins (that are found in between the inner and outer NE), nuclear pores and finally the cytoskeleton. The outer membrane of the NE then expands into the peripheral ER (PER). The PER is made up of a series of interconnected domains. These domains have two morphologies which are i) flattened sheets and ii) cylindrical tubules. The flattened sheets have little membrane curvature except along the edges where the lipid bilayer folds into itself. The cylindrical tubules, which expand from the NE, and the flattened sheets have a high membrane curvature (figure 1). The tubules are also connected at three way junctions, which results in a loose polygonal array that spreads throughout the cytosol to various parts of the cell in a way that allows other organelles to traffic around it (Figure 1.1). Along with this, the ER tubules are also highly dynamic, which means that they are continuously forming and re-arranging. The dynamic nature of these ER structures suggest that the morphology and function of the ER are linked, meaning that the cell is able to modify each of the structural domains of the ER to meet specific cellular needs (Westrate et. al. 2015, Shibata et. al. 2006). This is in line with early reports by Palade (1955a) and Palade (1956) where it was demonstrated that the ER has rough outer surfaces and smooth outer surfaces whose ratio differs depending on the function of the cell. For example, smooth ER was mainly observed in cells such as adipose cells and adrenal cortex cells which specialise in lipid metabolism (Palade, 1956), whereas rough ER which is characterised by membrane bound ribosomes attached to the outer surface (Palade, 1956) was identified in acinar cells and striated muscle fibres (Palade, 1955b). Though the studies by Palade had managed to show the distinction between the cisternae and tubules,

later studies managed to demonstrate using electron microscopy studies in yeast that the flattened cisternae had a higher density of ribosomes compared to the cylindrical tubules which had none (West et. al. 2011, Shibata et. al. 2006). Another critical difference between sheets and tubules which has been postulated to give these two structures different functions is that tubules have a higher surface-area-to-volume ratio compared to cisternae (Westrate et. al. 2015) which Shibata et. al. postulated increased the efficiency of lipid synthesis by maximising access to cytosolic phospholipid-interacting proteins (Shibata et. al. 2006). Westrate et. al. also postulated that this feature of tubules makes them better suited for surface dependent functions; however, beyond this, tubule functions are not well understood but have been postulated to include signalling between the ER and other organelles and also lipid synthesis (Westrate et. al. 2015, Shibata et. al. 2006). With regards to the flattened sheets, Westrate et. al. postulated that sheets were better suited to luminal processes including translation, translocation, folding, the secretion of newly synthesised proteins and post-translational modifications (West et. al. 2011, Westrate et. al. 2015). These processes have been studied extensively and will be discussed later in this chapter.

With ER morphology being correlated to the function of the ER, it is interesting that the ratio of sheets and tubules differs between cell types. This means that the organization of the ER and therefore ER functions will also differ between varying cells types.

1.2 Protein Folding and ER Quality control

The majority of what is known of the ER protein folding machinery was gleaned from biochemical studies of ER proteins and enzymes and genetic studies from yeast (Dean and Pelham 1990). More recently, an important study in understanding ER function was one conducted by Gilchrist et. al. (2006) who through an experimental proteomics approach isolated rough and smooth ER along with the Golgi apparatus in rat livers to provide a comprehensive list of ER proteins and their function.

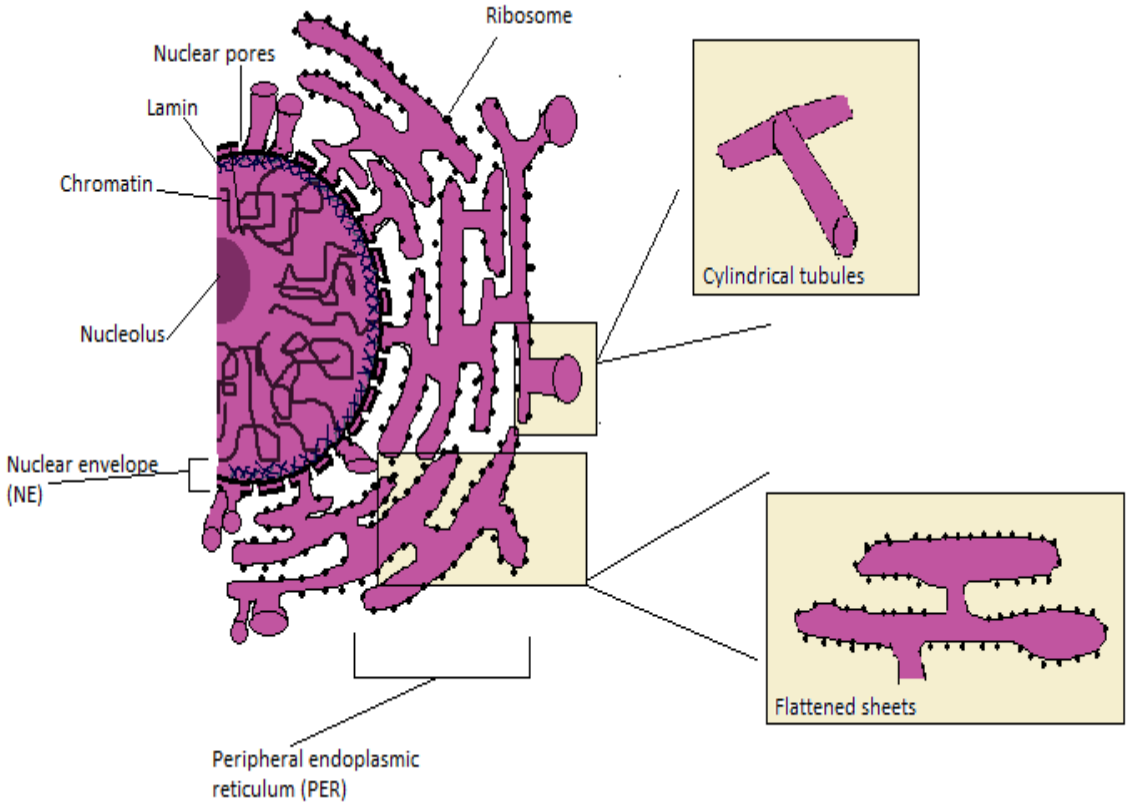

Figure 1.1. The morphology of the endoplasmic reticulum

The endoplasmic reticulum has two domains, the nuclear envelope (NE) and the peripheral endoplasmic reticulum (PER). The NE consist of inner and outer membranes which form a bilayer with proteins of the inner membrane binding to chromatin, lamin, linker proteins, the nuclear pore and the cytoskeleton to maintain the NE's structure. The PER consist of interconnected domains which have two morphologies; flattened sheets and cylindrical tubules with these having low and high membrane curvature respectively.

It was identified that the most abundant proteins in the rough ER were those involved in protein synthesis and folding and less relevantly, the most abundant proteins in the smooth ER being those involved in detoxification (Gilchrist et. al. 2006).With one of the most important functions of the ER being the folding of secretory, transmembrane and ER resident proteins, several studies over many years have been undertaken to elucidate the exact mechanisms by which proteins are folded and how these can be manipulated to treat protein folding linked diseases.

Many of the proteins that are involved in protein folding are known as chaperones (proteins that aid in the assembly or disassembly of macromolecular structures but are not permanent components of said structures) (Henderson and Pockley 2005). Chaperones belonging to a range of different families have been identified including the Hsp70 class chaperones (e.g. BiP) and lectin-like chaperones (e.g. calnexin/calreticulin) and others which have been listed in table 1. With there being numerous different chaperones, ER quality control is a tightly regulated process (Brodsky and Skach 2011). In the early stages of protein folding (a process that is initiated as soon as the translation of mRNA occurs on cytosolic ribosomes and then ends when the folded protein is packaged into vesicles and exits the ER), the nascent polypeptide chain passes from the ribosome through to the ER via an aqueous pore composed of the sec61 complex (Crowley et. al. 1994, Becker et. al. 2009). This pore is also tightly controlled as it has two key functions: i) opening and translocating a nascent polypeptide when the polypeptide chain reaches seventy amino acids in length and ii) ensuring that the nascent polypeptide chain is translocated to the right region of the ER (Crowley et. al. 1994). The regulation of this process was demonstrated by Liao et. al. (1997) who showed that the aqueous pore undergoes a series of tightly regulated conformational changes which ensure that the cytosol and ER lumen are alternatively gated. This alternative gating then allows specific domains of membrane proteins to be directed to the cytosol and secretory proteins to the ER lumen (Liao at. al. 1997, Brodsky and Skach 2011). Once nascent proteins enter the ER lumen through the translocon, they

almost instantaneously encounter chaperones and begin to fold a short distance into the lumen of the ER (Kowarick et. al. 2002). Before proteins can fold however, they are glycosylated early while the nascent peptide is passing through the translocon. The enzyme oligosaccharyltransferase (OST) attaches an oligosaccharide to the nascent polypeptides, which promotes stability, reduces aggregation and also presents calnexin (CXN) and calreticulin (CRT) with a binding site. It was reported by Shibatani et. al. that the OST enzyme forms complexes with ribosomes even following nascent polypeptide release and that the main association was with the Sec61αβ complex (Shibatani et. al. 2005), meaning N-linked glycosylation can occur co-translationally as the polypeptide enters the ER through the translocon (to help ensure more efficient folding). In the ER lumen following the attachment of the oligosaccharide composed of two N-acetylglucosamine, nine mannose and three glucose molecules ($GlcNAC_2Man_9Glc_3$) to nascent proteins, the glucosidase I enzyme removes the terminally attached glucose and glucosidase II removes the second glucose leaving a $GlcNAC_2Man_9Glc_1$, for which CRT and CXN have high specificity (Kozlov et. al. 2010). With CXN being a membrane protein, it is able to bind to substrates co-translationally while CRT is a soluble protein so it binds soluble luminal glycoproteins. Once bound, CXN/CRT (Kozlov et. al. 2010) are able to retain proteins in the ER, prevent them from aggregating thus shielding them from degradation and finally facilitating their folding by recruiting other chaperones such as ERp57 and PDI (Brodsky and Skach 2011) which both have a role in oxidative protein folding (Rutkevich et. al. 2010). Once the protein is folded, it can then leave the ER. However, if the protein is unfolded or misfolded and still contains hydrophobic regions, then there are two main events that can occur: i) the unfolded protein can be re-glycosylated by the enzyme UDP-Glc:glycoprotein glycotransferase and re-enter the CNX/CRT cycle or ii) it can be assigned to BiP/GRP78 (which has been shown to complex with several chaperones and folding enzymes including GRP94, P5 PDI, PDI and the co-chaperone HSP40) which assist in the re-folding of the protein (Meunier et. al. 2002).

Table 1. The main quality control proteins involved in ER protein folding

Family	Principle ER Members	Functions
HSP70	BiP	Chaperone
Glycan processing enzymes	ER glucosidase I and II	Trimming of glucoses from N-glycans
	ER mannosidases	Removal of terminal mannoses
Oxidoreductases	ERO1α/β	Disulphide bond formation
Protein Disulphide Isomerases	ERp57, ERp72 and PDI	Involved in disulphide bond formation, reduction and isomerization
HSP90	Grp94	Chaperone
Lectin-like chaperones	Calnexin, calreticulin	Chaperone

1.3. Protein Misfolding and the Unfolded Protein Response

Even though ER networks are tightly regulated (Brodsky and Skach 2011) and the majority of proteins are synthesised, processed and folded correctly, there are certain stimuli which can be physiological, environmental or even pathological that can cause the disruption of ER homeostasis and cause the accumulation of unfolded/ mis-folded proteins which ultimately leads to ER stress (Janssens et. al. 2014). The ER however, has mechanisms that deal with transient and chronic accumulation of misfolded proteins. These mechanisms are ER associated degradation (ERAD) and the unfolded protein response (UPR). ERAD is a complex system which targets misfolded/unfolded proteins for ubiquitination by the proteasome and involves several key steps which include i) the recognition of misfolded protein ii) retro-translocation into the cytosol iii) ubiquitination and finally iv) degradation. The UPR is a complex set of stress induced signal transduction cascades that aim to restore ER homeostasis after it has been disrupted by the accumulation of unfolded proteins in ER lumen (Brodsky and Skach 2011, Janssens et. al. 2014).

The UPR has three main sensors localized in the ER lumen these are: Activating Transcription Factor 6 (ATF6), protein kinase R -like ER kinase (PERK) and Inositol Requiring Enzyme 1 (IRE1). Through these three sensors, the UPR is then able to restore ER homeostasis by i) increasing the ER folding capacity by upregulating the transcription of genes encoding for chaperones, ii) reducing the further accumulation of unfolded proteins by transiently inhibiting protein translation and iii) activating apoptosis when ER homeostasis cannot be attained (Janssens et. al. 2014, Oyadomari and Mori 2003, Harding et. al. 2000).

1.3.1. ATF6

ATF6, as shown by Haze et. al. is a type II transmembrane glycoprotein that can be proteolytically cleaved into two forms (Haze et. al. 1999). AFT6, usually a 90kDa (p90ATF6) protein, is constitutively expressed. However, upon ER stress p90ATF6 is converted to a 50kDa protein (p50ATF6) (Yoshida et. al. 1998). It was later shown by Haze et.al. 1999 through fractionation experiments using HeLa cells that these two forms of AFT6 (p90ATF6 and p50ATF6) localise in different cellular compartments. It was found that p90ATF6 co-localised with CXN (a known ER transmembrane protein) in the membrane fraction which suggested that p90ATF6 was also a transmembrane protein. However, p50ATF6 (which was only detected in ER stressed cells) was found to localise in the nuclear pellet faction. Further fractionation experiments by Haze et.al. 1999 on the nuclear pellet also found that more than half of p50ATF6 was found in the supernatant which ultimately lead to the conclusion that p50ATF6 was a soluble protein that was able to translocate to the nucleus (Haze et.al. 1999), where its translocation could be correlated with increased BiP levels. This corroborated results found by Yoshida et. al. who identified an ER stress response element (ERSE) CCAAT(N)9CCAGG upstream of the genes encoding BiP, GRP94 and calreticulin to which ATF6 could bind. These ERSEs were crucial for the up-regulation of these genes, with the corresponding protein levels increased 5-8 fold, 8-fold and 4 fold respectively under chemically induced ER stress compared to when the ERSE was removed (Yoshida et. al. 1998). Although ATF6's role in upregulation of ER chaperones was clear, it was unclear how p90ATF6 was converted to p50ATF6 until a study by Ye et. al. 2000 who found that after ER stress ATF6 is translocated to the Golgi apparatus where it is processed by site-1/site-2 protease enzymes in a way that releases the N-terminal cytoplasmic domain. This domain then translocates to the nucleus and activates ER chaperone proteins as shown in Figure 1.2 (Ye et. al. 2000, Schindler and Schekman 2009, Yoshida et. al. 1998, Haze et. al. 1999).

1.3.2. PERK

Mammalian PERK was first characterised in 1998 as a transmembrane protein rich in hydrophilic regions. Through immunoblot analysis, it was shown that upon ER stress, PERK auto-phosphorylates at threonine residues and goes on to phosphorylate the alpha subunit of eIF2 at serine 51. In this same study it was shown that PERK, through its phosphorylation of eIF2α, is able to somehow regulate translation (Shi et. al. 1998), though the details of this regulation were not elucidated in that particular study. Instead, a later study by Harding et. al. (2000) was able to expand on the findings by Shi et. al. (1998) findings and expanded on them. They were able to show that PERK has an important role in attenuating translation during ER stress. Using $PERK^{-/-}$ mouse embryonic stem cells, it was shown that ER stress did not result in the attenuation of translation; rather, there was an increase (postulated to be because of a decrease in mature protein secretion) in cellular radioactively labelled proteins (proteome) compared to wildtype ($PERK^{+/+}$) ER stressed cells which suggested that PERK had an essential role in translation attenuation (Harding et. al. 2000). The full picture of PERK signalling during ER stress responses through eIF2α is now more understood. It has been shown that the phosphorylation of the alpha subunit of eIF2α by PERK decreases the translation of most mRNAs (Harding et. al. 1999). On the other hand, eiF2α can also increase the translation of mRNAs with a short upstream open reading frame. This results in the upregulation of proteins that are directly involved in the UPR (Vattem and Wek 2004). One such protein is ATF4 which has been shown to be important in PERK mediated signalling (B'Chir et. al 2013). Harding et. al. (2000) were able to show that during tunicamycin induced ER stress, the PERK/ATF4 signalling pathway upregulates genes involved in the import and metabolism of amino acids and genes involved in the resistance of oxidative stress, with ATF4 being the major regulator of these genes. This was found using $AFT4^{-/-}$ fibroblasts, which had impaired activation of genes relating to amino acid import, metabolism and protection against oxidative stress (Harding et. al. 2003). ATF4 has also been shown to regulate the transcription of genes relating to cell survival during the UPR, mainly autophagy genes including MAP1LC3 (discussed in section 1.4) (B' Chir et. al. 2013) and apoptosis associated genes such as CHOP (discussed in section 1.4) (Averous et. al. 2003).

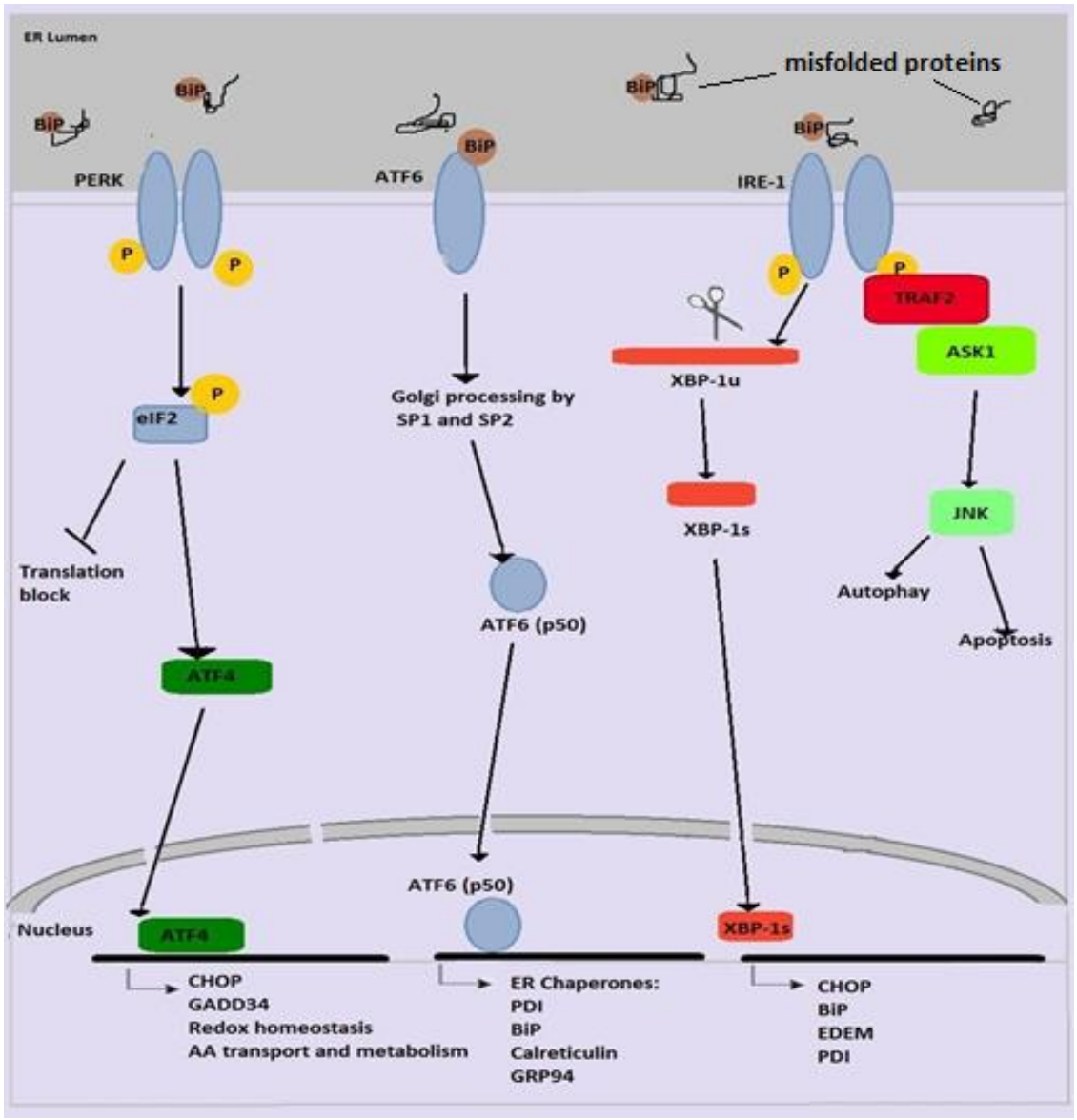

Figure 1.2: The Unfolded Protein Response

The UPR has 3 main branches: the PERK, ATF6 and IRE1 arms. Firstly upon protein mis-folding, BiP dissociates from PERK, ATF6 and IRE1 and binds to misfolded proteins to aid in their folding. Upon BiP dissociation, PERK and IRE1 oligomerize and auto-phosphorylate. ATF6 Golgi localization signals are activated allowing ATF6 to translocate to the Golgi apparatus. Once at the Golgi apparatus, ATF6 is cleaved by site 1/2 proteases releasing their N-terminal domain (ATF6p50). ATF6p50 then translocates to the nucleus where it binds to ERSE motifs in the promotors of ER stress responsive genes. Activated PERK phosphorylates eIF2α, activating it. Activated eIF2α activates the transcription factor ATF4 which facilitates the transcription of CHOP, GADD34 and genes involved in redox homeostasis. eIF2α can also block general translation. Activated IRE1 can cleave and splice XBP-1. Spliced XBP-1 (XBP-1s) then goes on to activate genes involved in ERAD and increases ER folding capacity. Activated IRE1 can also recruit TRAF2, leading to the activation of the JNK pathway, which can lead to either apoptotic or autophagic responses.

1.3.3. IRE1

Unlike PERK and ATF6, IRE1 has dual functions in that it can activate two distinct pathways, one involving the transcription factor XBP-1 and the induction of ER chaperones and the other involving the recruitment of TRAF2 and subsequent activation of the JNK pathway (Zhu et. al. 2014). There are two IRE1 isoforms, IRE1α (ubiquitously expressed) and IRE1β (expressed in the gut and the respiratory epithelium) which both have a N-terminal ER lumen sensor domain and a C terminal cytosolic effector region which contain both an endoribonuclease domain and a kinase domain (Tirasophon et. al. 1998, Bertolotti et. al. 2001, Martino et. al. 2012 Iwagawa et. al. 2008). Following on from a 2001 study by Yoshida et.al. which demonstrated that ER stress activation of IRE1α leads to the upregulation (through ERSE response element) and splicing of XBP-1 (Yoshida et. al. 2001), Imagawa et. al. (2008) found that during ER stress conditions, the RNase domain of each of the isoforms have distinct functions. The RNase domain of IRE1β was found to have a pivotal role in the cleavage of 28S rRNA (which is also shared by IRE1α, albeit at low levels) and the RNase domain of IRE1α was found to have a pivotal role in XBP-1 splicing (Iwagawa et. al. 2008). Further studies (e.g. Lee et. al. 2003) then went on to show, through microarray analysis, that in tunicamycin treated MEF cells generated from XBP-1 deficient mice, known UPR target genes were not expressed whereas in wildtype cells, UPR target genes involved in the degradation and folding of mis-folded proteins were expressed (e.g. BIP, CHOP, EDEM and the Protein Disulphide Isomerase P5). Lee et. al. also showed that ATF6 can induce XBP-1 and BiP which suggested that the UPR pathways are dynamic and partly converge (Lee et. al. 2003) (Figure 1.2).

IRE1 has also been shown to regulate the TRAF2/ASK1/JNK pathway. A recent study (Zhu et. al. 2014) described how IRE1 mediates the TRAF2/ASK1/JNK pathway through ubiquitination by CHIP (carboxyl terminus of HSC70-interacting protein), an E3 ubiquitin ligase usually active during ERAD. Through immunoprecipitation assays, western blotting and mass spectrometry, along with some confocal microscopy, Zhu et. al. were able to show that IRE1 and CHIP can co-immunoprecipitate and co-localise and that the subsequent ubiquitination at Lys828 was crucial for IRE1/TRAF2 interaction and subsequent JNK activation (Zhu et. al. 2014). Earlier studies had also

shown that IRE1 co-immunoprecipitates with TRAF2 when cells were treated with ER stressors in a kinase and RNase dependent manner (Urano et. al. 2000). As shown in figure 1.2, TRAF2 can activate ASK1 which then activates JNK. This activation of the IRE1/JNK pathway has been linked to autophagy and apoptosis in ER stressed cells; if the cells cannot recover from ER stress, the apoptotic pathway can be initiated.

1.3.4. BiP/Grp78

As shown in figure 1.2, BiP binds to the luminal domains of all three UPR sensors. A study by Bertolotti et. al. was the first to identify the role of BiP in the activation of the PERK and IRE1 sensors (Bertolotti et. al. 2000). Immunoprecipitation experiments found that BiP co-immunoprecipitated with PERK and IRE1 which therefore meant that BiP formed individual complexes with either PERK or IRE1. BiP interactions with PERK/IRE1 were then tested under ER stress conditions and it was found that within minutes of inducing ER stress, BiPs association with PERK/IRE1 decreased which was then correlated with the activation and phosphorylation of PERK/IRE1. Bertolotti et. al. proposed a model for IRE1/PERK activation. This model states that BiP is constitutively bound to the two sensors which inhibits their oligomerization; however, in response to misfolded proteins, BiP dissociates from the sensors and binds to the exposed hydrophobic domains of misfolded proteins, thereby facilitating phosphorylation, oligomerisation and activation of IRE1 and PERK (Bertolotti et. al. 2000).

BiP binding to ATF6 is similar to that of PERK and IRE1. ATF6's ER luminal domain has several binding sites which BiP is able to bind. These binding sites have also been shown to have regions which mediate the transport of ATF6 to the Golgi apparatus, referred to as Golgi localization signals (Shen et. al. 2002). In unstressed cells, ATF6 is a transmembrane protein with which BiP associates; however, upon treatment with ER stress inducers and the subsequent accumulation of mis-folded proteins, BiP disassociates from ATF6 to prevent misfolded protein aggregation and promote folding. This dissociation of BiP causes the activation of the Golgi localization signals and the translocation of ATF6 to the Golgi apparatus where it can be processed (Shen et. al. 2002).

1.4. The UPR and cell survival

As mentioned previously the UPR has the main function of restoring ER homeostasis in response to a disruption. As explained in section 1.3, ATF6, IRE1 and PERK activate pathways which induce the transcription of several genes including chaperones to aid in the re-folding of misfolded proteins but also to aid in the degradation of unfolded proteins. However, what happens when ER stress is prolonged? Szegezdi et. al. has previously suggested that the different branches of the UPR are activated not at the same time but in sequence. It is thought that PERK/ATF6 pathways are activated first to halt translation (to minimize further accumulation of misfolded proteins) and to induce transcription of chaperones (to mediate refolding of misfolded proteins). The IRE1 pathway is postulated to be activated last, however there has been very limited evidence to support this theory. It has been demonstrated that initially the IRE1 arm aids in the reestablishment of ER homeostasis through XBP1 splicing; however, at a later stage the UPR is terminated (Szegezdi et. al. 2006) by inducing the expression of $P58^{IPk}$, which was found to interact with the kinase domain of PERK thereby attenuating its function and ultimately reducing BiP/CHOP expression (Yan et. al. 2002). Once $P58^{IPk}$ is expressed, the cell can either resume normal cellular functions if the ER stress has been resolved or trigger apoptosis and autophagy pathways through the IRE1-JNK pathway (and PERK) (Szegezdi et. al. 2006).

1.4.1. Autophagy and the UPR

In most tissues, autophagy has an important role in normal cellular functions as well as being involved in re-establishing ER homeostasis. There are several types of autophagy including macroautophagy (which involves the delivery of cargo for degradation to lysosomes through autolysosomes), microautophagy (which involves the direct engulfment of cytosolic components by lysosomes for degradation) and chaperone mediated autophagy (which involves the targeting of cytosolic proteins directly to the lysosomes for degradation) (Glick et. al. 2010). Here, the focus will be on macroautophagy, which will be referred to as autophagy.

Autophagy can be initiated by a variety of stimuli including amino acid starvation and ER stress. In response to a specific stimuli, as shown in Figure 1.3, the formation of a flat membranous phagophore is initiated in a sequence of events which requires two sets of protein complexes (Kaur and Debnath 2015). The first is the ULK1 complex composed of ULK1 (a serine/threonine kinase that is an essential regulator of autophagosome formation), Autophagy related protein-13 (ATG13) and focal adhesion kinase family interacting protein of 200kDa (F1P200), which are both required for ULK1 to localise to the isolation membrane and maximise ULK1 kinase activity (Ganley et. al. 2009). The second is the class III phosphatidylinositol-3-kinase (Ptdlns) complex which is composed of Beclin-1, human vacuolar protein sorting 34 (hvps34), p150 and Atg14L which are all essential for autophagosome formation (Matsunaga et. al. 2010, Itakura et. al. 2008, Petiot et. al. 2000). The next step after phagophore formation is the elongation and transition from a single membraned phagophore into the double- membraned autophagosome. This elongation step requires the action of two ubiquitin-like conjugation pathways and is catalysed by Atg7 (Tanida et. al. 2000, Tanida et. al. 2004 and Kaur and Debnath 2015). Firstly, Atg5 and Atg12 conjugate and together they form a complex with Atg16L. This multimeric Atg5Atg12-Atg16L complex then associates with the outer membrane of the phagophore in a process that can occur outside of autophagy (Mizushima et. al. 2003) to facilitate in the formation of the autophagosome (Kaur and Debnath 2015, Barth et. al. 2010, Glick et. al. 2010).

When autophagy is initiated, hsAtg4B proteolytically cleaves pro-LC3B to generate LC3B-I which exposes glycine at the C-terminus. To this C-terminus the highly lipophilic phosphatidylethanolamine (PE) is conjugated to LC3B-I in an Atg7 dependent manner forming LC3B-II-PE. The Atg5-Atg12-Atg16L complex then ensures that LC3B-II-PE is localised to the expanding phagophore membranes.
Once LC3B-II-PE is integrated into the lipid membrane of the phagophore to form the autophagosome (Barth et. al. 2010 and Dowdle et. al. 2014), the Atg5-Atg12Atg16L complex dissociates leaving LC3B in the autophagosome membrane (Kabeya et. al. 2000, Mizushima et. al. 2003). The integration of LC3B-II-PE is said to be required for the expansion and completion of the phagophore membrane to form the autophagosome (and is also thought to aid in the recognition of cargo for

degradation) (Mizushima et. al. 2003). The final steps, as depicted in figure 1.3, are the fusion of the lysosome with the autophagosome and the degradation of contents by lysosomal hydrolases and the recycling of degraded material such as amino acids (Kaur and Debnaur 2015).

Ogata et. al. demonstrated that autophagy can be initiated in response to chemically induced ER stress (using tunicamycin and thapsigargin). In neuroblastoma cells, a 3.4 fold increase in autophagosome formation was found in ER stressed cells compared to untreated cells (Ogata et. al. 2006). This group also identified IRE1 signalling as being required for autophagy initiation during ER stress. They used IRE1αβ$^{-/-}$ and IRE1α deficient MEF cells which under ER stress showed no GFP-LC3B dot formation (corresponding to LC3B-II conjugated into the phagophore membrane i.e. the autophagosome). However, when full length IRE1α was transfected into IRE1α deficient cells, GFP-LC3B dot formation was recovered *i.e.* autophagosomes formed. Along with testing the IRE1 pathway, Ogata et. al. also investigated the role of PERK and ATF6 using PERK deficient and ATF6αβ knockdown cells, respectively, in ER stress induced autophagy. They found that in PERK deficient cells undergoing ER stress, there was a significant increase in LC3B dot formation and in ATF6αβ knockdown cells, GFP-LC3B dot formation was comparable to that of control wild-type MEF cells. Taken together this suggested that the PERK/ATF6 pathways were not involved in ER stress induced autophagy but the IRE1 pathways were. Further experiments involving inhibiting of JNK activation revealed that the IRE1-JNK pathway is involved in ER stress induced autophagy (Ogata et. al. 2006).

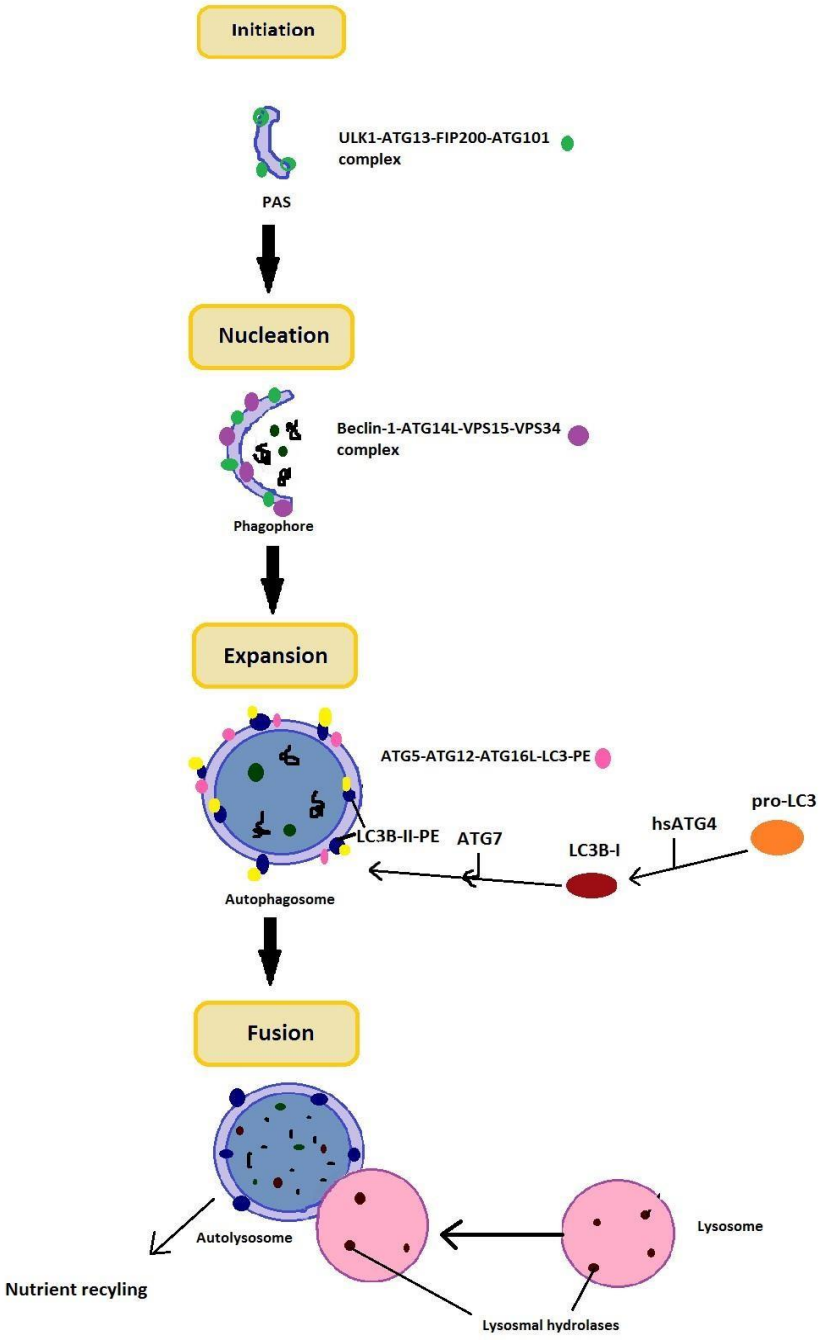

Figure 1.3: Overview of macroautophagy

Macroautophagy initiation begins with the formation of the phagophore at the phagophore assembly site (PAS). The phagophore elongates (Nucleation), engulfing cargo, and forms the autophagosome. Pro-LC3B is processed into LC3B-II (orange and red dots) and LC3B-II is incorporated within the membrane (purple and blue structure (expansion)). Prior to lysosomal fusion, LC3B-II dissociates back into the cytosol and the autophagosome fuses with a lysosome (pink). Lysosomal hydrolases then degrade the cargo, which is then recycled (fusion and degradation).

However, in contrast to Ogata et. al., Rzymski et. al. used a range of different cell lines and found that PERK pathways and not IRE1α pathways were involved in the induction of autophagy in response to ER stress. They initially tested the response of MDA-MB231 (breast adenocarcinoma), LS1-74T (colon adenocarcinoma), MCF7 (breast adenocarcinoma) and HCT 116 (colon carcinoma) cells to thapsigargin and tunicamycin induced ER stress and found that LC3B levels were increased (Tom et. al. 1979, Brooks et.al. 1973, Brattain et. al. 1981 and Sheridan et. al. 2006). However, in LS174T and HCT116 cells, which had the greatest fold increase of LC3B, there was no expression of GADD34, a protein which inhibits the ATF4 pathway. These authors went on to further substantiate these findings in MCF7 cells, were they found that PERK was activated and that there was an increased induction of ATF4 and processing of LC3B; however, in MCF7 cells silenced for ATF4, LC3B levels decreased when compared to wildtype MCF7 cells treated with thapsigargin. The LC3B promoter was also found to have an AFT4 as well as an XBP1 binding site (Rzymski et. al. 2010) meaning both the IRE1 pathway (which activates XBP1) and the PERK pathway may have a role in autophagy. Also in agreement with Rzymski et. al., B' Chir et. al. used stressed $PERK^{-/-}$ MEFs to show that the lack of ATF4, CHOP and activation of eIF2α was accompanied by a reduction in the expression of autophagy related genes. These genes were involved in the formation of the ubiquitin-like protein complex that is essential for autophagosome formation and included ATG12, MAP1LC3B encoding the LC3B protein, ATG5 and ATG7 the Beclin-1 protein and the SQSTM1 gene encoding the p62 protein (which directly binds to LC3B proteins and is essential for degradation) (Pankiv et. al. 2007). This data suggested that ATF4 and CHOP had an essential role in initiating transcription of genes involved in the elongation, formation and function of the autophagosome (B'Chir et. al. 2013). However, going back to the study by Ogata et. al. it seems that even though they had initially found no role for PERK in ER stress induced autophagy and the previously presented studies had, the differences between these two studies cannot be attributed to either the different cell types as both B'Chir et. al. and Ogata et. al. used MEFs or the method of ER stress induction as all studies presented here used tunicamycin and thapsigargin.
A later study by Raciti et. al. that was consistent with the findings of Ogata et. al., found a role for the IRE1-JNK pathway in autophagy that did not dismiss a role for

PERK. Raciti et. al. found that JNK2 had a role in controlling the final steps of autophagy through the regulation of UPR genes such as CHOP (downregulated UPR genes) and BiP (upregulated UPR genes) and others which may regulate lysosomal and autosomal function thereby promoting cell survival (Raciti et. al. 2012). These two papers suggest that the IRE1 pathway and the PERK pathway may have roles in different phases of autophagy.

Interestingly, the expression, activation and cleavage of LC3B has been shown to be dependent on different branches of the UPR in different cell types. For example, a study by Milani et. al. showed LC3B activation to be dependent on ATF4 in MCF7 and MDA MB 231 cells in response to severe hypoxia (Milani et. al.2009). However in Tanaka et. al. showed JNK to regulate the induction of LC3B activation in lung epithelial cells again in response to hypoxia (Tanaka et. al. 2012). This suggested that different cell types can activate different pathways that lead to the same responses, which could have implications in therapies directed towards autophagy.

1.4.2. Apoptosis and the UPR

There are two apoptotic pathways, called the extrinsic and the intrinsic pathways, which each converge on an execution phase which is delivered by the executioner caspases 3, 6 and 7. The extrinsic pathway is initiated by the ligation of members of the TNF receptor superfamily including Fas. Following Fas receptor ligation, the adapter molecule Fas-associated death domain protein (FADD) is recruited to the Fas receptor to form the death inducing signal complex (DISC) (Kischkel et. al. 1995) which in turn recruits and activates caspase 8 (Boldin et. al. 1996). Following its activation, caspase 8 can directly activate other caspases including caspase 3 (Enari et. al. 1996, Takahashi et. al. 1997), caspase 6 (Takahashi et. al. 1997) and caspase 7 (Fernandes-Alnemri et. al. 1995, Takahashi et. al. 1997) leading to apoptosis. The DISC can also initiate apoptosis through a pathway involving the mitochondria (Scaffidi et. al. 1998). This pathway involves the pro-apoptotic molecule BID. Caspase 8 cleaves BID at its carboxyl terminal to form a fragment referred to as p15 (tBID). tBID then translocates to the outer membrane of the mitochondria where it initiates the release of

cytochrome c thus initiating the execution phase of apoptosis (Gross et. al. 1999) as seen in figure 1.4. From here on the intrinsic pathway will be discussed and will be referred to as apoptosis. The intrinsic pathway is initiated and mediated by the Bcl-2 family of proteins whose transduction is triggered by cellular stresses that include growth factor deprivation and ER stress. Some of the main transducers of apoptosis include the pro-apoptotic Bax and Bak proteins. Upon their activation, Bax and Bak homo-oligomerize and form pores within the membrane of the mitochondria (Wei et. al. 2001, Bratton and Salvesen 2010). Through these pores, cytochrome c is able to translocate from the mitochondria and into the cytosol (Bratton and Salvesen 2010) and bind to and activate Apaf-1 (Zou et. al. 1997). Apaf-1 homo-oligomerizes into an activating complex known as the apoptosome complex. Once the apoptosome is assembled, pro-caspase 9 is recruited to the apoptosome and activated by cleavage into Caspase 9. Processed caspase 9 (with a molecular weight of either 35kDa or 37kDa) then recruits and activates caspase 3 (Bratton et. al. 2001), thus initiating the caspase cascade and subsequently apoptosis as shown in figure 1.4.

As mentioned in section 1.4, apoptosis can be activated by ER stress. Zinszner et. al. created a $CHOP^{-/-}$ mouse and found that cells derived from this mouse were resistant to apoptotic changes, with the appearance of characteristic apoptotic features being delayed when compared to wildtype control cells. This implicated CHOP in ER stress induced apoptosis, along with the UPR, since UPR pathways induce CHOP transcription (Zinszner et. al. 1998). McCullough et. al. then later determined the role of CHOP in apoptosis. Their study found that the overexpression of CHOP in rat1, MEF and A49 cells reduced the expression of Bcl-2 and further experiments showed that CHOP inhibited Bcl-2 promoter activity in a dose dependent manner. This lead to the conclusion that CHOP has an important role in down-regulating the transcription of the anti-apoptotic factor bcl-2 (McCullough et. al. 2001). These findings implicated PERK dependent pathways in ER stress induced apoptosis, as though all the components of the UPR can activate CHOP, PERK/eIF2α signalling is indispensable for the upregulation of CHOP (Szegezdi et. al. 2006).

IRE1α has also been implicated in apoptosis initiation. Firstly, overexpression of IRE1 has been linked to apoptosis as it was shown to induce CHOP mRNA and increase its protein levels (Wang et. al. 1998). Specifically, the IRE1-JNK axis has been implicated in

apoptosis, with ASK1 overexpression inducing apoptosis in a caspase dependent manner (Hatai et. al. 2000). Finally, JNK has also been linked to apoptosis induction through its role in phosphorylating the anti-apoptotic factor bcl-2, thereby suppressing its activity (Szegezdi et. al. 2006). ATF6 has also been linked with apoptosis initiation. Nakanishi et. al. demonstrated that ATF6 is required for the activation of caspase 12 initiated apoptosis during myotube formation in mice albeit not as a response to chemically induced ER stress (Nakanishi et. al. 2005).

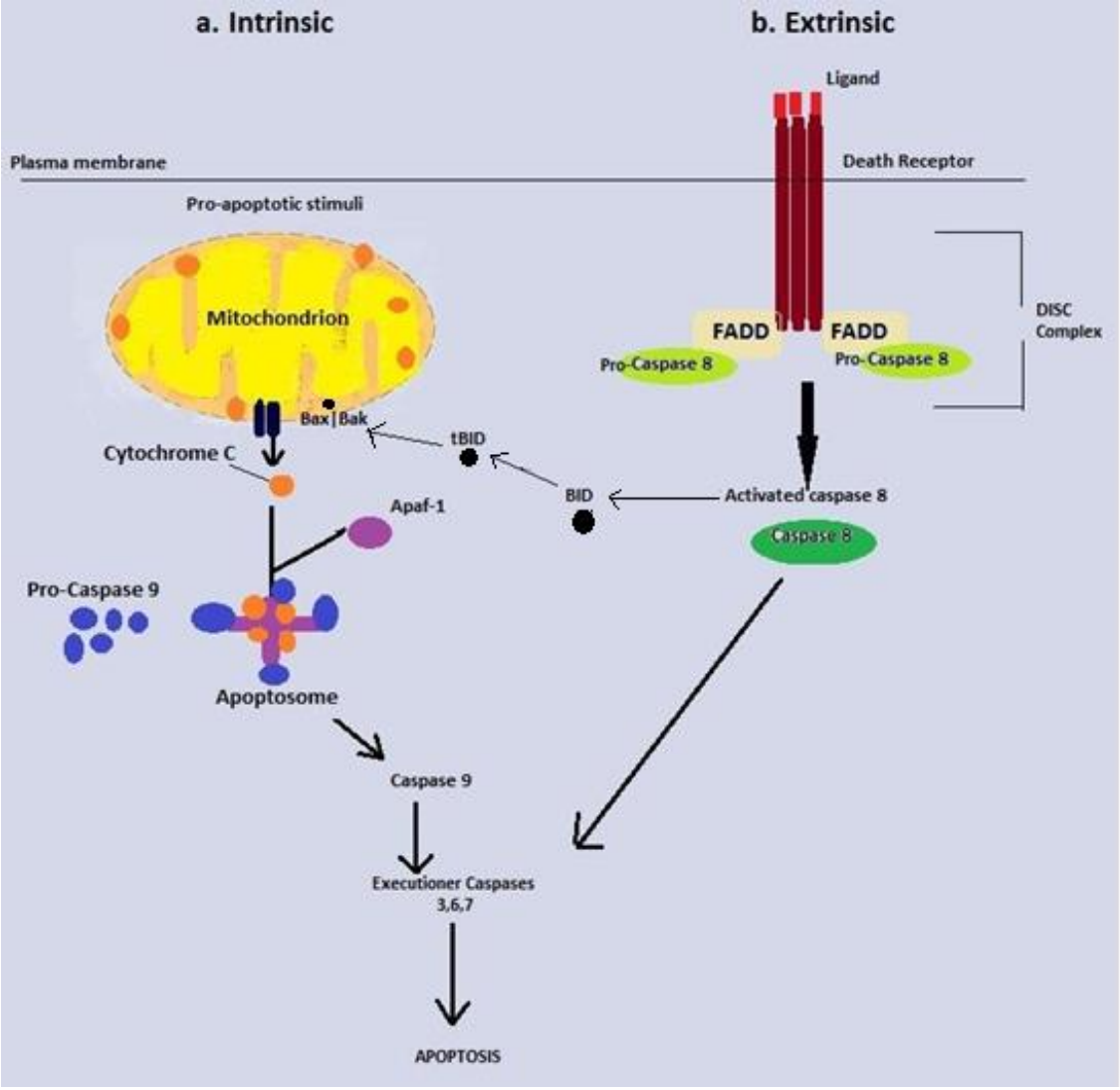

Figure 1.4: An overview of the Intrinsic and Extrinsic pathways of Apoptosis

A. The intrinsic pathway of apoptosis is initiated when Bax/Bak proteins oligomerize within the mitochondria allowing outflux of cytochrome c from mitochondria into the cytosol. Apaf1 and cytochrome c form the apoptosome which recruits and activates procaspase 9 forming caspase 9. Caspase 9 then activates caspases 3 which then activates the caspase cascade and activates apoptosis.
B. The extrinsic pathway involves the binding of a ligand such as Fas onto the Fas death receptor, which leads to the recruitment of FADD to form the DISC complex. The DISC complex then recruits and activates procaspase 8 forming caspase 8. Caspase 8 can either 1) cleave BID forming tBID, tBID then translocates to the mitochondria and initiates the release of cytochrome c thus initiating the execution phase of apoptosis or 2) Caspase 8 can activate caspase 3 which then leads to the activation of the caspase cascade and apoptosis.

1.5. The UPR, Inflammation and Ankylosing Spondylitis

1.5.1. The UPR and Inflammation

Numerous studies have shown cross-talk between the UPR and inflammatory responses with each arm of the UPR having been shown to intersect with inflammatory pathways at various levels. With the PERK branch of the UPR, it has been hypothesised that the inhibition of translation through PERK-eIF2α signalling leads to a disequilibrium in the ratio of short lived IkB (an inhibitor of NF-kB) to longer lived NF-kB which ultimately results in the activation of NF-kB (Deng et. al. 2004). IRE1 is also known to directly phosphorylate IκB in a TRAF2 dependent manner and ATF6, through the kinase Akt is also known to activate NFκB (Janssens et. al. 2014).

The IRE1-JNK arm of the UPR has been shown to mediate the induction of proinflammatory cytokines. These cytokines include IL-1β, IL-8 and GM-CSF which are important in leukocyte activation, proliferation and migration (Oltmanns et. al. 2003). Zha et. al. also recently showed that in myocardial cells infected with Coxsackievirus group B type 3, tunicamycin-induced ER stress induced the proinflammatory cytokines IL-6, IL-12, TNF-α and MCP-1 through with NF-κB interaction with the IRE1 pathway; however, the exact nature of the interaction was not investigated (Zha et. al. 2015). Also recently it was shown by Kim et. al. in RAW 264.7 macrophages that following chemical induction of ER stress, IL-1β and TNF-α gene expression was upregulated. They also noticed that the expression of GSK-3β (which is involved in NF-κB mediated inflammatory pathways) was increased during ER stress responses. Through several other experiments they also found that IRE1α may mediate pro-inflammatory signalling through GSK-3β (Kim et. al. 2015) adding more weight to the hypothesis that states that the UPR activates inflammation. However, there has been limited evidence to support the notion that the UPR activation on its own is enough to trigger the production of inflammatory mediators. True to this statement, the study by Zha et. al. which subjected myocardial cells to tunicamycin treatment in the presence or absence of Coxsackievirus group B type 3, showed that tunicamycin administered to myocardial cells infected with Coxsackievirus group B type 3 resulted in a drastic increase in pro-

inflammatory cytokine expression whereas tunicamycin treatment alone only resulted in a small increase in cytokine expression (Zha et. al. 2015).
Conversely, in the study by Kim et. al. ER stress as a result of tunicamycin or thapsigargin administered to RAW 264.7 macrophages, resulted in a robust increase in the expression of pro-inflammatory cytokines (both mRNA and protein expression), which was inconsistent with findings that UPR activation on its own is not enough to cause robust inflammatory signalling. In an effort to reconcile the Zha et. al. and Kim et. al. studies, the main differences in tunicamycin/ thapsigargin induction of inflammatory mediators can perhaps be attributed to the types of cells used (Zha et. al. used mouse myocardial cells and Kim et. al. mouse RAW 264.7 macrophages) which suggests that perhaps different cells may be more susceptible to inflammatory signalling (Zha et. al. 2015, Kim et. al. 2015). Several studies have demonstrated that the activation of inflammatory mediators is highly cell specific with some cells, like dendritic cells, only producing cytokines (IL-6) at the transcriptional level but not at the protein level in response to tunicamycin induced ER stress (Janssens et. al. 2014). In contrast, in other cells such as MEFs and immortalized B cells, IL-4 and IL-13 signalling was attenuated during tunicamycin-induced ER stress responses (Arensdorf and Rutkowski 2013).

1.6. The UPR and Ankylosing Spondylitis

The UPR has been linked to several inflammatory diseases, including inflammatory bowel disease, rheumatoid arthritis, diabetes and ankylosing spondylitis (AS) (Turner et. al. 2005, Layh-Schmitt et. al. 2013, Janssens et. al. 2014). AS is a chronic inflammatory autoimmune disease mainly affecting the spine and sacroiliac joints, where there is inflammatory back pain and eventual loss of spinal mobility. AS can also present with many extraskeletal manifestations, showing that AS is a disease that affects several different cell types whether directly or indirectly. The extraskeletal manifestations include anterior uveitis, psoriasis, chronic inflammatory bowel disease (Zambrano-Zaragoza et. al. 2013). AS patients also have an increased risk of cardiovascular manifestations such as congestive heart failure and cardiac conduction abnormalities (Ehrenfeld, 2012), and also reduced aerobic capacity (Hsieh

et. al. 2014). The human leukocyte antigen-B27 (HLA-B27), a Major Histocompatibility Complex class I molecule, has been shown to have the strongest association with AS susceptibility through genome wide association studies (GWAS) and other genetic studies (Reveille et. al. 2010, Laval et. al. 2001, Lin et. al. 2011). HLA-B27 has several subtypes which have been associated with AS susceptibility these include HLA-B*2705, B*2702, B*2704 and B*2707 which have been reported to have an association with AS in Europe whereas subtypes such as B*2706 and B*2709 are common in Southeast Asia, but have not been associated with AS (Zambrano-Zaragoza et. al. 2013). HLA-B27 is expressed in more than 90% of AS patients (Huang et. al. 2011), indicating that it has a major role in disease susceptibility, aetiology and pathogenesis; however to date, the exact aetiology and pathogenesis of AS is unknown. Interestingly, only approximately 6% of the world's population that express HLAB27 actually develop AS, and there 5-10% of AS patients who are HLA-B27 negative, which indicates that there must be other factors, both genetic and environmental, that are involved in AS disease susceptibility and pathogenesis (Zambrano- Zaragoza et. al. 2013). To this regard, GWAS studies have identified additional genes associated with AS. For example, Reveille et. al. reported the first GWAS for AS (Reveille et. al. 2010). They used samples from 2,053 AS patients of European descent and 5,140 ethnically matched individuals unaffected by AS. This group identified six independent loci with twenty-five associated SNPs that were significantly associated with AS. These loci corresponded to ERAP1, IL23R, ANTXR2 and IL1R2 genes which, for the most part, are linked to inflammatory signalling (Reveille et. al. 2010, Cui et. al. 2003, Peng et. al. 2010, Chen and Zhang 2015 and Eken et. al. 2013). ERAP1 is function is linked with that of HLA class I molecules. ERAP1 is involved in the trimming of peptides of 9-16 residues in length for MHC class I presentation (Chang et. al. 2005).

A later study by Lin et. al. conducted in Han Chinese individuals (n=1,837 AS individuals and n=4,231 healthy controls) found two additional susceptibility loci whose corresponding genes are associated with cartilage development and new bone formation. These loci were found between EDIL3 and HAPLN1 and ANO6. Along with these genes, Lin et. al. also confirmed that HLA-B had the strongest association to AS susceptibility, which has also been shown by numerous past genetic studies (e.g. Reveille et. al. 2010 and Laval et. al. 2001). Taking all these studies into account, the

MHC (HLA-B27) has the strongest association with AS (Laval et. al. 2001, Lin et. al. 2012, and Reveille et. al. 2010). Subsequently, many studies have focused on HLA-B27 and its possible role in AS pathogenesis. HLAB27 has unique characteristics compared to other MHC class I molecules which include i) a propensity to mis-fold, ii) its catholic peptide specificity and iii) a tendency to form heavy chain homodimers in the ER and on cell surfaces. From this, several hypothesis have been put forward to explain AS aetiology, these are i) presentation of self arthritogenic peptides, which proposes that self-peptides that resemble microbial peptides are presented by folded HLA-B27 and are targeted by autoreactive CD8+ T cells unique to HLA-B27. This leads to cytotoxicity and chronic inflammation (Zambranno-Zaragoza et. al. 2013). ii) Aberrant re-folding of HLAB27 heavy chains at the cell surface, which proposes that HLA-B27 heavy chain homodimers (instead of heterodimers with β_2 macroglobulin) form on cell surfaces. These homodimers then bind to specific receptors on immune cells such as NK cells and T cells (Zambrano-Zaragoza et. al. 2013). However homodimer formation is not exclusive to AS as the HLA-B*2706 subtype which is protective against AS also forms homodimers (Van Gaalen, 2012). iii) Enhanced intracellular microbial survival which is based on the observation that individuals that are positive for HLA-B27 are unable to eradicate some intracellular pathogens including those of the *Yersinia, Chlamydia* and *Shigella* genera. As a result, the immune system becomes abnormally activated leading to exaggerated bacterial multiplication and their postponed clearance. However, though bacteria have been observed in triggering reactive arthritis (Ikawa et. al.1998), an infectious trigger for AS has not yet been demonstrated (Zambrano-Zaragoza et. al. 2013). Iv) HLA-B27 heavy chain mis-folding in the ER (a key hypothesis relating to the work in this thesis), proposes that AS develops, in part, as a result of an accumulation of mis-folded HLA-B27 heavy chain molecules in the ER, which results in activation of the UPR. Activation of UPR signalling pathways eventually leads to inflammation and in AS, chronic inflammation in the spine can lead to the fibrosis and ossification of bone (Janssens et. al. 2014).

Recent studies have mainly focused on the link between AS, inflammation (most genetic susceptibility genes are involved in the inflammatory response) and the UPR. For example, Turner et. al. showed that in macrophages derived from the bone

marrow of HLA-B27 transgenic rats with inflammatory disease, up-regulation of HLA-B27 is associated with the activation of the UPR, as shown by elevated transcripts of UPR associated genes like BiP, CHOP and spliced XBP-1 (Turner et. al. 2005). In a later study, Turner et. al. 2007 showed how up-regulation of misfolded HLA-B27 heavy chains in macrophages correlated with UPR activation; however, in splenocytes treated in the same way, no robust UPR activation was seen (Turner et. al. 2007), suggesting that biologically, HLA-B27 misfolding may have different consequences in different cell types. These findings beg the question: could protein misfolding in different cell types lead to the activation of different ER stress pathways? And could this have implications in disease pathogenesis, since AS is a disease that affects multiple organ systems?

Many studies have demonstrated that the UPR activation induced by the misfolding of HLA-B27 heavy chains leads to the activation of inflammatory signalling. A study by DeLay et. al. conducted in macrophages from the gut of mice showed that HLA-B27 misfolding and subsequent UPR activation leads to the activation and dysregulation of IL-23 signalling (Delay et.al. 2009). Interestingly, IL23 signalling has been shown to enhance the formation of osteoclasts (Chen et. al. 2008) which is of interest because the anatomical areas which are inflamed in AS have been shown to readily respond to IL-23 stimulation (Sherlock et. al. 2012). These studies highlight several questions. For example what UPR pathways are mainly involved in the activation of inflammatory signals like IL-23, when are they activated and are these pathways activated in all cell types? This is of particular importance with regards to IL-23 as recent studies have implicated IL-23 in AS pathogenesis, with a study by Appel et. al. observing IL-23 positive cells in fibrous tissue and subchondral bone marrow of chronic AS patients (Appel et.al. 2013). More importantly, a recent study by Milanez et. al. found that current AS therapies including anti-TNFα do not influence the IL-23/IL-17 pathway as IL-23 levels were elevated even after long term anti-TNFα therapy. This may account for an anti-TNFα treatment not being able to reduce radiological AS progression (Milanez et. al. 2016). This highlights the need for new therapeutic targets that reduce IL-23 levels.

1.7. The UPR can be activated by chemical inducers

As mentioned throughout section 1, the UPR can be activated by chemical inducers, which disrupt specific functions of the ER. These chemical inducers include tunicamycin, DTT and thapsigargin and their structures are depicted in Figure 1.5.

1.7.1. Tunicamycin

During the folding of nascent polypeptide chains, glucose is required for N-liked glycosylation, which prevents protein misfolding and aggregation, and promotes chaperone binding. Tunicamycin is a family of bacterial nucleoside antibiotic homologues that hinder the glycosylation of proteins by inhibiting the transfer of GlcNAc-1-phosphate from UDP-acetylglucosamine to dolichol phosphate through the inhibition of the enzyme UDP-GlcNAc dolichol phosphate-GlcNAc-1phosphaletransferase (Duskin and Mahoney 1982). This inhibition of protein glycosylation causes the misfolding of newly synthesised proteins (Merksamer et. al. 2008), and prevents chaperones such as CXN/CRT from binding and assisting in folding, thus promoting glycoprotein aggregation and misfolding, leading to the activation of the UPR stress signalling responses (Calfon et. al. 2002).

1.7.2. Thapsigargin

As well as being important in protein folding, the ER is also the key intracellular calcium store. There are several calcium dependent chaperones (e.g. calnexin and calreticulin) within the ER, so when ER calcium homeostasis is disrupted, these proteins lose their chaperone activity. Nascent proteins are not folded and thus unfolded/misfolded proteins accumulate within the ER, leading to the activation of UPR stress signalling (Oslowski and Urano 2011). Thapsigargin, a lactone derived from the *Thapsia gaganica* plant, is a specific inhibitor of sarcoplasmic/ER calcium transport ATPase (SERCA). Inhibition of SERCA leads to calcium depletion in the ER and the onset of the UPR (Inesi and Sagara 1992).

1.7.3. DTT

The ER maintains an oxidising environment, which is favourable for the formation of disulphide bonds that act to stabilise the folding and assembly of proteins. DTT is a cell permeable reducing agent that reduces disulphide bonds causing the unfolding of proteins which leads to activation of the UPR stress signalling responses (Merksamer et. al. 2008).

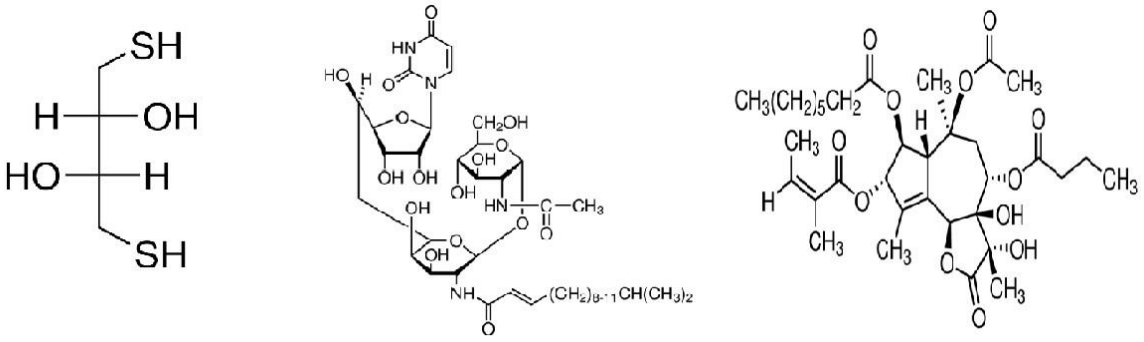

Figure 1.5: The structure of three chemical inducers of the UPR:

DTT, Tunicamycin and Thapsigargin

1.8. Aims of project

The UPR has been linked to the pathogenesis of many diseases, including AS. In AS, the MHC class I HLA-B27 heavy chain has a tendency to mis-fold, which can activate the UPR. However it is not known how mis-folding events lead to differing responses between different cell types. In this study, tunicamycin and DTT were used to induce and study ER stress in two different cell lines, HeLa and HT1080, which were previously shown by the laboratory to have differential sensitivity to ER protein misfolding (Lemin and Benham, unpublished observations). The findings from this study can be taken forward into HLA-B27 expressing antigen presenting cells and translated into AS disease models.

- The main objectives of this thesis were:
    - To study the UPR using different pharmacological agents to induce ER stress responses in different cell types.
    - To explore differences between cell types in acute and chronic ER stress in terms of responses to UPR activation from distinct ER stressors.
    - To use novel imaging techniques to study the behaviour of cells under ER stress.
    - To explore UPR activation and inflammation by examining the effect of genistein, a tyrosine kinase inhibitor, on UPR induction.

2. Methods and Materials

2.1. Cell lines and Tissues

HeLa human cervical cancer cells were maintained in MEM, minimum nonessential medium (22561-021; Gibco, Invitrogen) and HT1080 human fibrosarcoma cells were maintained in D-MEM, Dulbecco's Modified Eagle's Medium (21063-029; Gibco, Invitrogen). Both cell lines were supplemented with 8% fetal calf serum (10106151; Sigma-Aldrich), 2 mM Glutamax (A122860-01 Invitrogen), 100 units ml^{-1} penicillin and 100µg ml^{-1} streptomycin (15140-122; Invitrogen). The cells were kept at 37°C at 5% CO_2 and passaged every 3-4 days when they reached approximately 70% confluence. To passage cells, spent medium was aspirated off and cells were washed twice with phosphate buffered saline (PBS) without calcium and magnesium and trypsinised with 1ml of 1x trypsin-EDTA (Invitrogen) at 37°C for 1-2 minutes or until cells had detached from the surface of the petri dish. The cells were then re-suspended in 10ml of fresh medium and 1ml of this suspension was plated into 9ml of fresh medium. Cells were then left in the incubator at 37°C at 5% CO_2 to adhere and grow.

2.2. Antibodies

Antibody information including dilutions, antibody specificity and supplier information can be found in table 2.1.

Table 2:1. Antibody information including dilutions for Western blot and Immunofluorescence

Antibody name	Antibody specificity	Dilution	Supplier information
HC10 (mAb)	MHC class I B and C	1:200	J. Neefjes, Netherlands Cancer institute
Anti-PDI (pAb)	PDI as described by Benham et al. 2000	1:1000 (WB), 1:400 (IF)	A Benham
Anti-β-Actin (mAb)	Beta Actin	1:1000 (WB)	Mabacam 88224, Abcam
Anti-JNK (pAb)	SAPK/JNK	1:1000 (WB)	#9252, Cell signal
Anti-P-JNK (pAb)	SAPK/Phospho-JNK Thr 183/Tyr185	1:1000 (WB)	#4671, Cell signal
Anti-ASK1 (pAb)	ASK1	1:1000 (WB)	#8662, Cell signal
Anti-P-ASK1 (pAb)	Detects ASK1 phosphorylated only at threonine 845.	1:1000 (WB)	#3765, Cell signal
Anti-PERK (mAb)	PERK	1:1000 (WB)	#3192, Cell signal
Anti-Phospho-tyrosine-100 (pAb)	wide range of phosphopeptides	1:1000-1:2000 (WB)	#9411, Cell signal
Anti-LC3B (pAb)	LC3-B	1-500-1:1000 (WB), 1:400 (IF)	#2775, Cell signal
Anti-STAT3 (pAb)	STAT3	1:1000 (WB)	#9132, Cell signal
Anti-Phospho-STAT3	Phospho-STAT3 (Tyr705)	1:1000 (WB)	#9131, Cell signal

2.3. Dyes

ER Tracker™ Blue-White DPX (E-12355, Life Technologies), ER Tracker™ Green (BODIPY FL Glibenclamide) (E34251, Life Technologies) and LysoTracker Deep Red (L12492, Life Technologies) are all available commercially.

Table 2.2. ERTracker and LysoTracker dye dilutions for live cell imaging analysis

Dye	**Dilution**
ER Tracker™ Blue-White DPX	1:1000-1:2000
ER Tracker™ Green (BODIPY FL Glibenclamide)	1:1000
LysoTracker Deep Red	1:5000

2.4. Cell Treatments

Confluent HT1080 and HeLa cells were passaged into 6cm dishes at an appropriate dilution and left to grow at 37^{o}C at 5% CO_2 until they were confluent. Confluent cells were then treated with chemical inducers of the UPR; these were 1 µg/ml tunicamycin and 5 mM DTT (Sigma Aldrich) at the times specified in later sections. Cells were also treated with 140 µg/ml genistein at the specified times in later sections. Following treatment, cells were washed twice in PBS and were either, dispersed into the appropriate lysis buffer either MNT or RIPA lysis buffer for protein analysis (section 2.5-2.7), prepared for immunofluorescence (section 2.8) or prepared for live cell imaging (section 2.9).

2.5. Cell lysis

Post treatment of cells with either vehicle control or specific UPR inducers, cells were lysed for protein analysis by SDS-PAGE. Cells were lysed at 4^{o}C in either 300 µl MNT (1% v/v Triton X-100, 30 mM Tris-HCL, 100 mM NaCl, pH 7.4), supplemented with protease inhibitors antipain, chymostatin, leupeptin and pepstatin A (Sigma Aldrich) 20 mM N-ethylamleimide (NEM) (Sigma-Aldrich) and phosSTOP (which inhibits acid, alkaline, serine/threonine, tyrosine and dualspecificity phosphatases) (Roche) or 300 µl RIPA lysis buffer (1% v/v Triton X-100, 50 mM Tris HCl pH8, 150 mM NaCl, 0.5% w/v Na-deoxycholate, 0.1% w/v SDS) supplemented with protease inhibitors antipain, chymostatin, leupeptin and pepstatin A (Sigma Aldrich) 20 mM N-ethylamleimide (NEM) (Sigma-Aldrich) and phosSTOP (Roche). Cells were then scraped off the surface of the dish on ice and transferred to Eppendorf tubes, which were incubated on ice for 10 minutes. Cells were subsequently vortexed and then centrifuged for 10 minutes at 4^{o}C at 14100 rpm. Once spun, the supernatant was removed and transferred to a fresh Eppendorf tube and the pellet discarded. The lysates were then snap frozen and kept at -20^{o}C. Protein quantification was determined using the bicinchoninic acid protein assay (BCA) (#23227; Thermo Scientific). Cell samples were incubated with BCA working reagent for 30 minutes at 37^{o}C and then a spectrophotometer set at 562 nm was used to measure absorbance. From this protein concentration was determined.

2.6. SDS-PAGE

Lysates were prepared for SDS-PAGE separation by mixing them with 2x Laemmli loading buffer (1 M Tris pH 6.8, 20% (w/v) SDS, 5% (v/v) glycerol, 0.01% (w/v) bromophenol blue) with the addition or absence of 50 mM DTT (Sigma-Aldrich) to break down disulphide bonds. The samples were then boiled at 95^{o}C for 5 minutes and spun down in a centrifuge for 1 min at 16100g. Gels were cast using Hoeffer casting apparatus. The resolving gel and stacking gels were made up of variable quantities for variable gel percentages using the following reagents to make a 12% (used for LC3-B analysis via western blotting) or 10% (for all other antibodies tested)

resolving gel and a 5% stacking gel. The resolving gel (v/v) was made up from: 40% acrylamide (Sigma-Aldrich), 1.5M Tris pH 8.8 (Sigma-Aldrich), 10% (w/v) SDS (Sigma-Aldrich), 10% ammonium persulfate (APS) (Sigma-Aldrich) and (v/v) N,N,N,N-Tetramethylethylenediamine (TEMED) (Sigma-Aldrich) and left to polymerise for approximately 40 mins with a layer of distilled water on top of the resolving gel layer to prevent drying out. The stacking gel (v/v) was made up from, 40% (v/v) acrylamide, 1M Tris pH 6.8, 10% (w/v) SDS, 10% (w/v) APS and TEMED. A comb was placed on top of the stacking gel and the gel was left to polymerise for approximately 20 mins. Once the gels were set, they were run for ~50 minutes at 40 mA in 1x Tris-glycine SDS buffer (SigmaAldrich). The protein marker used was the All Blue Precision Plus protein standard (250-10 kD) (#161-0373, BioRad), which consisted of ten proteins of the following sizes; 250 kDa, 150 kDa, 100 kDa, 75 kDa, 50 kDa, 37 kDa, 25 kDa, 20 kDa, 15 kDa and 10 kDa.

2.7. Western Blotting

PVDF membranes (Millipore) were primed in methanol for approximately 30-40 seconds and transferred to transfer buffer (190 mM glycine, 25 mM Tris and 20% (v/v) methanol). Wet transfer of gels was then performed in 1x transfer buffer for 2 hours at 150 mAs. Following transfer, the membranes were blocked in either 5% (w/v) milk in TBS-T (0.1% Tween, 150 mM NaCl, 2.68 mM KCl and 10 mM Tris-base) or 5% (w/v) BSA (bovine serum albumin) in TBS-T overnight or for 60 minutes on a shaker. Following blocking, membranes were washed in TBS-T 3x for 5 minutes each and then incubated with desired primary antibody at the desired dilution (see Table 2.1). Antibodies were diluted in 5% (w/v) milk dissolved in TBST or 5% (w/v) BSA (A9418; Sigma-Aldrich) in TBS-T for 60 mins or overnight at 4^{o}C depending on the suggested primary antibody protocol. Membranes were then washed in TBS-T 5 times for 5 minutes each. Following washing, membranes were incubated with the corresponding secondary horseradish peroxidase antibody at 1:3000 in 5% (w/v) milk in TBS-T for 45-60 minutes. After antibody incubation, membranes were washed 5 times for 5 minutes each with TBS-T. Enhanced Chemiluminescence fluid (Amersham) was then used to visualise proteins. The membrane was incubated with the solution at room temperature for approximately 1 minute and subsequently drained off. The

membranes were then wrapped in saran wrap to prevent them from drying and luminescent stickers were placed onto saran wrap to assist in the interpretation of the exposure. The membranes were then exposed to film (Kodak) at different exposure times depending on protein of interest. Once exposed, the film was then developed using an X-ray developer machine.

2.8. Immunofluorescence

HT1080 and HeLa cells were grown on sterile coverslips (VWR) in 6cm dishes at appropriate dilution until cells reached 70% confluence. Cells were then washed twice in PBS supplemented with calcium and magnesium ions (PBS++) (Invitrogen) and cells were then fixed onto coverslips using 4% (v/v) paraformaldehyde (VWR) at room temperature for 10 minutes or in 100% ice cold methanol at -20^{o}C for 15 minutes. The cells were then placed in 0.1% (v/v) Triton X100 (T8787; SigmaAldrich) for 5 minutes at room temperature to permeabilize membranes. PBS ++ was then used to wash coverslips. Following this step, each coverslip was blocked in 0.2% (w/v) Bovine serum albumin (BSA) (Sigma-Aldrich) at room temperature for 30-60 minutes and each of the coverslips was washed in PBS ++ once. Coverslips with cells were then incubated with the desired antibody at the appropriate concentration (0.2% (w/v) BSA in 1X PBS or 1X PBS / 1% BSA / 0.3% Triton X-100) at room temperature for 45 minutes at room temperature or overnight at 4^{o}C . Coverslips were then washed to remove excess primary antibody and then were incubated for 30-60 minutes with secondary antibodies which were either swine anti-rabbit Alexa Fluor 488 of 594 (Invitrogen) or donkey anti-mouse Alexa Fluor 488 or 594 (Invitrogen) diluted in 0.2% (w/v) BSA in PBS or 1X PBS / 1% BSA / 0.3% Triton X-100. Coverslips were then washed in PBS and stained with 1x DAPI for 5 minutes in a dark chamber and a final wash with PBS was performed. Finally, hard-setting Vectashield (Vector Laboratories) was used to mount coverslips onto glass slides and after drying, cells were analysed using either Zeiss Axiovert 200M Apotome or the Zeiss LSM 510 META Laser Scanning Confocal Microscope.

2.9. Live cell imaging

For live cell imaging, HT1080 and HeLa cells were grown to 70% confluence in 2cm glass bottomed dishes. Once confluent, cells were washed twice in 1X PBS and fresh medium was added. To the fresh medium, ERTracker™ Blue-White DPX (E12355, Life Technologies) or ER Tracker™ Green (BODIPY FL Glibenclamide) (E34251, Life Technologies) and LysoTracker Deep Red (L12492, Life Technologies) were added together at the specified dilutions listed in Table 2.2. Cells were initially incubated with the dyes for approximately 90 minutes before imaging. Cells were then treated with ER stress inducers (1µg/ml tunicamycin or 5 mM DTT) and images were taken at specific time intervals for a period of 18 hours using the Andor Revolution XD, Spinning Disc Confocal Laser Microscope, Leica SP5 Confocal Laser Scanning Microscope SMD or the Zeiss Cell Observer. While capturing images, cells were maintained at 37^{o}C and at 5% CO_2 and 95% humidity. Images and videos obtained from live cell imaging were analysed using ImageJ software.

2.10. Statistical Analysis

The student t-test was used for statistical analysis along with a P value of <0.05 to signify statistical significance.

3. The Effects of Tunicamycin Induced Endoplasmic Reticulum Stress on the Induction of Cell Survival Pathways in Two Different Human Cell Lines

3.1. Introduction

The mechanisms utilised by different cell types to cope with acute and chronic ER stress from morphological changes to molecular changes will be investigated, to garner information on whether these responses are the same or if they differ in different cell types, in the hopes of identifying therapeutic targets.

As mentioned previously in section 1.1, the structure of the ER is very dynamic in that the sheets and tubules that form the ER are continuously being formed and remodelled while remaining continuous (Westrate et. al. 2015, Shibata e.t al. 2006, Schuck et. al. 2009). A study by Schuck et. al. conducted in the yeast *Saccharomyces cerevisiae* showed that during DTT and tunicamycin induced ER stress, the formation of cisternal sheets was increased (there was a higher luminal volume to surface area ratio compared to tubules), which ultimately contributed to (along with the activation of lipid biosynthesis genes) the expansion of ER membranes. This expansion of the ER membrane was able to mitigate ER stress independently of the upregulation of chaperones. This response was postulated to be a result of a larger ER lumen which was able to accommodate more misfolded proteins which thereby encouraged their folding due to a decrease in aggregation potential (Schuck et. al. 2009). It would be interesting to see whether this response also occurs in human cells exposed to ER stress.

At a molecular level, in the event of unabated ER stress, cells can activate either cell survival (autophagy) or cell death pathways (apoptosis), which can be activated mainly through PERK/AFT4 and IRE1α/JNK pathways (section 1.4). The activation of these two UPR branches has been shown to potentiate crucial modulators of the autophagy and apoptosis pathways, including, LC3B and Caspase 9 (section 1.3) respectively. The expression, activation and cleavage of LC3B is dependent on different branches of the UPR in different cell types in response to the same stimuli

(Milani et.al. 2009, Tanaka et. al. 2012). For example, Milani et. al. showed LC3B activation to be dependent on ATF4 in MCF7 and MDA MB 231 cells in response to severe hypoxia (Milani et. al. 2009). However, Tanaka et. al. showed JNK to regulate the induction of LC3B activation in lung epithelial cells again in response to hypoxia (Tanaka et. al. 2012) which could have implications in therapy. It would be interesting to observe any further differences in autophagy activation, particularly the time of autophagy activation and when pro-apoptotic pathways are initiated in different cell types.

3.2. Results

3.2.1. Imaging changes to the morphology of the endoplasmic reticulum in response to chemically induced ER stress using fluorescent dyes

To visualise the dynamic morphological changes which may have occurred in response to ER stress induction within the ER, imaging experiments were conducted on live HT1080 and HeLa cells stained with fluorescent dyes.

To optimise live cell imaging conditions, ER staining dyes and microscope conditions were varied. The two dyes used were ERTracker blue/white and ERTracker green (BODIPY Glibenclamide; both Invitrogen ThermoFisher) that are highly selective for the ER (Section 2.3, table 2.2). These dyes stain the ER through different mechanisms. The ERTracker green dye (which has an excitation/emission spectrum of 504/511 is conjugated to the drug Glibenclamide, which binds to the sulphonylurea receptors that comprise part of the ATP sensitive K+ channels located within the ER (Hambrock et. al. 2002). In contrast, ERTracker blue/white (which has an excitation/emission spectrum of ~374/430-640) does not bind to sulphonylurea receptors but is highly selective for the ER lipid membrane environment (Cole et. al. 2000).

To investigate the uptake and specificity of the two ER trackers in our system, HeLa (not show) and HT1080 cells were incubated with the ERTracker blue/white (1:1000 dilution) and ERTracker green (1:1000) dyes and subjected to live cell imaging for 0-100 minutes. As shown in Figure 3.1A, both the dyes stained the perinuclear area directly around the nucleus (black space surrounded by staining) that corresponds to the ER with little to no background staining, particularly in cells stained with ERTracker blue. HT1080 cells stained with ERTracker green in medium (rather than PBS) showed a

noticeably high background compared to ERTracker blue/white stained cells. In contrast HT1080 cells stained with ERTracker green but incubated in PBS (rather than medium) showed little to no background (figure 3.1A). This suggested that because PBS incubation dramatically reduced the background fluorescence, the combination of ERTracker green and medium components caused an increase background fluorescence. However, because incubating cells in PBS for extended periods of time is not compatible with cell viability, in subsequent experiments, cells to be stained with ERTracker green were stained and incubated in medium rather than PBS and microscope settings were adjusted.

To determine the time of dye take up that would give optimal imaging conditions, HT1080 and HeLa cells were initially incubated in ERTracker green dye for 30 mins prior to imaging and the optimal dye take up was determined by measuring fluorescence intensity at 30, 40, 60, 80 and 100 mins for each cell line (Figure 3.1B). The fluorescence intensity was highest at 40 mins and 60 mins for HT1080 and HeLa cells which lead to the conclusion that the different cells had different rates of dye uptake, so subsequent experiments were conducted under these conditions i.e. HT1080 cells were incubated for 40 mins and HeLa cells for 60 mins (figure 3.1B).

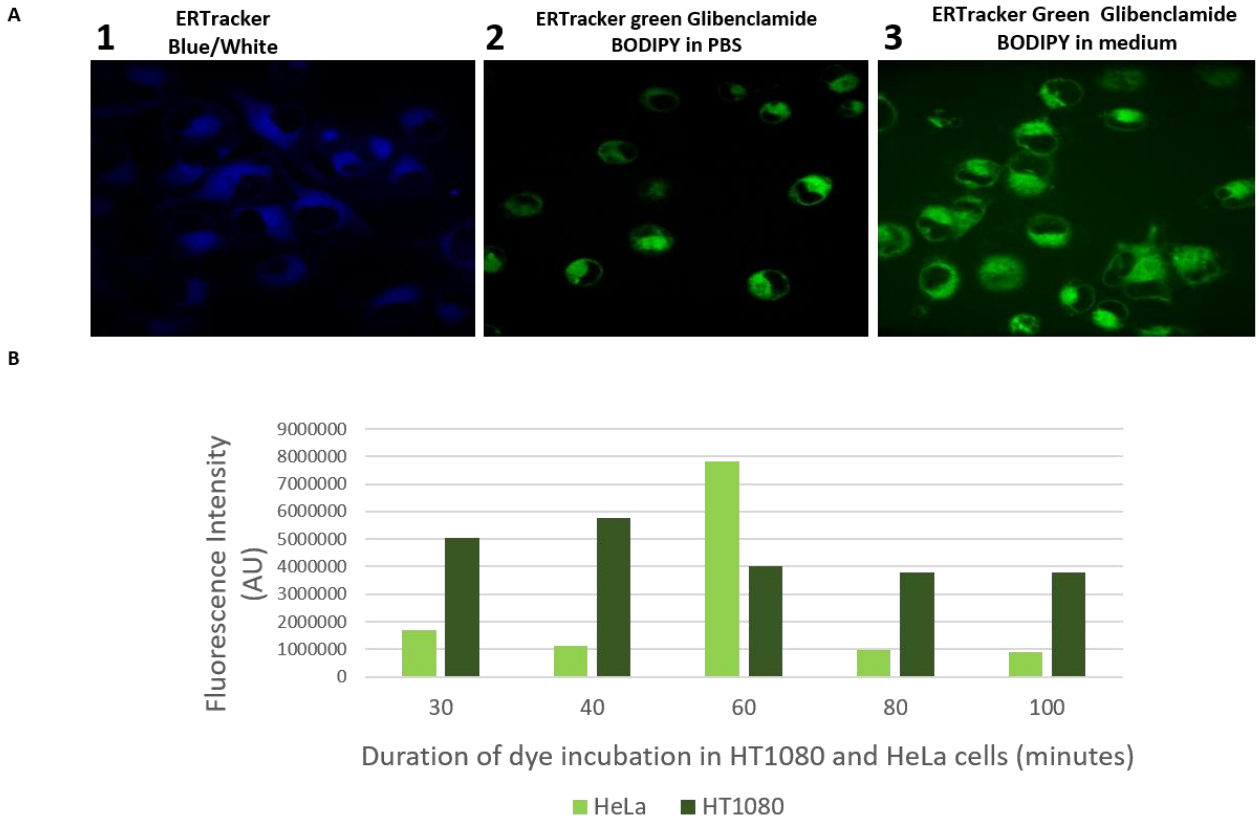

Figure 3.1 Optimisation of dye uptake in HT1080 and HeLa cells

A. HT1080 cells were incubated for 30 minutes in either ERTracker blue/white in DMEM medium (left panel), ERTracker Glibenclamide green in PBS (middle panel) and ERTracker Glibenclamide green in DMEM medium (right panel).The panels show the appearance of the ER at 20 mins. Both dyes showed specificity for ER. ERTracker blue/white in medium and ERTracker green in PBS showed no background however ERTracker green dye in medium showed background fluorescence.
B. HT1080 and HeLa cells were incubated for 30, 40, 60, 80 and 100 minutes with ERTracker Glibenclamide green in DMEM medium. The fluorescence intensity of the ER was highest at 60 mins in HeLa cells and 40 mins in HT1080 indicating that optimal dye take up occurs at these times. In the fluorescence intensity calculations, background readings were subtracted from cell fluorescence.

Live cell imaging of living cells facilitates in the study of real-time dynamic processes from single molecules, to cells and even tissues. With many advances in microscopy, gaining insight into the many dynamic cellular processes that are occurring within live cells depends largely on the methodology (a combination of i) the fluorescent dyes that are used, ii) maintenance of cell health and iii) the microscope used) so with this mind, microscope conditions were also optimised (Brown, 2014, Salipalli et. al. 2014).

Firstly, HT1080 cells were mock, DTT and tunicamycin treated for 90 mins and incubated with 1:1000 ER tracker Blue/white for 90 mins prior to imaging. Live stained cells were imaged on the Zeiss Cell Observer microscope under 5% CO_2 and 37^{o}C (figure 3.2). The resolution of images obtained from this experiment were poor due to number of factors including the plastic petri dishes used and the microscope resolution. These limitations restricted observation of the fine detail of the ER. Nevertheless, the ER was specifically stained and no gross differences were seen in ER morphology between mock, DTT and tunicamycin treated cells, with all treatment groups showing ER blebbing to some extent, as most clearly seen in the close-up of the x40 magnification of the tunicamycin treated cells (figure 3.2D). Because of the poor resolution of these images, even after switching from plastic petri dishes to glass bottom dishes, the Leica SP5 Confocal Laser Scanning Microscope SMD was used in the next set of experiments. However, though this microscope had better resolution compared to the former, this particular microscope was not compatible with the experimental set-up as image capture time was too slow (approximately 5 mins) (data not shown). Thus the experiment was repeated using an Andor Revolution XD Spinning Disc Confocal Microscope (data not shown). This microscope (which was designed specifically for live cell imaging) was compatible with the experimental set-up and could capture images at a much faster rate when compared to the Leica SP5 CLSM without affecting image quality. So in subsequent experiments, the Andor spinning disk confocal microscope was used.

3.2.1.1. High laser power and ERTracker green conditions lead to decreased cell viability

Following optimisation, a study into how HeLa cells ER morphology changes with ER stress was conducted (figure 3.3). HeLa cells were labelled with ERTracker green, treated with either DMSO vehicle control or tunicamycin and imaged for 18 hrs.

In tunicamycin treated HeLa cells, at 1 hr, the ER morphology varied between cells, from an elongated appearance to a round perinuclear appearance which was similar to the vehicle control (figure 3.3A, panels 1 and 5). The different ER morphologies seen in these experiments may reflect differences in cell movement and polarisation; in some cases cells have moved out of the plane of focus (figure 3.3A, panels 1, 2 and 5, F). The ER also exhibited structures that appear to be either tubules or sheets, whose sizes increased (e.g. between 1 hrs to 2 hrs; see figure 3.3A, panel 5-6, arrows) and whose structure became more defined as exposure to tunicamycin continued. These structures were not seen to the same extent in the ER of vehicle control cells. By 4 hrs of tunicamycin treatment, some tubular/sheet structures were more defined and moved with time reflecting the dynamic nature of the ER (figure 3.3B panel 7-14, box). However, the overall structure of the ER remained consistent. By 12 hrs, cells had begun to round up, bleb and detach from the dish (arrows, figure 3.3C, panels 18-20) up until 18 hrs (figure 3.3D, panel 4), when 80% of the cells within the field of view showed these characteristics. Unexpectedly, the ER morphology of vehicle control cells showed similarities to the tunicamycin treated cells. By 4 hrs, tubules/sheets became visible and increased in size (figure 3.3A-B, panel 2-10, boxes).

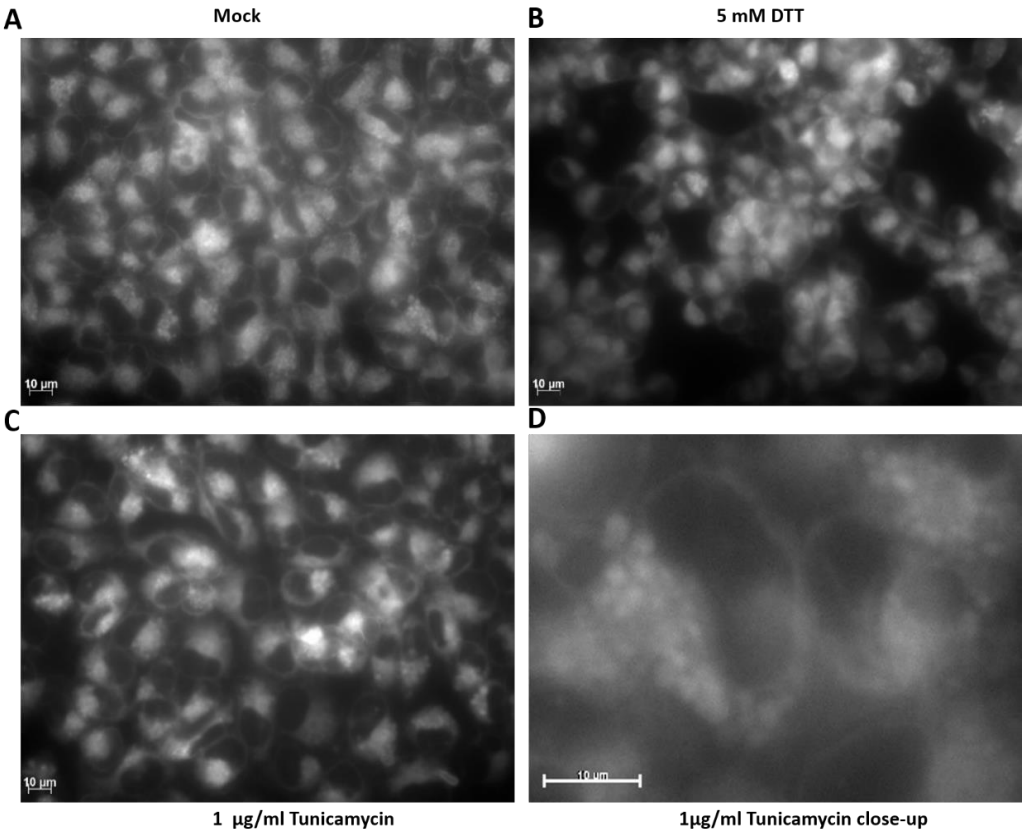

Figure 3.2: Imaging ER labelled cells using the Ziess Cell Observer microscope

HT10080 cells were mock treated, treated with 5mM DTT (panels: A and B) or treated with 1 ug/ml tunicamycin (Tun; panels: C and D) for 1.5 hrs prior to imaging on the Ziess Cell Observer microscope. Although resolution using this microscope was poor, all cells showed characteristic ER staining and the tunicamycin treatment resulted in blebbing which can be seen more clearly in the Tun close-up (panel D).

By 9hrs, control cells had begun contracting, detaching and blebbing (as indicated by arrows, figure 3.3C from panel 17) and by 18 hrs most cells in the field of view showed characteristics similar to those of cells having undergone cell death compared to 0 hrs treatment (Figure 3.3D, panel 1-2) . This was unexpected as DMSO at these low concentrations was not expected to cause cell death.

Investigations were then undertaken to unveil the cause of the cell death. Temperature and $C0_2$ conditions remained constant throughout the experiments. Laser settings were then investigated. It was found that the laser adversely affected cell viability. Re-setting of the laser power allowed imaging of cells at lower exposures i.e. from 2500 ms to 60 ms meaning cells were exposed to less laser power which significantly increased cell viability. However at these lower laser power settings, it was discovered that imaging ER staining with ERTracker green in combination with DMEM/MEM medium at low laser power produced significant background so subsequent experiments were conducted using ERTracker blue/white (data not shown).

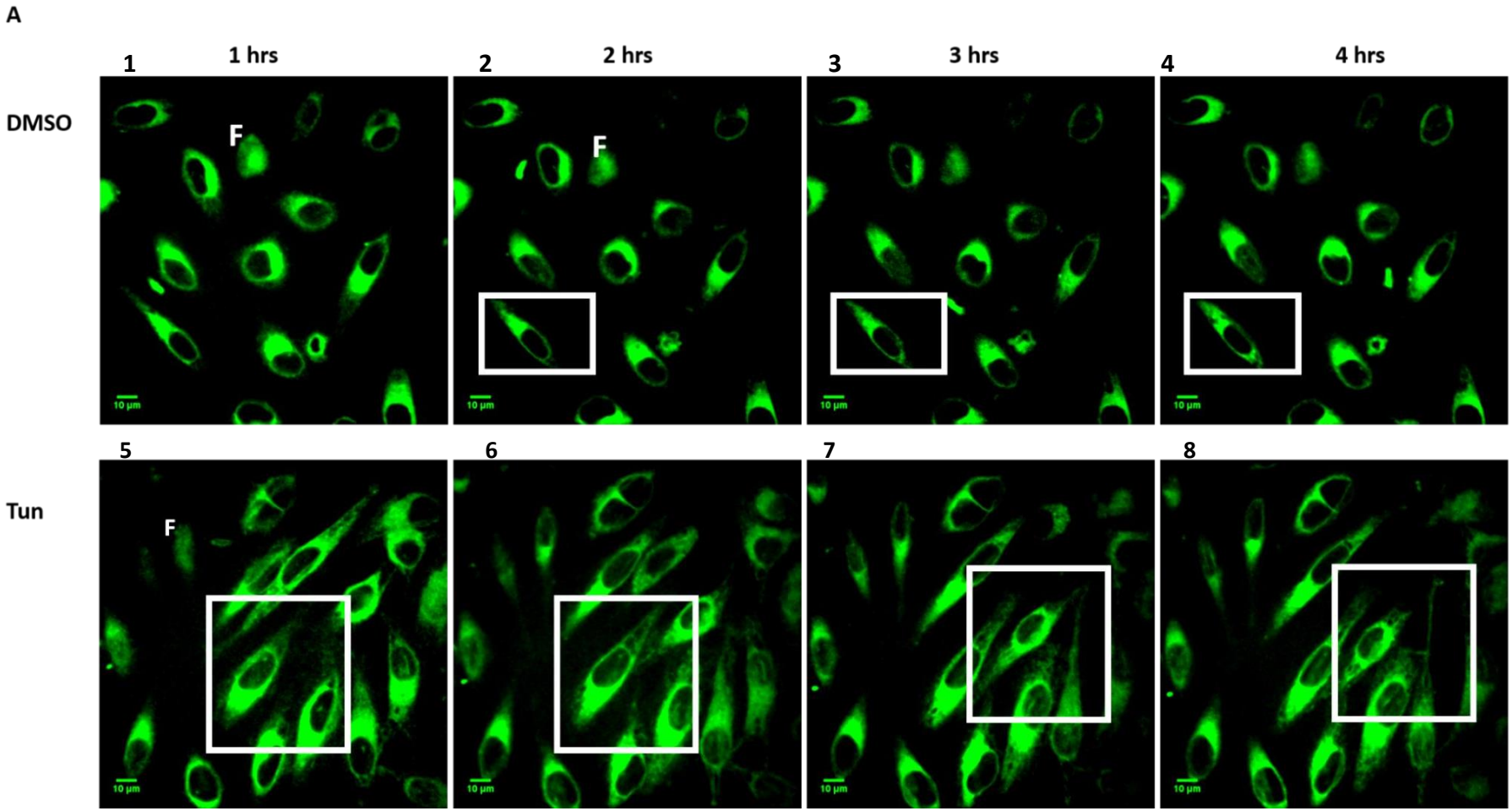
A
1
1 hrs
2
2 hrs
3
3 hrs
4
4 hrs
DMSO
F
F
5
6
7
8
Tun
F
10 µm

B

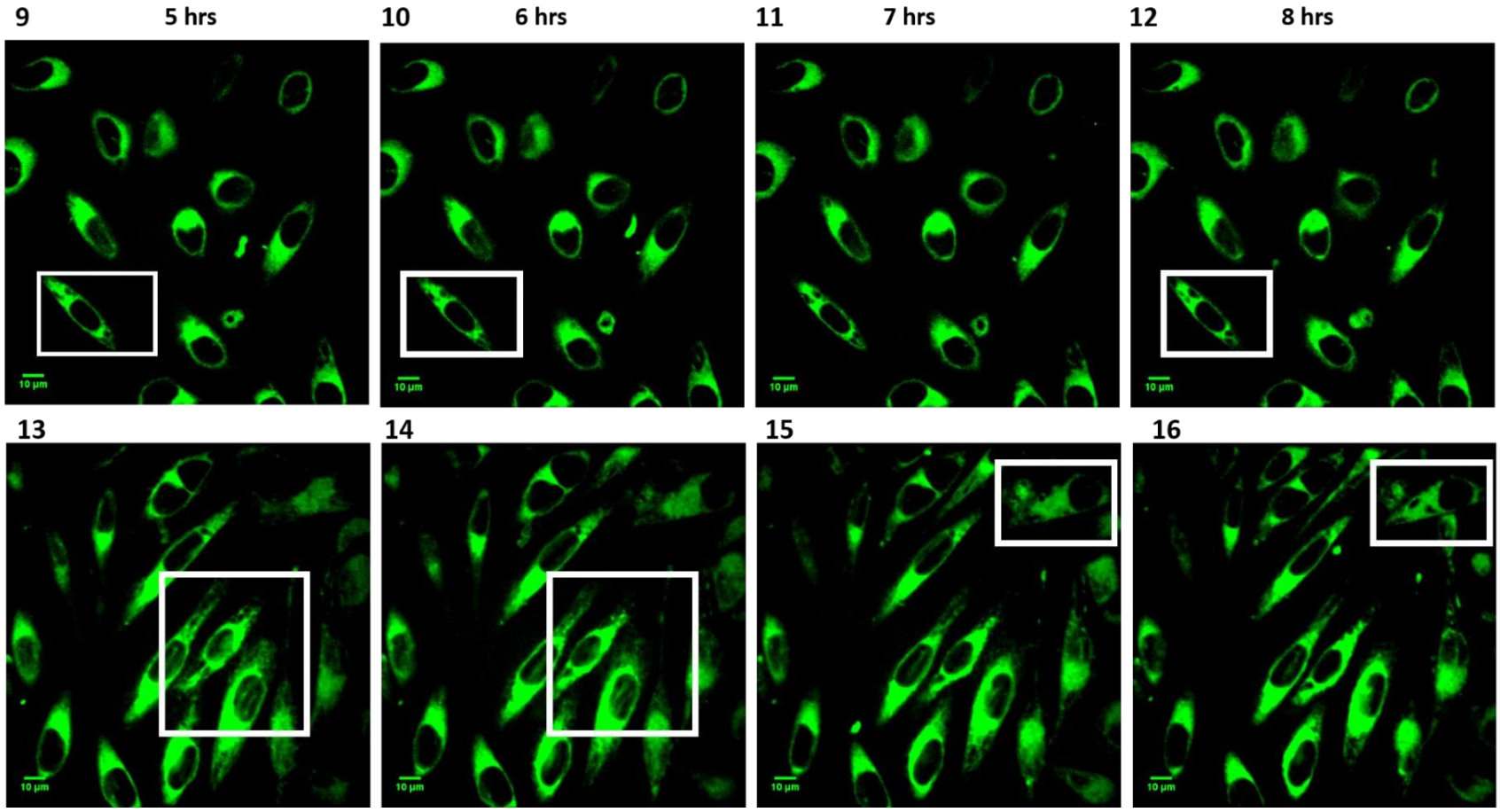

C

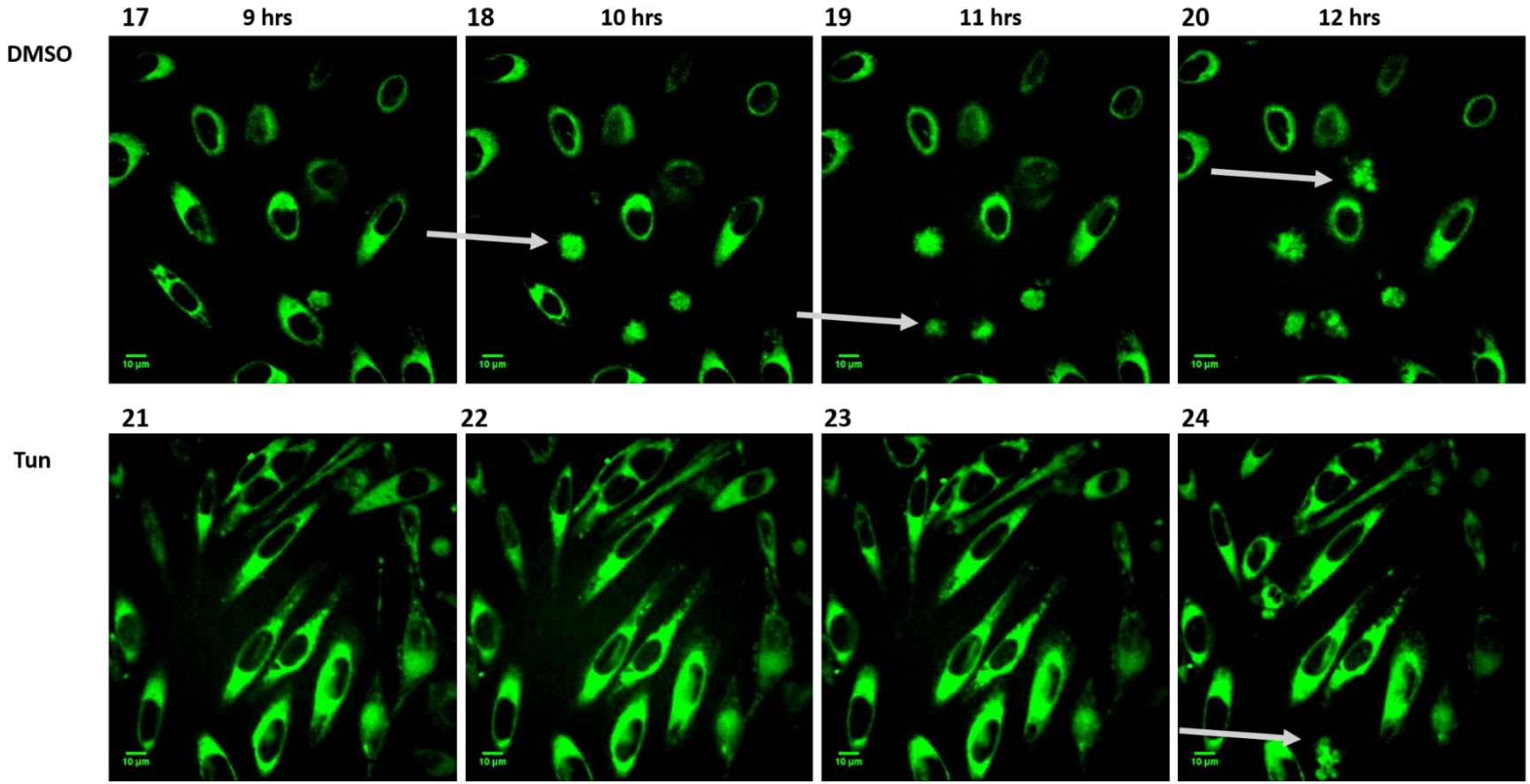

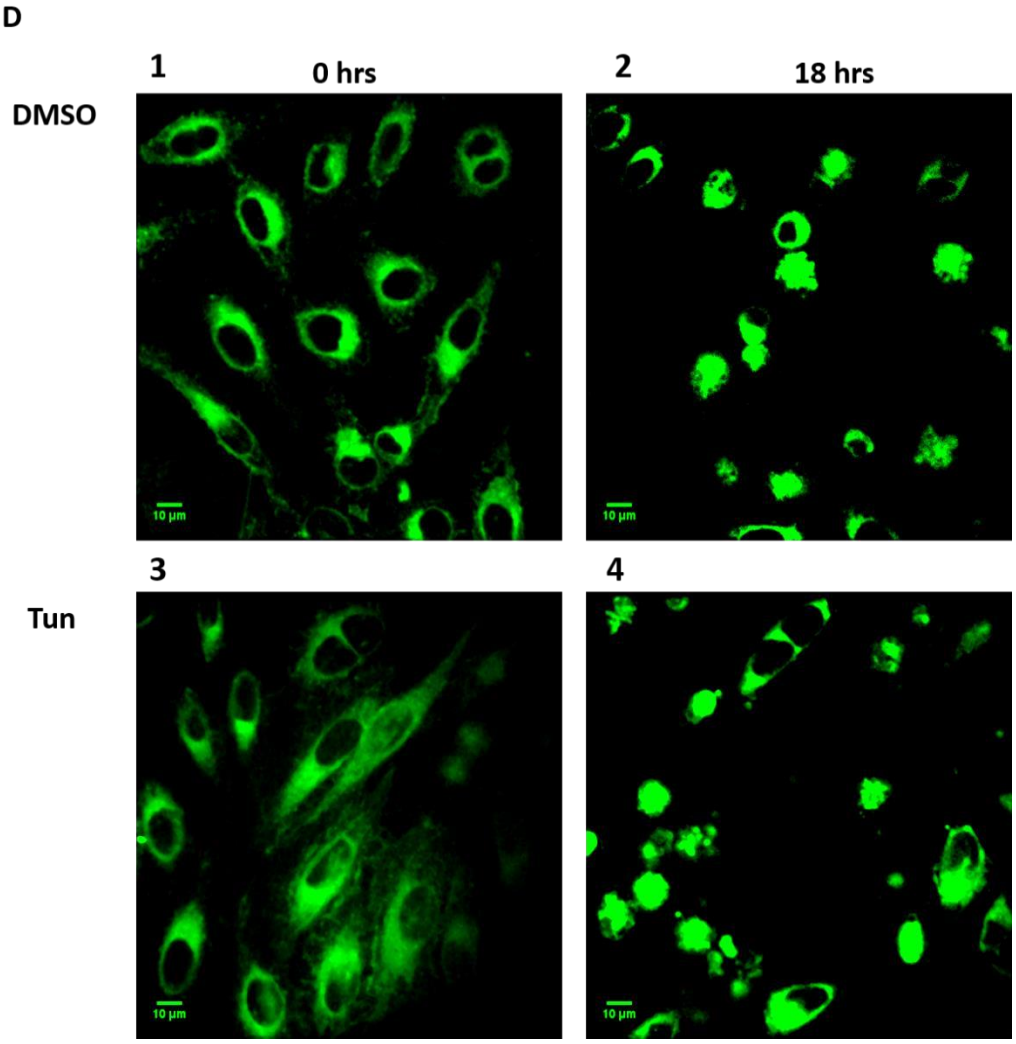

Figure 3.3: Imaging at high laser power leads to a decrease in cell viability

HeLa cells were incubated for 1 hour in with ERTracker green Glibenclamide BODIPY prior to imaging for 18 hrs at 30 second intervals and treated with DMSO only or Tun for 18 hours under 5% CO_2 at 37^{o}C.

A. (1-4 hrs) Structures resembling either sheets or tubules appeared in both control and ER stress induced cells with changes seen in Tun treated cells as early as 1 hrs compared to 4hrs in control cells (panels 1-4, boxes).

B. (5-8 hrs) The sheet/tubular structures became more prominent in both DMSO and Tun treated cells (panels 9-12, boxes)

C. (9-12 hrs) The ER rounded, blebbed and detached in a way that resembled cell death in both DMSO control and Tun treated cells at ~9 hrs and 12 hrs respectively (panels 18-20, arrows (showing detached and blebbed cells)).

D. (0 and 18 hrs) A comparison of HeLa cells at 0 hrs and 18 hrs post Tun revealed the extent of the effect high laser power has on cell viability after 18 hrs.

3.2.1.2. The effect of tunicamycin induced ER stress on ER morphology in different cell types

A comparative study looking at the effects of ER stress on the morphology of HT1080 and HeLa cell ER as then conducted. HT1080 and HeLa cells were first stained with ERTracker blue/white and treated with DMSO vehicle control, tunicamycin and DTT to induce ER stress (section 2.3, 2.4 and 2.9) cells were then imaged for 18 hrs. Figure 3.4 and 3.5 show a comparison between HeLa and HT1080 cell ER morphology at 0.5 hrs, 1 hrs, 3 hrs, 6 hrs, 12 hrs and 18 hrs.

From 0.5 -3 hrs there were no significant changes to tunicamycin treated Hela and HT1080 ER membrane area compared to control cells (figure 3.4), however, there were changes in ER morphology. In HeLa cells from 0.5 -1 hrs tunicamycin treatment, though ER morphology was variable (reflecting the morphology of the cells, ranging from elongated (e), oval (o) and rounded (r)), this was comparable with DMSO control treated cells (figure 3.5A-B, panel 1, 2, 7 and 8, e, o, r). From 0.5 – 1hrs, the ER of HT1080 cells treated with tunicamycin, like that of HeLa cells, was comparable to the ER of control treated cells and like HeLa cells, there was a faint appearance of tubule/sheet structures at the periphery of the ER (figure 3.5A panels 1, 2, 4 and 5, arrows), this characteristic was also observed with ERTracker green but much less clearly (data not shown). However, in contrast to HeLa ER, by 1 hrs in HT1080 cells, the faint tubular/sheet structures became more prominent in both DMSO control and tunicamycin treated cells (figure 3.5B, panels 10-11, arrows), suggesting some differences in the fluidity of the ER between cell types.

A

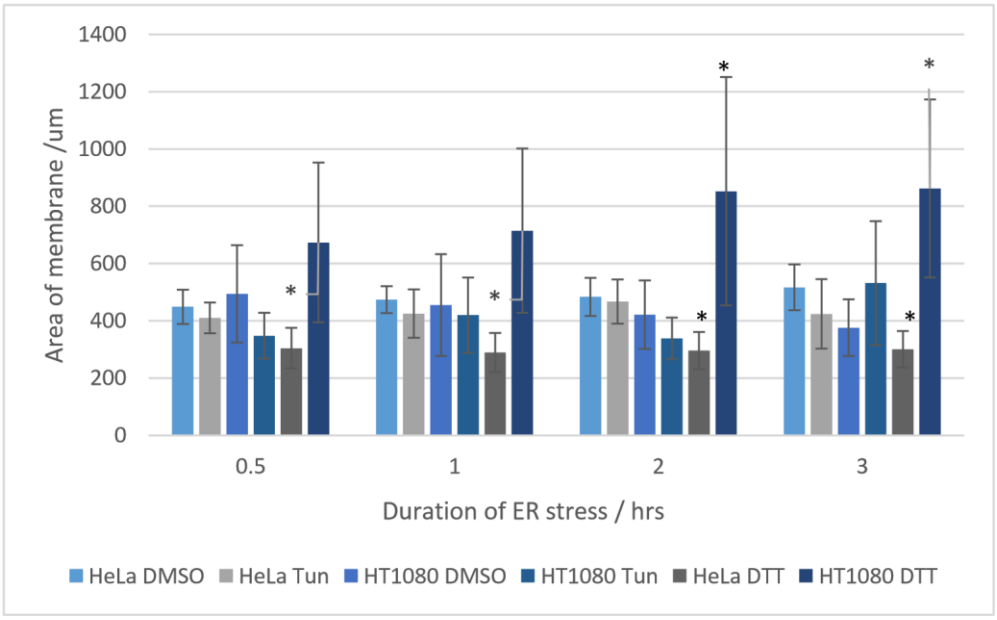

B

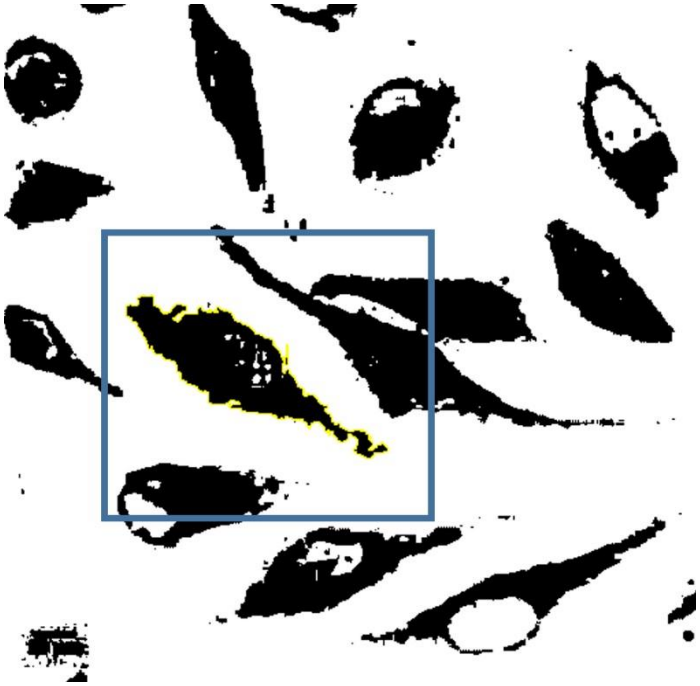

Figure 3.4: Quantification of ER membrane expansion during tunicamycin and DTT induced ER stress

HT1080 and HeLa cells were incubated with medium containing ERTracker Blue/white (1:1000) dye prior to imaging on Spinningdisk confocal under 5% $C0_2$ and 37^{o}C for 18 hrs. Right before imaging Tun and/or DTT was added.

A. Quantification of ER membrane expansion from images in figure 3.4.

B. ImageJ was used to quantify ER membrane area. ER periphery was measured (yellow outline, box).

n=9, *=p <0.05

A

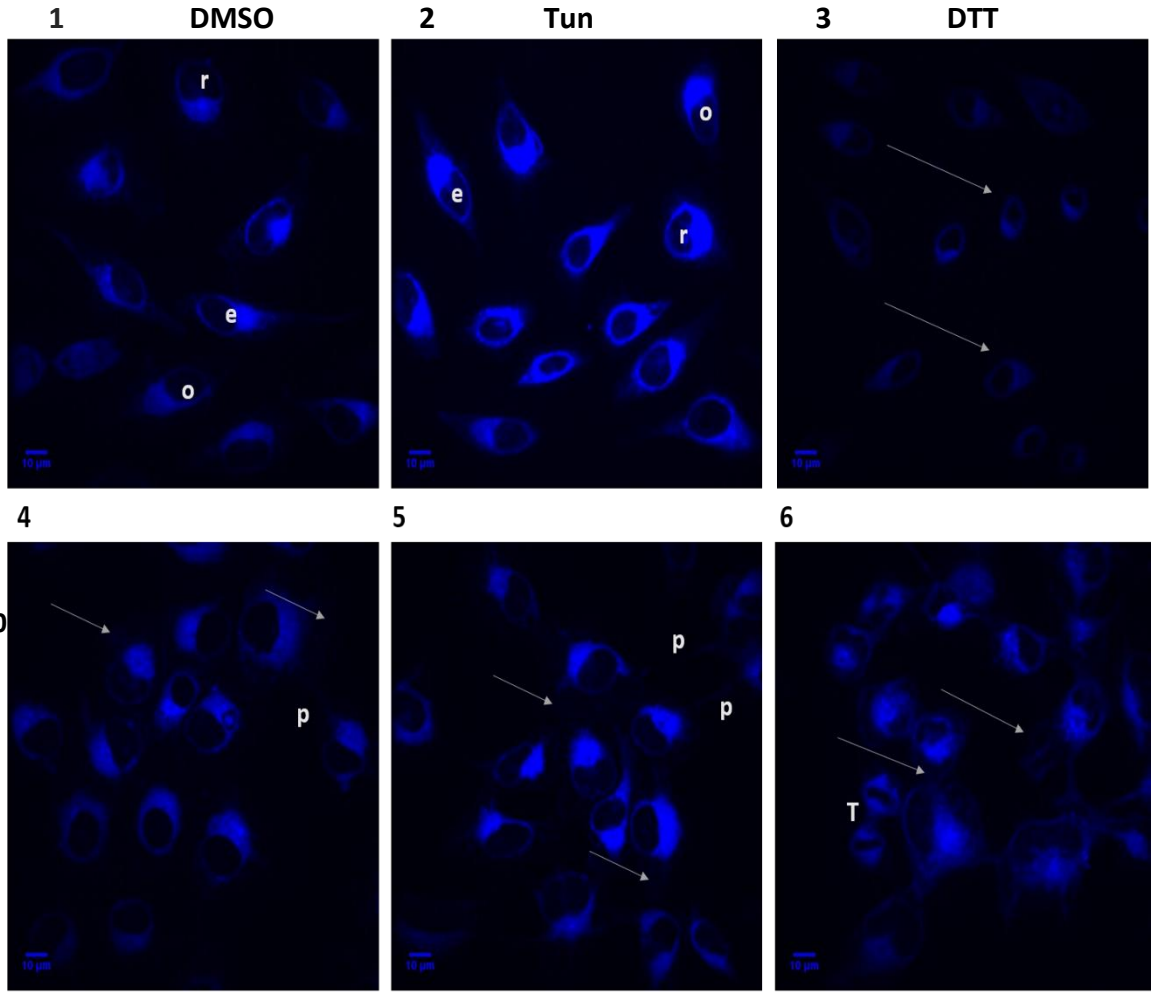

0.5 Hrs

B

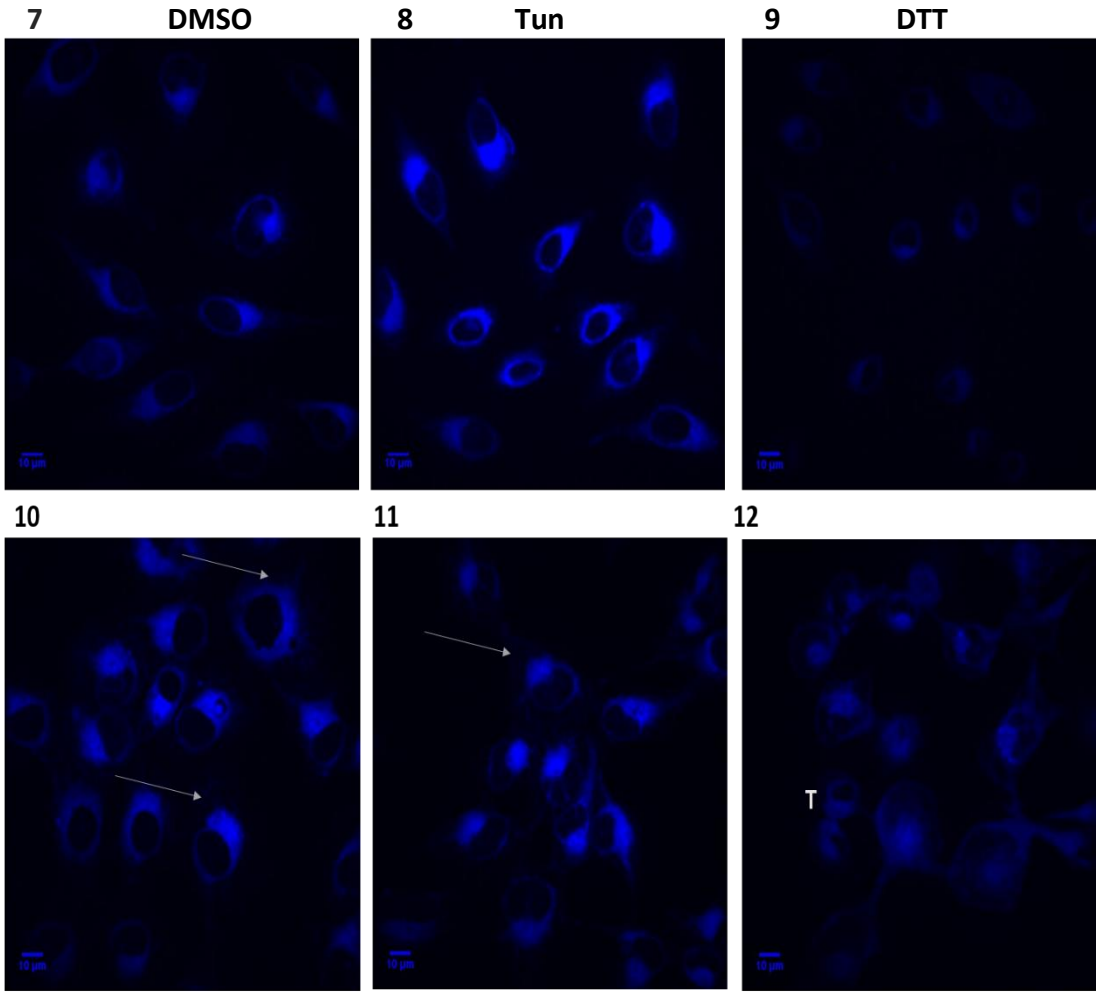

1 hrs

C

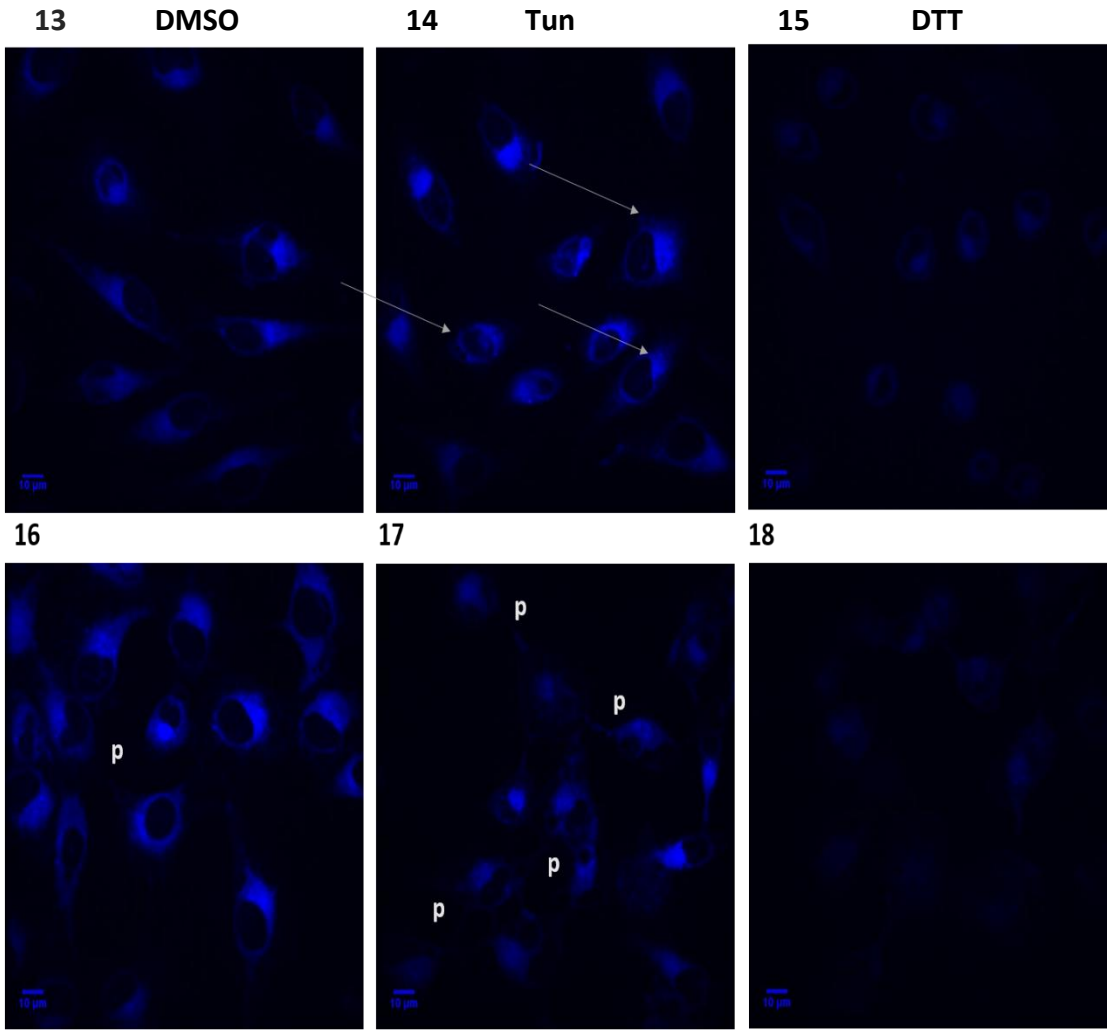

D

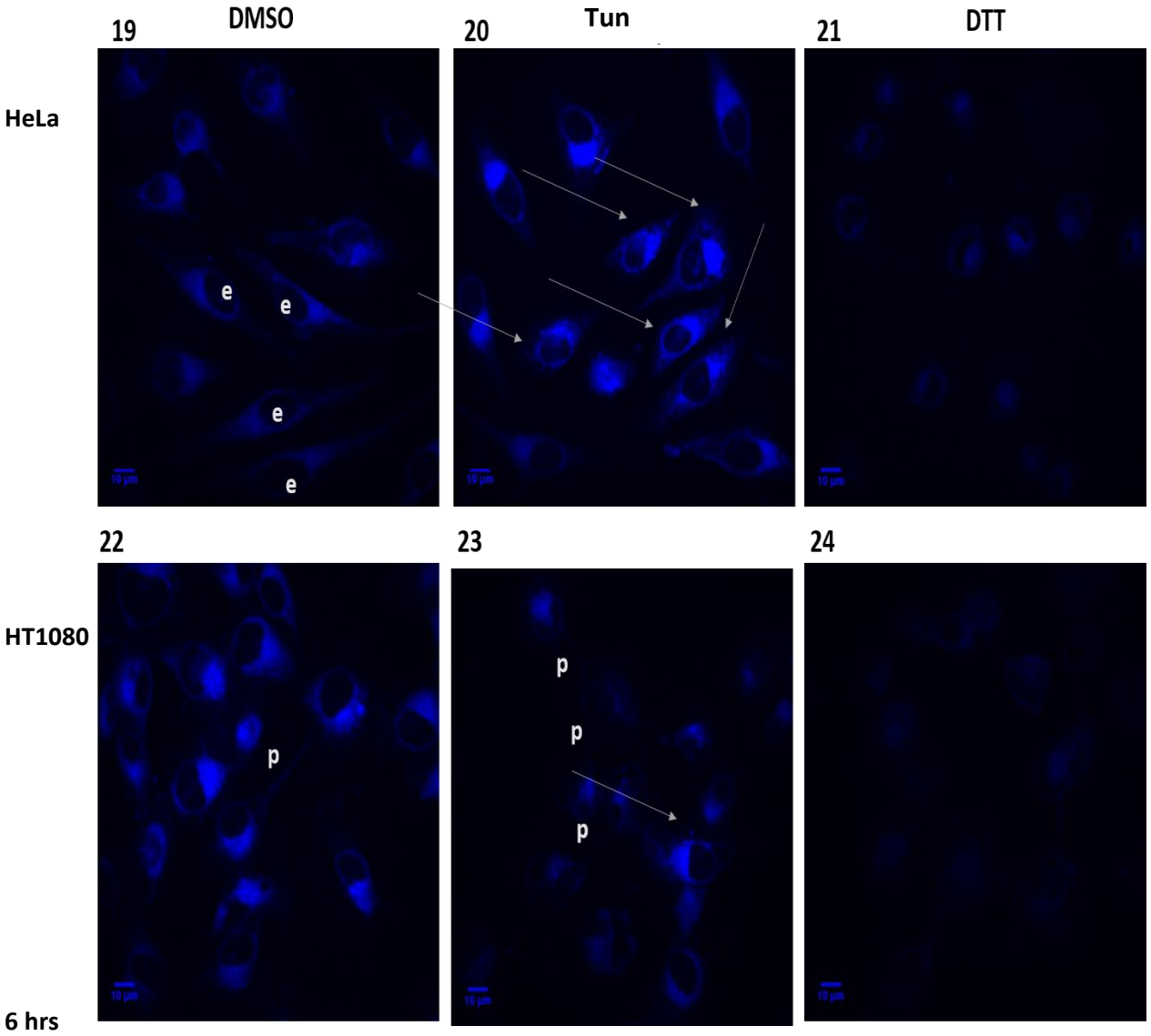

E

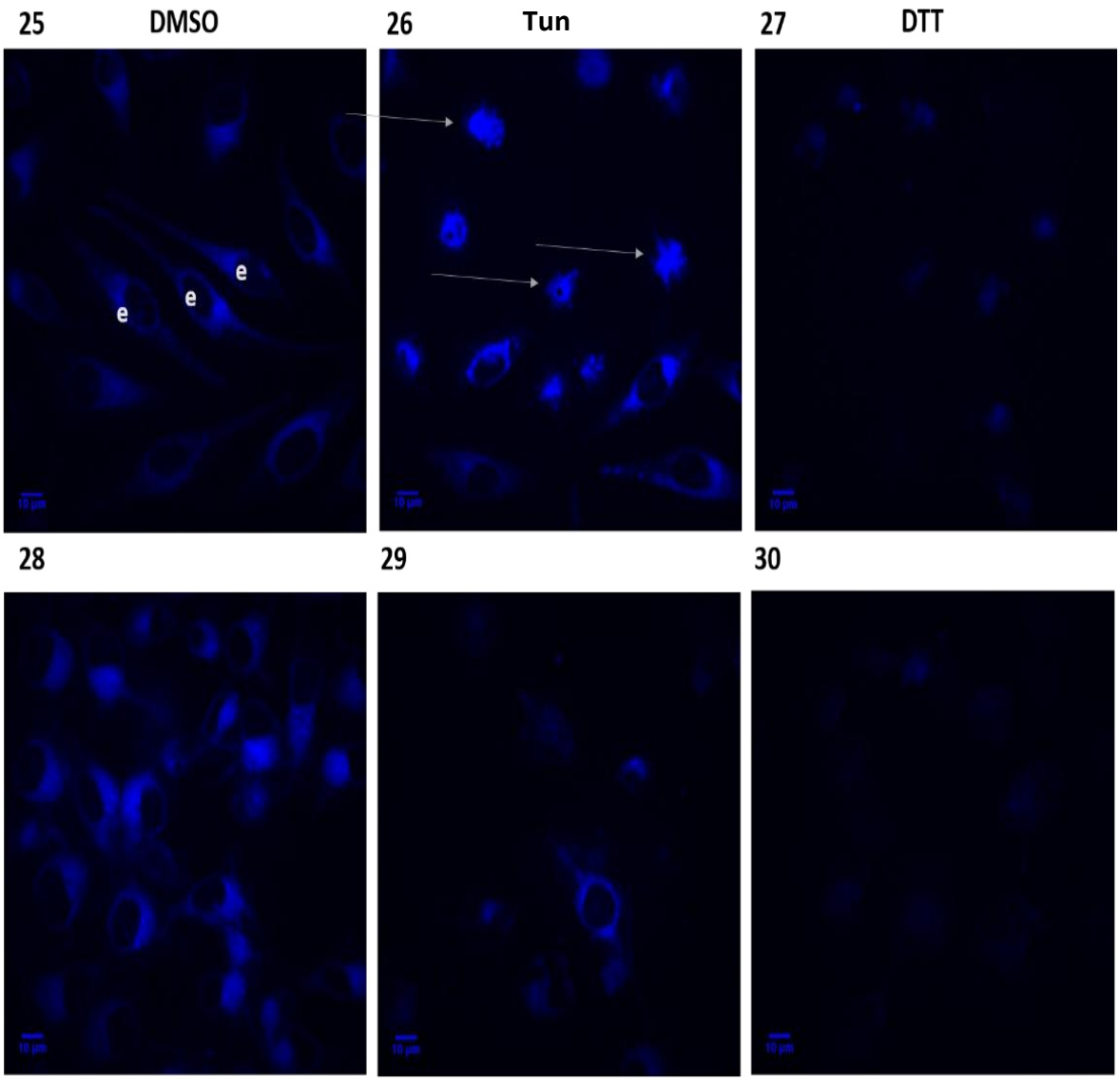

12 hrs

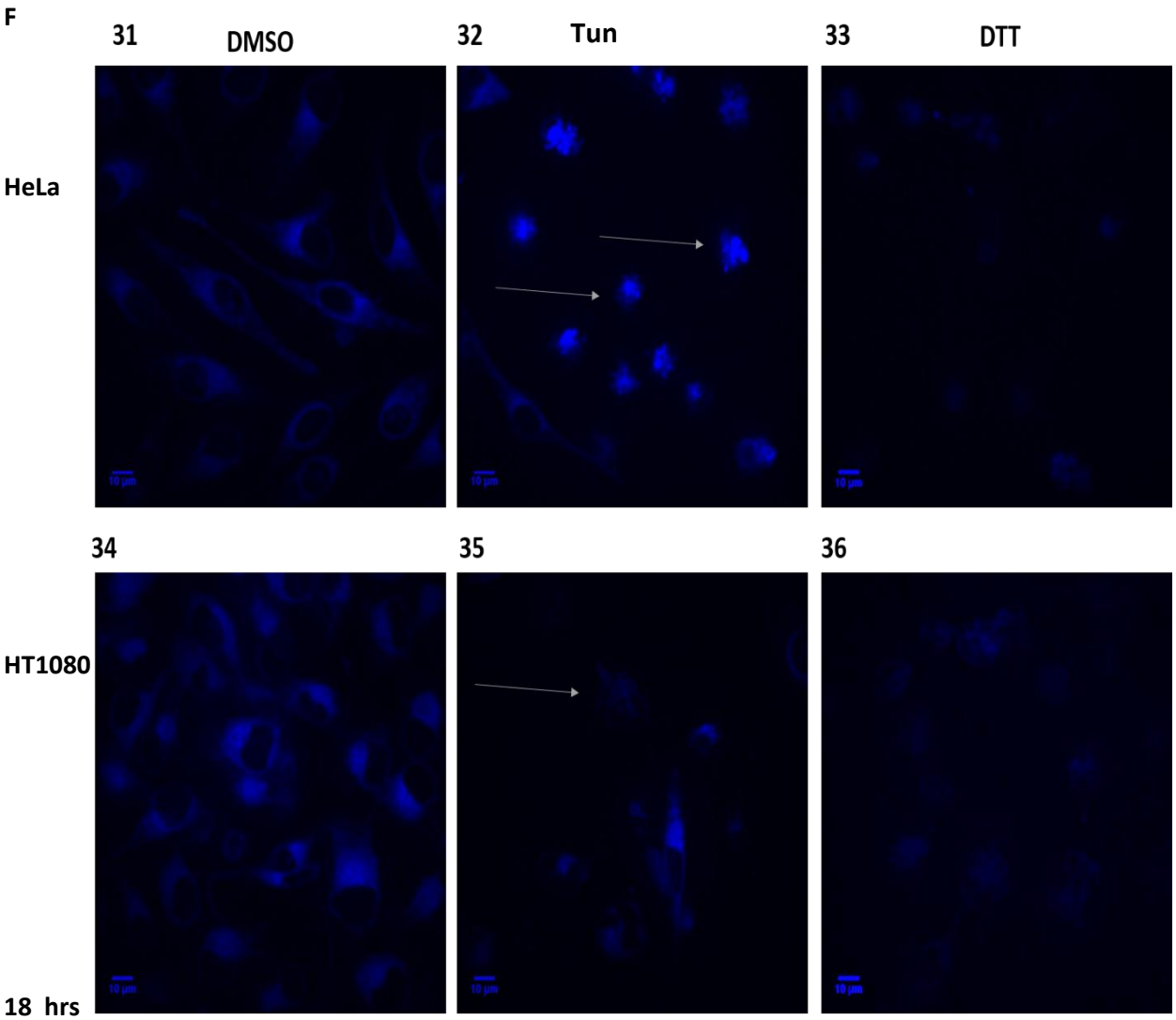

Figure 3.5: Tunicamycin induced ER stress leads to decrease in cell viability in HT1080 and HeLa cells

HT1080 and HeLa cells were incubated in medium containing 1 mM ERTracker blue for 120 mins prior to imaging. The cells were treated with DMSO (left hand panels), Tun (middle panels) and DTT (right hand panels) for 18 hours under 5% CO_2 and at 37^{o}C.

A. At 0.5 hrs, no significant changes in both HeLa and HT1080 cells treated with Tun compared to DMSO control.
B. At 1 hrs, tubular/sheet structures were visible in HT1080 ER treated with Tun but not HeLa ER (arrows, panel 11).
C. At 3hrs, HeLa cells showed tubular/ sheet structures (arrows panels 3-23). In HT1080 cells, ER morphology became abnormal.
D. At 6hrs, tubular/ sheet structures are no longer visible in HeLa. Projections seen in HT1080 cells (p, panel 23)
E. At 12hrs, DMSO treated HeLa cells began to elongate (e, panel 25) while Tun treated cells began to round and bleb (arrows, panel 26).
F. (18hrs) In both cell lines DMSO treated cells remained viable however in HT1080 and HeLa cells treated with Tun and DTT, the ER rounded, blebbed and the cell detached from the dish (arrows, panels 32, 33, 35,36) in a way that resembled cell death.

Key: e-elongated, o-oval, r-rounded T-telophase and P-protrusions.

Cellular protrusions and thick and thin filamentous structures appeared to be connect HT1080 cells from 1 hrs to 6 hrs (figure 3.5B-D, panel 10, 11, 16, 17, 22 and 23, P) which was in contrast HeLa cells which did not exhibit these filamentous structures. Three hours into tunicamycin treatment, the ER of some HeLa cells showed more distinct tubular/sheet structures compared to control (figure 3.5C, panel 14, arrows), whereas none could be seen in the ER of HT1080 cells, which remained fairly constant. By 6 hrs tunicamycin treatment, tubular/sheet structures of HeLa cells had become more prominent (figure 3.5D, panel 20 and 23, arrows) in contrast to the ER of HT1080 cells whose morphology had remained fairly constant. By 12 hrs in both cell types, dramatic changes had occurred in ER morphology. In tunicamycin treated HeLa cells, 69% of the ER had detached and blebbed compared to control ER (figure 3.5E, panel 26, arrows and table 3.1). In tunicamycin treated HT1080 cells, approximately 100% of cells had lost their oval ER morphology compared to 0% in control cells. And by 18 hrs in tunicamycin treated HeLa cells, 92% had detached and blebbed compared to control cells which remained attached, dividing (table 3.1) and migrating (figure 3.5C, panels 31-32), which was also seen in HT1080 control ER (Figure 3.5F, panel 34), as seen in table 3.1. Tunicamycin treated HT1080 cell ER also resembled that of HeLa in that there was no cell movement and cells had detached, no nuclear space was visible and no cellular protrusions could be seen (figure 3.5F, panels 31, 32, 34, 35, arrows).

In contrast to tunicamycin treated HT1080 and HeLa ER, the ER of DTT treated HeLa cells, appeared smaller (which significantly decreased compared to control cells (figure 3.4)) and rounder (which remained constant throughout 18 hrs of DTT treatment), reflecting the fact that DTT is a potent reducing stress reagent that rapidly induces cell rounding (figure 3.5A, panel 3, arrows). The ER membrane area of HT1080 DTT treated cells showed a significant increase compared to the ER membrane area of DMSO control 0.5 -3 hrs (figure 3.4) along with the appearance of prominent tubule/sheet structures at the ER periphery (figure 3.5A, panel 6, arrows). However from 0.5 hrs onwards, the ER morphology of DTT treated cells remained consistent. It was expected that DTT treatment would be more potent than

tunicamycin treatment however tunicamycin did induce the death of both HT1080 and HeLa cells.

In HeLa cells the first cell death was seen from 459 mins after tunicamycin treatment and in HT1080 cells from 122 mins after tunicamycin treatment. The difference in time of death was unexpected, as previous laboratory findings had suggested that HT1080 cells were more resistant to ER stress induced by tunicamycin (unpublished data). However, it is possible that the accelerated death of tunicamycin-treated HT1080 cells may have been caused by an additive effect on the laser. Taken together, the results demonstrate that both tunicamycin and DTT have an effect on ER morphology in HT1080 and HeLa cells.

Table 3. 1 Chemical induction of ER stress affects cell viability

Cell Type	Treatment	Percentage of detached and blebbed cells / %						Approximate number of cell divisions
		0.5 hrs	1 hrs	3 hrs	6 hrs	12 hrs	18 hrs	
HeLa	DMSO	0	0	0	0	0	0	7
	Tun	0	0	0	0	69	92	0
	DTT	0	0	100	100	100	100	0
HT1080	DMSO	0	0	0	0	0	0	4
	Tun	0	7	15	38	100	100	0
	DTT	0	100	100	100	100	100	0

3.2.2. The effect of tunicamycin and DTT on the glycosylation and reduction of MHC class I proteins

To study the different signalling pathways that are activated in different cell lines during early and late UPR stress responses, chemical inducers of the UPR, tunicamycin and DTT (section 1.7) were used. Tunicamycin was used as the principle agent of interest as it was suspected from previous unpublished studies in our laboratory to induce differential UPR activation in HeLa cells compared with HT1080 cells. Tunicamycin effects glycosylation, which is a pivotal modification that occurs on many nascent secretory pathway polypeptides before they can be folded correctly and efficiently (Shibatani et. al. 2005, Kozlov et. al. 2010). So inhibiting the glycosylation of many proteins and subsequently causing mass misfolding, rather than studying the effects of one misfolded protein, provides better insight into how the UPR in general can respond to ER stress and the pathways that are activated in these responses.

To assess whether the concentrations of tunicamycin used in these experiments had an effect on the steady state pool of MHC class I heavy chains, HT1080 cells were treated with tunicamycin and DTT for 60 mins, along with mock treated cells and followed by lysis, SDS-PAGE and western blotting (as described in the materials and methods section 2.4-2.7). Lysates were run under reducing or non-reducing conditions and the HC10 monoclonal antibody (table 2.2) was used to probe for MHC class I molecules, HLA B/C, which are glycosylation (Barbosa et.al. 1987). As seen in figure 3.6, the class I heavy chain molecular weight remained consistent when subjected to tunicamycin, DTT and mock treatment under reducing conditions (Figure 3.6A, lanes 5-7). Under non-reducing conditions, the MHC class I heavy chains migrated more rapidly and were more compact because of the presence of disulphide bonds (Figure 3.6A, lanes 5-7). Tunicamycin appeared to have no visible effect on the mobility of the heavy chain pool (Figure 3.6A, lanes 5-7), which would have corresponded to the molecule having a lower molecular weight due to inhibition of sugar attachment. This is consistent with the notion that the MHC pool is distributed between the ER, secretory pathway and plasma membrane and that in this experiment, tunicamycin was likely altering the glycosylation of a minor pool of newly synthesised MHC class I heavy chains. Hence

HLA-B/C turnover was not great enough to visualise a significant change in global HLA-B/C molecular weight, a change which may have been seen with a longer tunicamycin treatment. DTT treatment of the cells did not lead to the complete reduction of the MHC class I molecules when the samples were analysed in vitro since the band in the non-reducing gel migrated at a similar height to the mock-treated MHC class I molecules (figure 3.6A, compare lanes 2 and 5). Actin was used as a loading and blotting control (Figure 3.6B). Taken together with other data from the laboratory, the results suggest that these conditions are sufficient to cause ER stress (Lemin thesis), but do not cause gross reduction or deglycosylation of the overall secretory protein pool.

Taking this result into consideration, a range of short and long tunicamycin incubation times were used in subsequent experiments to represent acute and chronic ER stress responses.

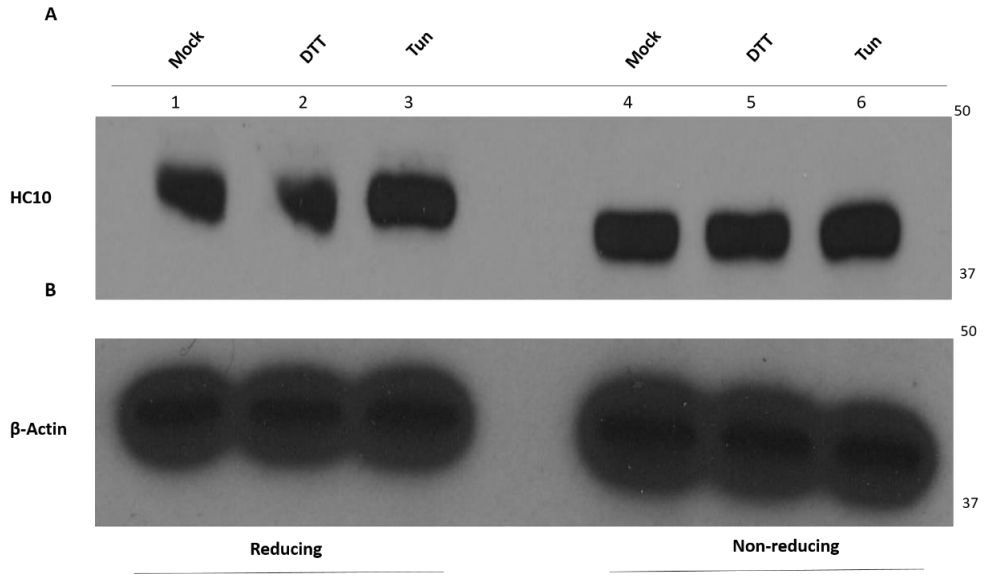

Figure 3.6: Analysis of HLA B/C heavy chains in HT1080 cells treated with DTT and tunicamycin.

HT1080 cells were either mock treated (lanes 1 and 4), treated with 5 mM DTT for 60 mins (lanes 2 and 5) or treated with 1 µg/ml of Tun for 60 mins (lanes 3 and 6) prior to lysis and analysis by SDS-PAGE and Western blotting.

A. Samples were probed with HC10 under reducing (lanes 1-3) and non-reducing (lanes 4-6) conditions. No change in HLA B/C molecular weight was seen in response to Tun treatment at 60 mins.

B. Samples were probed with anti-actin under reducing (lanes 1-3) and nonreducing (lanes 5-7) conditions as a loading control. Molecular weight markers are indicated on the right.

3.2.3 The effects of tunicamycin induced ER stress on cell survival and apoptotic pathways in different cell types

3.2.3.1. The effect of tunicamycin induced ER stress on the activation of ASK-JNK in different cells

The imaging experiments showed that cell death occurred after prolonged tunicamycin treatment of both HT1080 and HeLa cells as seen previously (section 3.2.1). However, the question remained, what cell survival pathways were activated and when were they activated? The ASK-JNK pathway was investigated first because it is pivotal in the ER stress response (Figure 3.7).

With ASK1 being essential in for JNK activation (Nishitoh et. al. 1998), ASK1 protein expression in both HT1080 and HeLa cells was investigated. HT1080 and HeLa cells were treated with tunicamycin for 30 mins, 60 mins and 6 hrs and with DTT for 60 mins and processed as described in section 2.4-2.7. Cells were lysed (in a lysis buffer that did not contain an alkylating agent) and ASK1 expression was investigated by reducing SDS-PAGE followed by Western blotting. Under reducing conditions, a band was seen at the expected molecular weight of ASK1 (155kDa (Xuhong et. al. 1996)), but only in HeLa cells (figure 3.8, panel A). Unexpectedly, there was a band present between 50kDa and 75kDa at approximately 62kDa that was seen under both reducing and non-reducing (not shown) conditions in the absence of NEM (figure 3.8 panel B). β-actin was used as a loading control (figure 3.8, panel C).

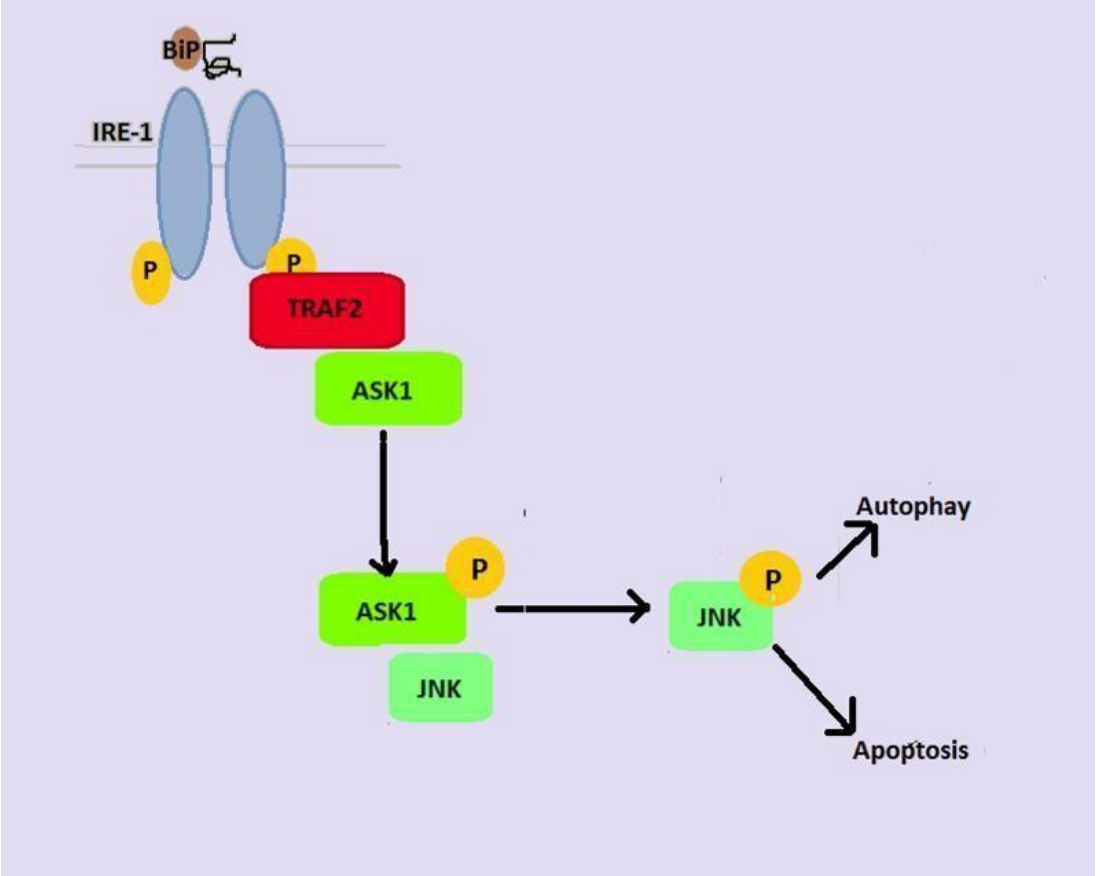

Figure 3.7: The activation of the IRE1-JNK pathway

IRE1 can be activated following ER stress. Once is activated it recruits TRAF2 which then phosphorylates ASK1.Phosphrylated-ASK1 then activates JNK by phosphorylation, which can lead to either apoptotic or autophagic responses.

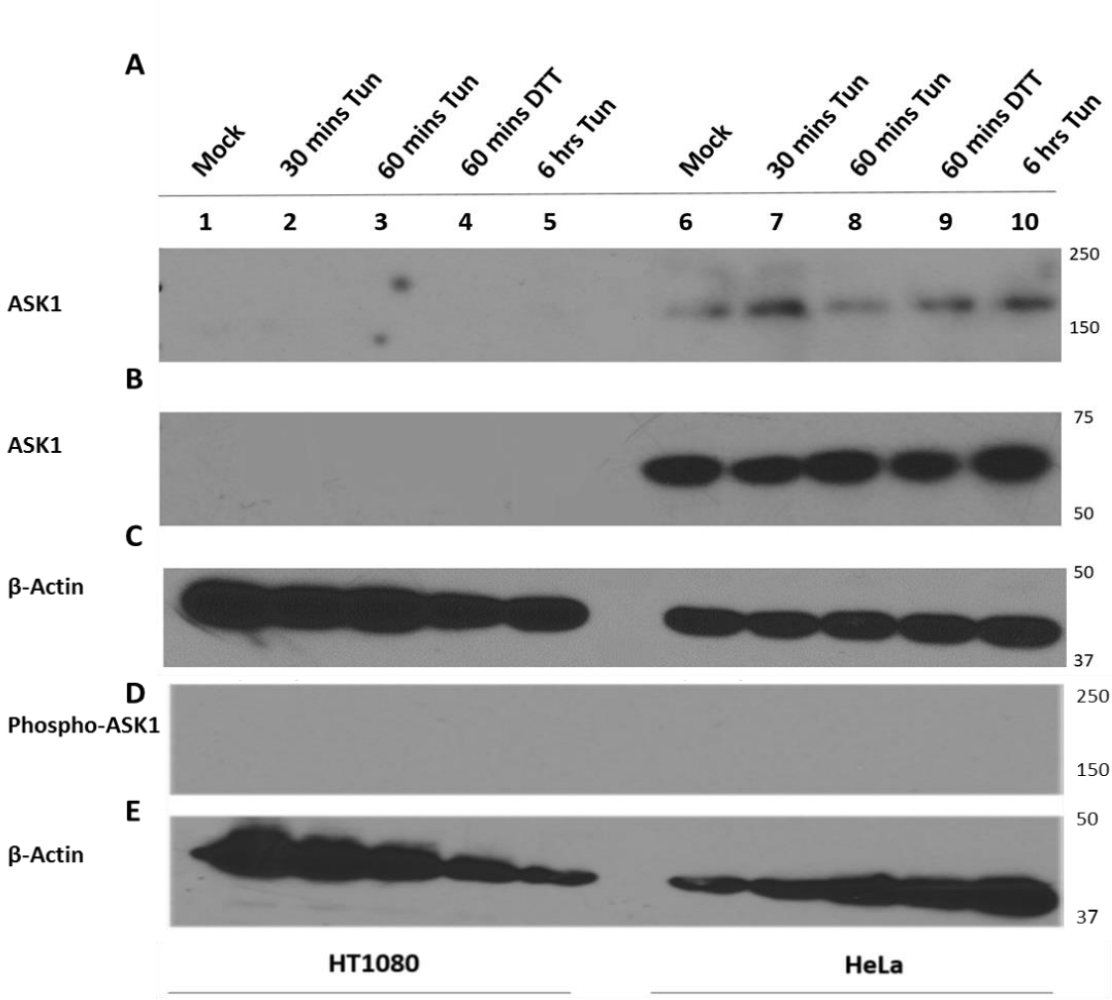

Figure 3.8: ASK1 expression in HT1080 and HeLa cells

HeLa and HT1080 cells were either mock treated (lanes 1 and 6) treated with 1 µg/ml Tun for 30 mins (lanes 2 and 6), 60 mins (lanes 3 and 8) and 6 hrs (lanes 5 and 10) and with 5 mM DTT for 60 mins (lanes 4 and 9) prior to lysis in RIPA lysis buffer without NEM and analysis by SDS-PAGE and Western blotting.

A. ASK1 was detected only in HeLa cells at ~155kDa (lanes 6-10). ASK1 expression appeared stronger after 30 mins (lane 7) and 6 hrs (lane 10) Tun treatment.

B. Unexpected appearance of a ~60-65kDa band whose expression was seen both under non-reducing (not shown) and reducing conditions in HeLa cells and not HT1080 cells.

C. β-actin was used as a loading control however it shows that in HT1080 cells more protein was loaded compare to HeLa cells. Nevertheless no expression of ASK1 was seen in HT1080.

D. No phosphorylated ASK1 expression was seen in both HeLa and HT1080 cells under ER stress conditions and no 60-65kDa ASK1 associated band were seen.

E. β actin was used as a loading control.

In a repeat experiment, ASK1 expression was also investigated again under both reducing and non-reducing conditions in the presence of NEM. At the expected molecular weight of ASK1 (155 kDa), no ASK1 band was seen in both HT1080 and HeLa cells however, the ~62kDa band was present in HeLa cells and its mobility remained unchanged under both reducing and non-reducing conditions, indicating an absence of disulphide bonds (data not shown). There was no change in the steady state level of ASK1 after either DTT or tunicamycin treatment in HeLa cells. Treatment of HT1080 cells with tunicamycin or DTT did not induce the expression of ASK1 (data not shown).

Next, ASK1 phosphorylation was investigated in HT1080 and HeLa cells. As shown in figure 3.8D, no P-ASK1 band was seen in either cell type. This result may be because endogenous phosphorylated ASK1 is expressed at low levels so a transfection experiment may be needed to see the appearance of P-ASK1.

Given the potential difference in ASK (or a cross-reactive ASK family protein) expression between Hela and HT1080 cells, it was decided to analyse the expression of JNK, which is downstream of ASK and can be phosphorylated in response to ER stress through the IRE1 pathway (figure 3.7). Firstly, JNK and PJNK antibody specificity was investigated. Initially, HT1080 cells were treated with tunicamycin for 60 mins, 120 mins and 24 hrs or with DTT for 60 mins, 120 mins and 24 hrs and processed as previously described (section 2.4-2.7). As seen in Figure 3.9A, total JNK expression was seen at all time points except 24 hr treatment with DTT (figure 3.9, panel A, lane 2) (which may have been due to loss of material from dead cells). In tunicamycin treated HT1080 cells, total JNK signal was observed at all time points, which was consistent with reports showing that JNK is constitutively expressed (Raciti et. al. 2012).

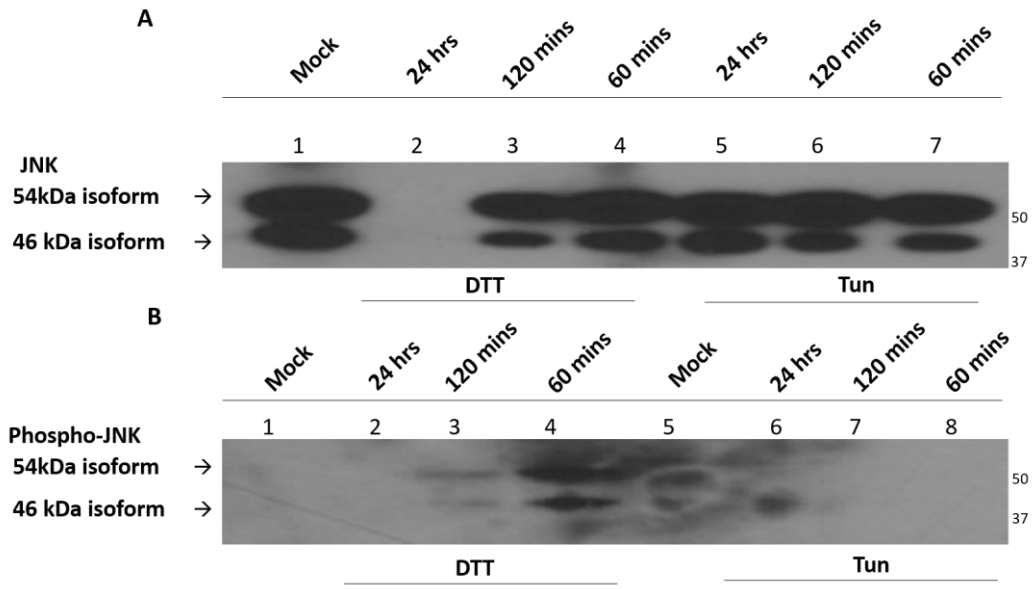

Figure 3.9: Anti-JNK and anti-Phospho-JNK antibodies recognise JNK and Phospho-JNK respectively

HT1080 cells were either mock treated (lanes 1 (A) and 1 and 5 (B)) or treated with 5 mM DTT (lanes 2-4 A and B) or 1 µg/ml Tun (lanes 5-7 (A), 6-8 (B)) for 60 mins, 120 mins and 24 hrs prior to lysis in MNT lysis buffer and analysis by SDS-PAGE and Western blotting. Anti- JNK and anti-phospho-JNK antibodies were used to detect total JNK and its active form phospho-JNK respectively.

A: JNK expression was seen at all time points excluding 24 hrs DTT treatment indicating that the antibody recognized both total JNK isoforms (46kD and 54kD). Overall JNK expression was similar when stressed cells were compared to mock treated cells, indicating that JNK is constitutively expressed.

B: Phospho-JNK expression was only seen at 120 mins and 60 mins DTT treatment, consistent with the transient nature of phosphorylation. No Phospho-JNK was detected after Tun treatment.

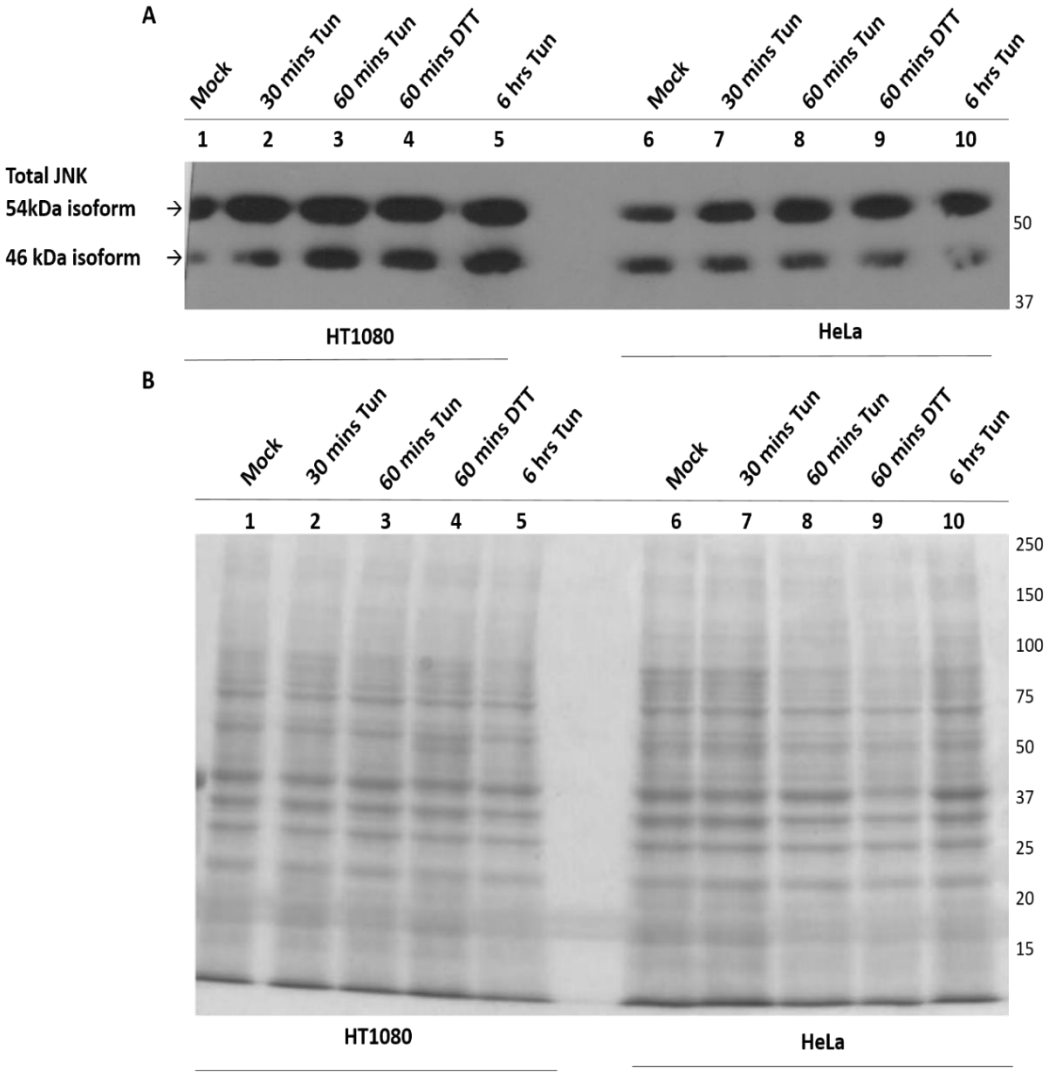

Figure 3.10: JNK is constitutively expressed in both HT1080 and HeLa cells HT1080 and HeLa cells were either mock treated (lanes 1 and 6) or treated with 1 µg/ml Tun for 30 mins (lanes 2 and 7), 60 mins (lanes 3 and 8) and 6 hrs (lanes 5 and 10) or 5 mM DTT for 60 mins (lanes 4, 9) prior to lysis in RIPA lysis buffer (to maximise protein extraction) and analysis by SDS-PAGE and Western blotting.

A. In both HT1080 and HeLa cells, JNK expression is comparable to mock at all Tun and DTT treatment times suggesting that total JNK is constitutively expressed. Two JNK isoforms were visible at 54kDa and 46kDa.

B. Coomassie blue staining was used as a control to show protein levels in the lysates that were used for Western blotting in A and in figure 3.14.

Also seen in figure 3.9A are two JNK bands at approximately 46kDa and 54kDa which were in both DTT and tunicamycin treated cells. This was consistent with literature reports of JNK, which is known to be found as two isoforms of 46kDa and 54kDa. The P-JNK antibody only gave a signal at 60 and 120 mins DTT treatment (figure 9 panel B, lanes 3-4). This correlated with previous findings that showed that JNK activation (i.e. phosphorylation) is transient (Read et. al. 1997). The P-JNK antibody also recognised both isoforms of JNK (figure 3.9, panel B, lanes 3 and 4).

A comparative study of HT1080 and HeLa cells was then undertaken to observe any differences in the activation and expression of JNK (figure 3.10A). HT1080 and HeLa cells treated with tunicamycin for 30 mins, 60 mins and 6 hrs and with DTT for 60 mins were lysed in RIPA lysis and analysed by SDS-PAGE and western blotting. Both total JNK isoforms were expressed at all time points and treatments including mock treated cells, which again was consistent with previous findings (Raciti et. al. 2012). A Coomassie stained gel of the protein samples, shown in Figure 3.10B, demonstrated loading of samples. Overall this result suggests that both JNK isoforms are expressed in HT1080 and HeLa cells.

A comparison of P-JNK induction in HT1080 and HeLa cells was undertaken as seen in Figure 3.11A. In HT1080 cells, a band at ~50 kDa was seen at all time points and treatments, including mock treated cells, suggesting that this may have been a background band. A faster migrating, seemingly specific band likely to be the 46 kDa isoform of JNK was detected after 120 mins of DTT treatment in HT1080 cell lysates (lane 5). In contrast, in HeLa cells P-JNK expression was seen from 30 mins to 120 mins tunicamycin treatment. However, along with the 46kDa and 54kDa isoforms of P-JNK, there were additional bands expressed from 30 mins to 25 hrs tunicamycin treatment at approximately 100kDa in HeLa cells and which were also seen in HT1080 cells albeit weakly. Note that the HeLa and HT1080 cell lysates were run on the same gel. These observations suggest that either P-JNK phosphorylation differs between HT1080 and HeLa cells or that the P-JNK antibody was not specific or that conditions were not

optimal for P-JNK analysis. Subsequent P- JNK western blot analysis were inconclusive (data not shown), thus the molecular identity of the different bands in the P-JNK analysis remains to be determined.

Due to its role in both autophagy (section 1.4.1) and apoptosis (section 1.4.2), PERK expression in HT1080 and HeLa cells was also investigated using SDS-PAGE and Western blotting analysis. Little or no PERK expression was seen in either HT1080 or HeLa cell lysates treated +/- tunicamycin or DTT (figure 3.12A), even though the β-actin loading control showed that protein was present in the lysate (figure 3.12B). Repeat experiments with cells lysed under various conditions also yielded no signal, suggesting that an alternative antibody is required to visualise PERK activation after ER stress.

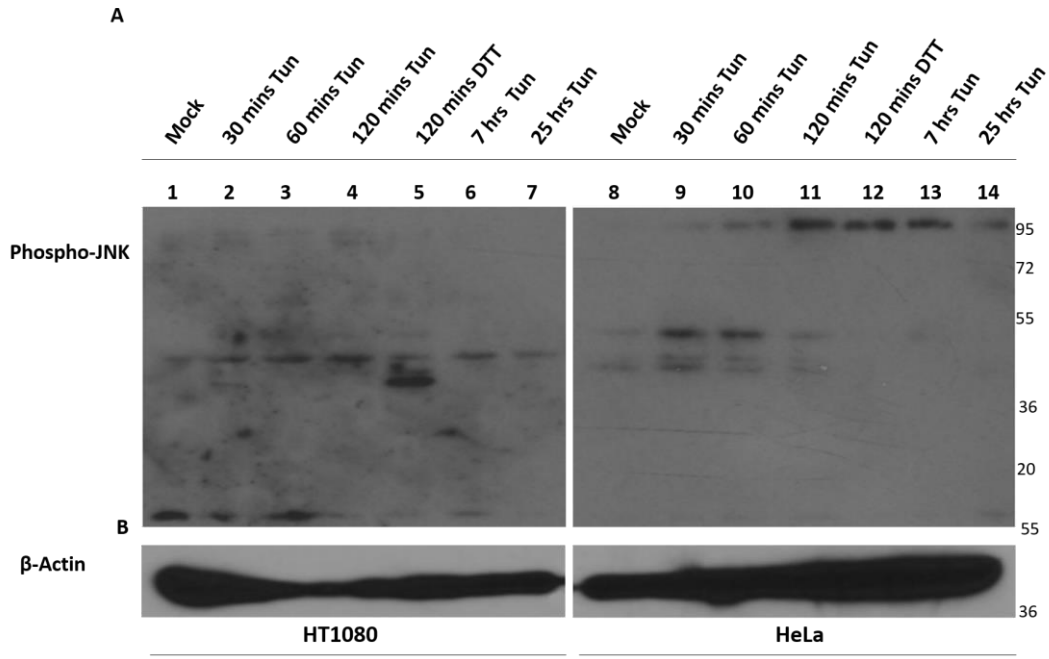

Figure 3.11: A comparison of Phospho-JNK expression in HT1080 and HeLa cells

HT1080 and HeLa cells were either mock treated (lanes 1 and 8) or treated with 1 µg/ml Tun for 30 mins (lanes 2, 9), 60 mins (lanes 3, 10) 120 hrs (lanes 4, 11), 7 hrs (lanes 6, 13) and 25 hrs (lanes 7, 14) or 5 mM DTT for 120 mins (lanes 5, 12) prior to lysis in RIPA lysis buffer (to maximise protein extraction) and analysis by SDS-PAGE and Western blotting.
A. HT1080 and HeLa cells show a different pattern of phospho-JNK expression. In HT1080 cells the JNK isoform appeared at 50kDa whereas in HeLa cells two bands were seen at ~ 46kDa and 50kDa. HeLa cells also showed additional higher molecular weight bands at ~96kDa. Anti phospho-JNK antibody was used to detect phospho-JNK.
B. β- actin was used as a loading control.

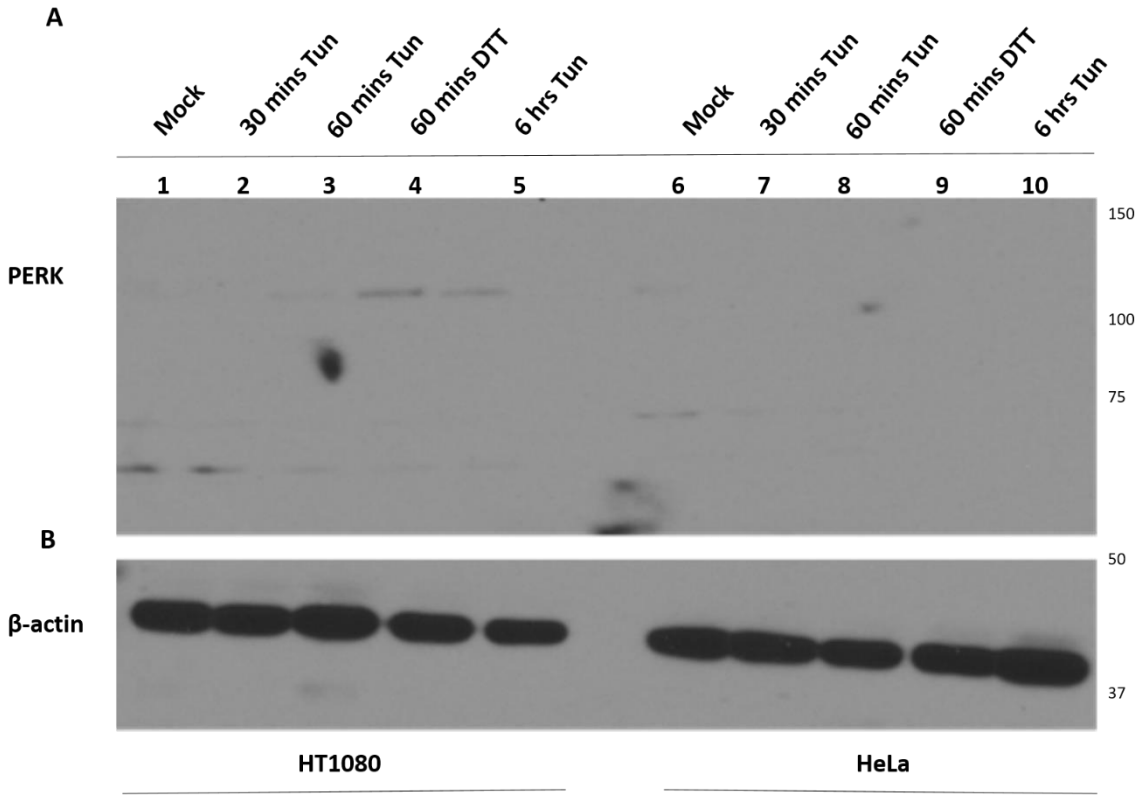

Figure 3.12 PERK analysis after ER stress in HeLa and HT1080 cells HT1080 and HeLa cells were either mock treated (lanes 1, 6) or treated with 1 µgl /ml Tun for 30 mins (lanes 2, 7), 60 mins (lanes 3, 8) and 6 hrs (5, 10) or with DTT for 60 mins (lanes 4, 9). Anti-PERK was used to probe for PERK (panel A) after SDS-PAGE and western blotting of the cell lysates.

A. Weak PERK expression was seen at the expected molecular weight of 140kDa in HT1080 cells but not in HeLa cells, except for a faint signal in mock treated HeLa cells.

B. The lysates shown in A were probed for β-actin as a loading control.

3.2.3.2. Tunicamycin induced ER stress responses lead to the activation of cell survival pathways in different cell types.

The expression, activation and cleavage of LC3B is dependent on different branches of the UPR in different cell types and because LC3B is a crucial component of autophagosome formation (section 3.1), LC3B was used to investigated if and when autophagy is activated and if survival pathway activation differs between cell types.

First, anti-LC3B antibody conditions were optimised. HeLa cells were treated with tunicamycin for 30 mins, 60 mins and 6 hrs and with DTT for 60 mins as described in section 2.4. The cell lysates were analysed by SDS-PAGE followed by western blotting (section 2.5-2.7). LC3B is known to form as a ~30kDa precursor that is then cleaved to form LC3-I (16kDa) from which LC3B-II (14kDa) formed (Kabeya et. al. 2000).

Initially, 10µg of protein was loaded onto a 12% gel and anti-LC3B used at a 1:1000 dilution, which resulted in a weak signal at ~34kDa corresponding to pro-LC3B (Figure 3.13A). Next 15µg of protein was loaded onto a 12% gel and anti-LC3B used at 1:1000 dilution (figure 3.13B). No band was seen around 14-16kDa, where LC3BI/II expression was expected; however expression of pro-LC3B expression was seen after 6 hrs tunicamycin treatment (figure 3.13, panel B, lane 5). Finally, 15µg of protein was loaded and anti-LC3B at a 1:500 dilution was used which resulted in the appearance of a band at ~16kDa, along with a band at ~34kDa that most likely corresponded to pro-LC3B. However, it was unclear as to which form of LC3B, LC3BI or II was visualised at~ 15kDa (figure 13, panel C). Nonetheless, subsequent experiments were conducted using 15µg protein and 1:500 anti-LC3B.

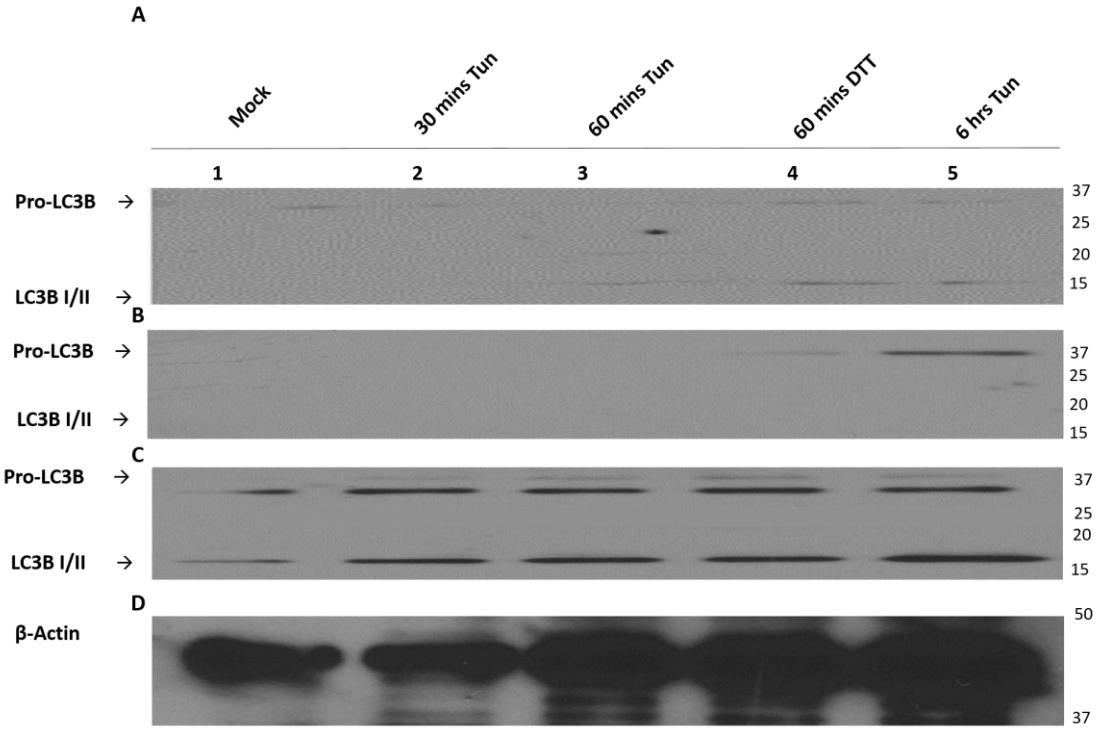

Figure 3.13: Optimisation of anti-LC3B antibody conditions

HeLa cells were either mock treated (lane 1) or treated with Tun for 30 mins (lane 2), 60 mins (lane 3) and 6 hrs (lane 5) and 60 mins and DTT for 60 mins (lane 4) prior to cell lysis in RIPA buffer and SDS-PAGE and Western blot analysis. Anti-LC3B was used to probe for LC3B (A-C). A. With 10µg of protein loaded per lane and 1:1000 anti-LC3B dilution, LC3B-I and LC3B-II band intensity was very low.

B. 15µg of protein was loaded per lane and 1:1000 of anti-LC3B used. Pro-LC3B was not observed in mock (lane 1) and 30 mins (lane 2), 60 mins (Tun and DTT (lane 3, 4)). No 16kDa/14kDa form was detected.

C. 15µg of protein was loaded per lane and 1:500 of anti-LC3B used. At all expected areas LC3B was detected except for doublet bands at 16kDa/14kDa.

D. D. β-actin was used as a loading control however lanes 3-5 where overloaded which corresponds with the results seen in panel B.

A comparison of HT1080 and HeLa cells was then undertaken. LC3B expression and processing after tunicamycin induced ER stress was then conducted in HT1080 and HeLa cells. As shown in figure 3.14, lane 10, in HT1080 cells, LC3B-I expression increased only after 6 hrs tunicamycin treatment along with LC3B-II expression. In HT1080 cells, the band at 14/16kDa was also seen after 60 mins of DTT treatment but only faintly. In HeLa cells, the band at 14kDa/16kDa was seen after 30 mins tunicamycin treatment (figure 3.14, lane 7) and by 6 hrs tunicamycin treatment, the 14-16kDa upper band had decreased; however the density of the lower 14/16kDa band increased compared to that of 30 mins and 60 mins tunicamycin treatment indicating an increase in antibody binding (figure 3.14). The western blot analysis suggested that LC3B-II activation was increased in HT1080 cells, whereas in HeLa cells, LC3B-II seemed to be present prior to ER stress induction which was consistent with the results seen in figure 3.13C.

To examine whether LC3B was differently distributed intracellularly in the cells, immunofluorescence was utilised to visualise changes in LC3B processing and localisation. Firstly, antibody conditions were optimised in HeLa cells treated with DMSO (vehicle control) and 20 mM NH_4Cl for 60 mins (which inhibits fusion of autophagosomes and lysosomes, resulting in LC3B-II accumulation) (figure 3.15), alongside HeLa cells that were treated with tunicamycin for 60 mins. Compared to DMSO control treated cells, which exhibited a diffuse pattern of LC3B staining in line with literature (Kabeya et .al. 2000), 60 mins tunicamycin and NH_4Cl treated cells both exhibited punctate structures along with very little diffuse staining (Figure 3.15A, panels 2, 5, 8, boxes). The diffuse and punctate staining can be seen clearly in figure 3.15B, panels 2, 5, boxes). This observation was in line with literature reports showing that punctate formation under tunicamycin induced ER stress corresponds to the processing of LC3B-I to LC3B-II (Ogata et. al. 2006). This experiment therefore showed that under these conditions, tunicamycin induced ER stress resulted in the conversion of LC3B-I to LC3B-II and the formation of autophagosomes.

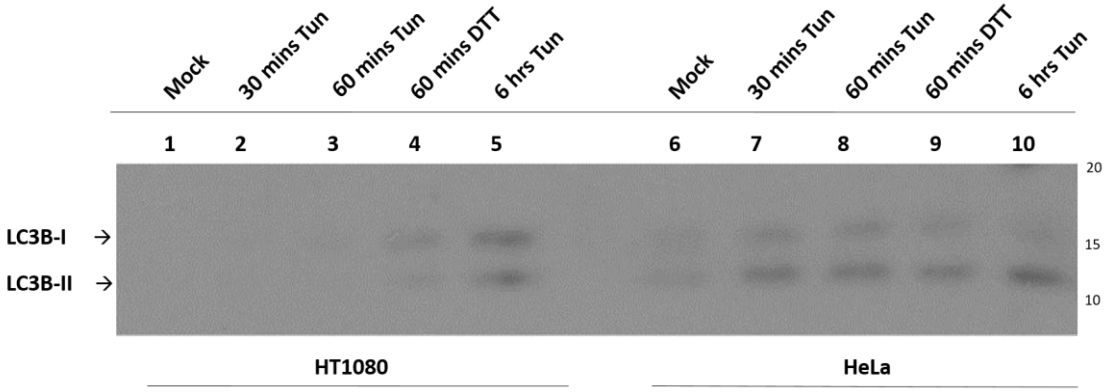

Figure 3.14: Differences in LC3B expression in HT1080 and HeLa cells

HeLa and HT1080 cells were mock treated (lanes 1 and 6) or treated with Tun for 30 mins (lanes 2 and 7), 60 mins (lanes 3 and 8) and 6 hrs (lanes 5 and 10) or treated with DTT for 60 mins (lanes 4 and 9) prior to cell lysis in RIPA lysis buffer and SDS-PAGE and Western blot analysis.

In HT1080 cells, LC3B-I and LC3B-II levels increased after 6 hrs Tun treatment (lane 5) and 60 mins DTT treatment (lane 4) with expression levels being higher after 6 hrs Tun treatment. In HeLa cells, LC3B-I increased from mock to 30 mins Tun treatment (lanes 6-7) then decreased at 60 mins DTT (lane 9) and could not be detected after 6 hrs Tun treatment (lane 10). LC3B-II expression increased from 30 mins Tun treatment and was at its highest after 6 hrs Tun treatment (lanes 6-10).

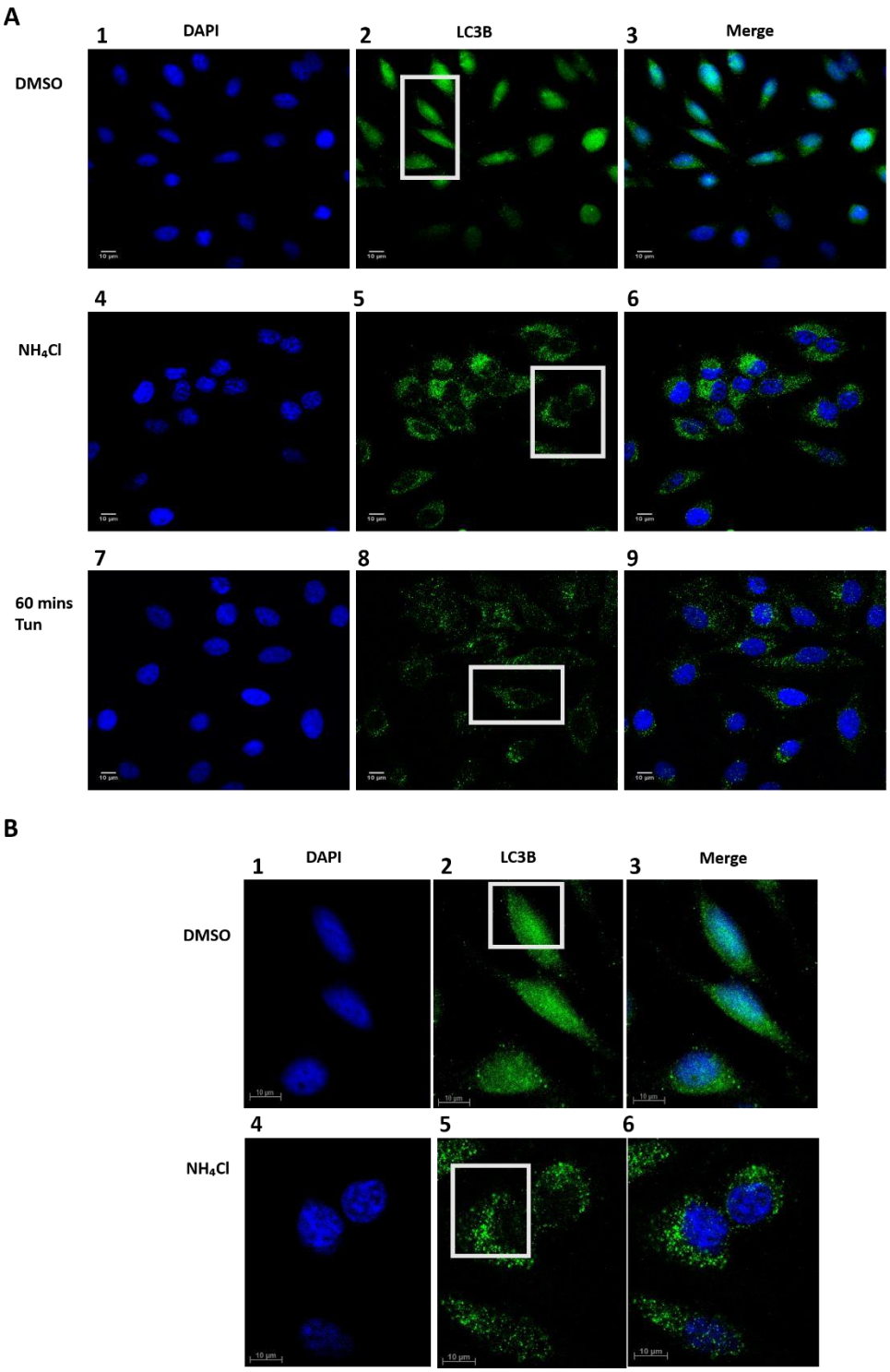

Figure 3.15: Tunicamycin induced ER stress induces punctate LC3B staining

HeLa cells were grown on coverslips, treated with either DMSO (panels 1, 2 and 3) NH_4Cl (panels 4, 5 and 6) or Tun for 60 mins (panels 7, 8 and 9) prior to immunofluorescence analysis. Cells were stained with DAPI nuclear stain (blue) and anti-LC3B (green).

A. Tun treated cells showed punctate LC3B staining in contrast to DMSO vehicle control treated cells which showed diffuse LC3B staining around the nucleus. NH_4Cl treated cells show punctate staining of LC3B around the nucleus.

B. Higher magnification of DMSO and Tun treated cells stained with anti-LC3B, clearly showing the two states of LC3B.

A comparison of HeLa and HT1080 cells was then conducted, where each cell line was treated with either DMSO, 20 mM NH_4Cl for 60 mins or tunicamycin for 30 mins, 60 mins and 6 hrs. In HeLa cells, all tunicamycin treatment times showed both diffuse and punctate staining which was comparable throughout the time course, even with the NH_4Cl positive control (Figure 3.16A, panel 2, 8, 11 and 14 ,boxes). However, DMSO control cells showed a more punctate than diffuse pattern which was unexpected and not comparable with previous experiments conducted under the same conditions (Figure 3.15, panel 2, 3). This suggests that the cells may have experienced an independent environmental stress prior to or during the experimental procedure.

In HT1080 cells treated the same way as HeLa cells, 30 mins, 60 mins and 6 hrs of tunicamycin treatment all resulted in punctate staining and little diffuse staining, which was comparable throughout all treatment times (Figure 3.16B, panel 5-15, arrows). In contrast, the DMSO control treated cells showed diffuse LC3B staining with very little punctate staining, while the NH_4Cl positive control treated cells showed punctate staining with no diffuse staining. This result suggest that tunicamycin induced ER stress induces the formation of autophagosome in HT1080 cells as early as 30 mins (figure 3.16B). The pattern of staining in HeLa cells was not consistent between experiments (Figures 3.16 and 3.16), particularly the DMSO and NH_4Cl controls, so a further analysis of punctate vesicle formation was conducted in both HeLa and HT1080 cells using different antibody concentrations (figures 3.17 and 3.18). For 1:400 anti-LC3B in HeLa cells, NH_4Cl showed more LC3B staining with both diffuse and punctate expression patterns compared to mock and DMSO treated cells (Figure 3.17A, panel 2, 5, 8, box), however, both mock and DMSO treatments again gave rise to some punctate vesicle formation with very little diffuse staining (Figure 3.18A, panel 2, 5, boxes). In HT1080 cells, mock, DMSO and NH_4Cl treatment resulted in diffuse and punctate staining which was comparable throughout all treatment conditions (Figure 3.17B, panel 2, 5, 8, boxes). This was unexpected, particularly for DMSO treatment and inconsistent with previous findings seen in figure 3.15 (figure 3.18B, panel 2, boxes). Anti-LC3B used at 1:200 dilution did not reveal diffuse LC3B staining for mock and DMSO controls in both cell types (figure 3.18A-B, panel 2, 5, boxes). Overall, although the LC3B antibody was clearly able to detect LC3B in punctate structures, it was not possible to accurately infer the induction of autophagy by ER stress using LC3B in an immunofluorescence assay.

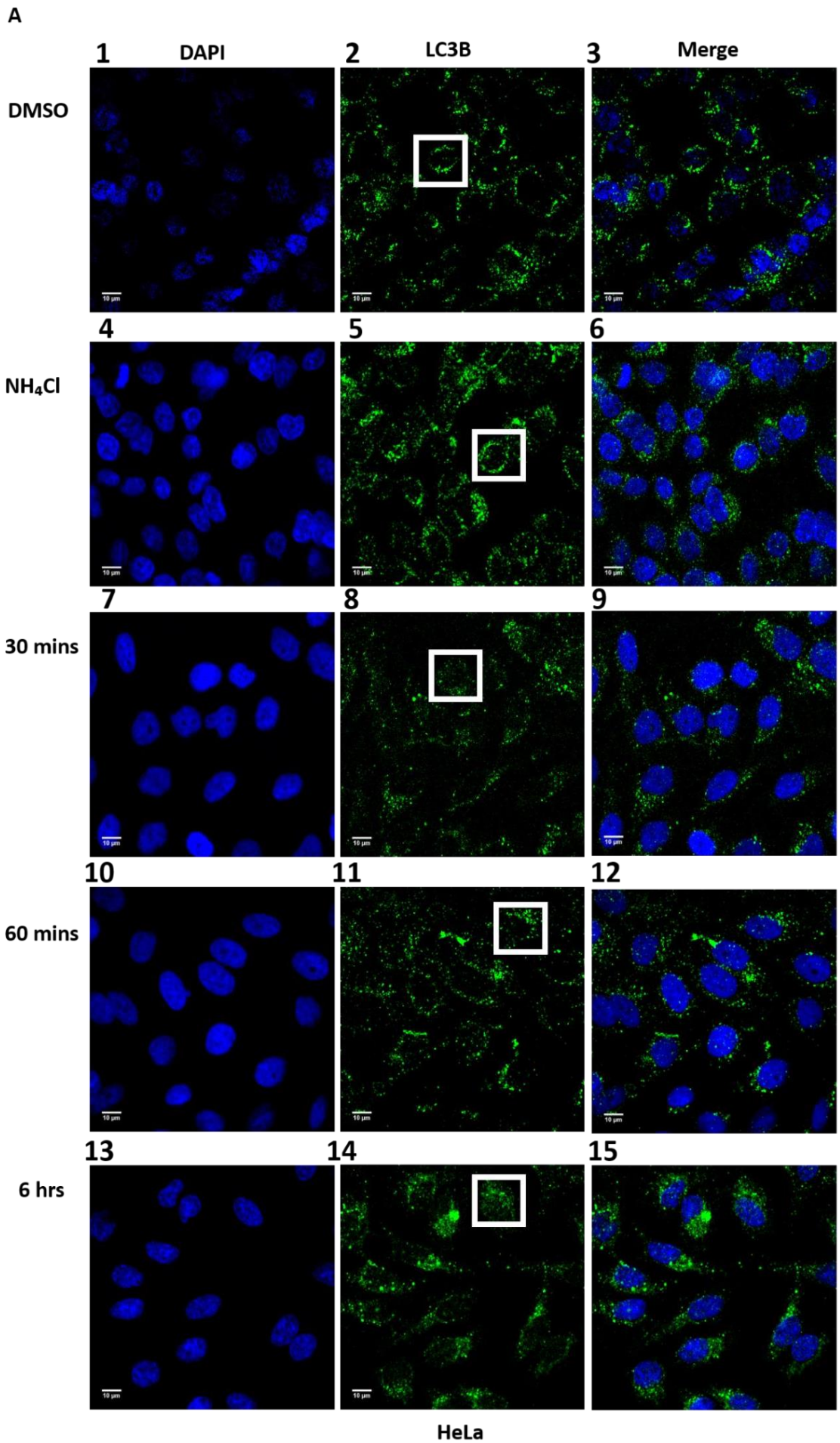
A
1
DAPI
2
LC3B
3
Merge
DMSO
4
5
6
NH4Cl
7
8
9
30 mins
10
11
12
60 mins
13
14
15
6 hrs
HeLa

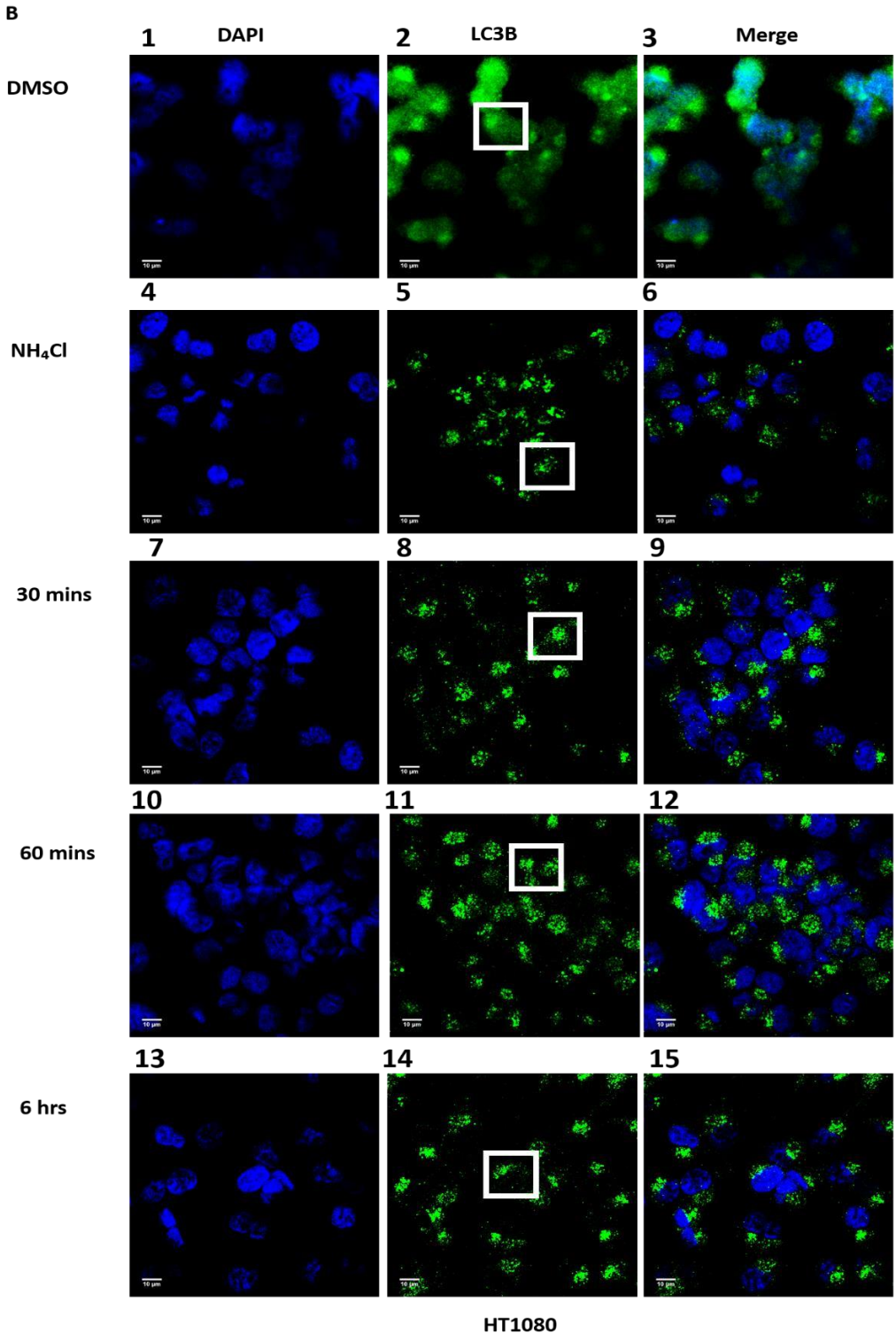

Figure 3.16: LC3B punctate formation increases with Tun treatment in HeLa cells HeLa (A) and HT1080 (B) cells were grown on coverslips, treated with either DMSO (panels 13), NH_4Cl (panels 4-6) or Tun for 30 mins (panels 7-9), 60 mins (panels 10-12) and 6 hrs (panels 13-15) prior to Immunofluorescence analysis. Anti-LC3B was used to stain cells (green) and DAPI was used to stain the nucleus (blue).

A. Punctate and little diffuse staining of LC3B was comparable throughout all treatments (panels 1 -15).

B. DMSO showed diffuse staining (panel 2-3, box) Punctate staining was comparable in all other treatments (panels 7-15). Boxes show pattern of LC3B staining.

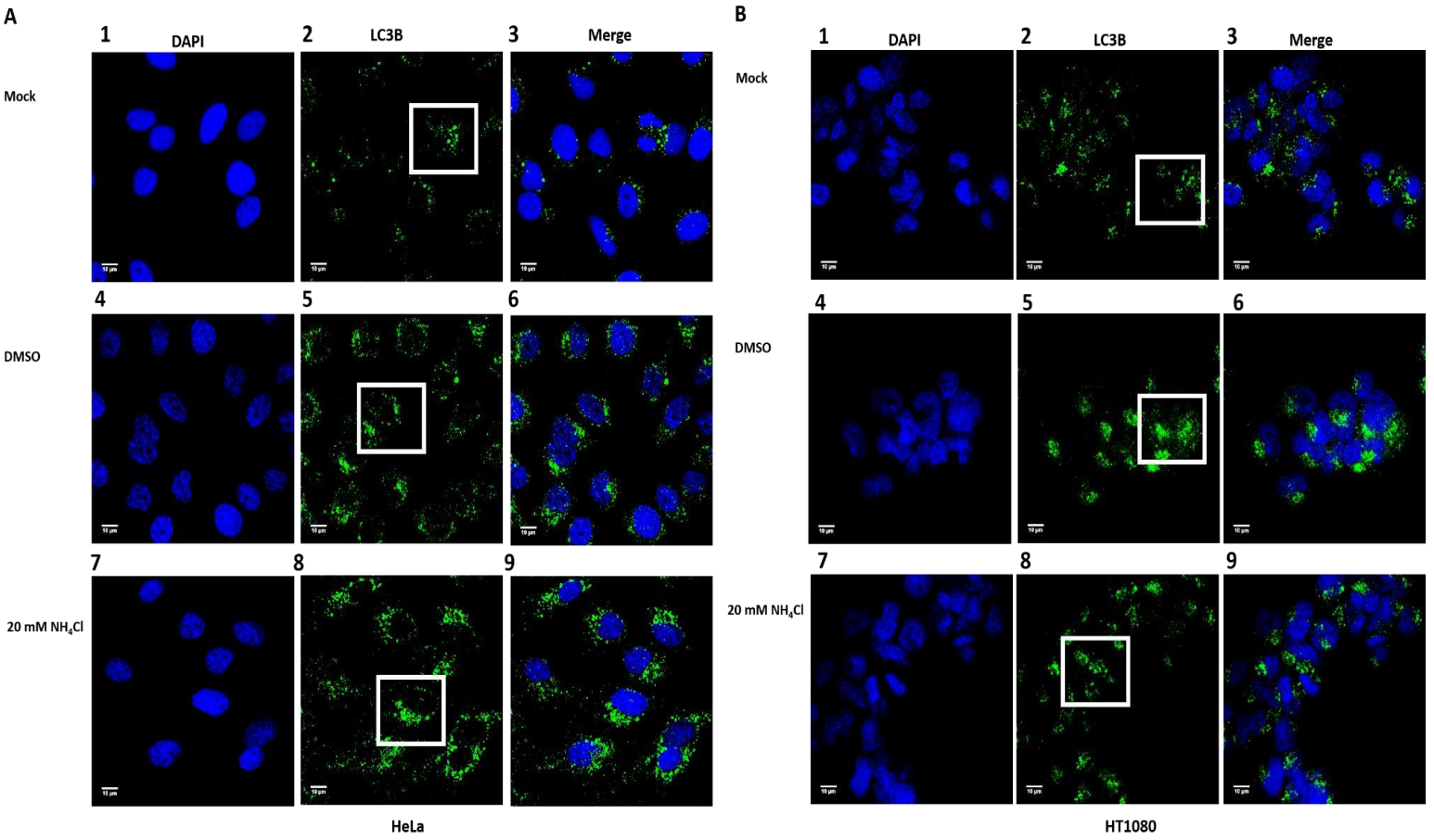

Figure 3.17 Analysis of LC3B dot formation in HT1080 and HeLa cells

HeLa (A) and HT1080 (B) cells were grown on coverslips, which were either mock (panels 1-3), DMSO (panels 4-6) or NH_4Cl (panels 7-9) treated prior to immunofluorescence analysis. Anti-LC3B antibody used to stain LC3B at 1:400 dilution (green) and DAPI was used to stain the nucleus (blue).

A. In HeLa cells, NH_4Cl showed more punctate and diffuse staining compared to mock (panels 2 and 3, boxes) and DMSO (panels 5 and 6, boxes) treated cells.

B. In HT1080 cells, mock (panels 1-3), DMSO (panels 4-6 boxes) and NH4Cl (panels 7-9, boxes) treated HT1080 cells all showed diffuse and punctate LC3B staining.

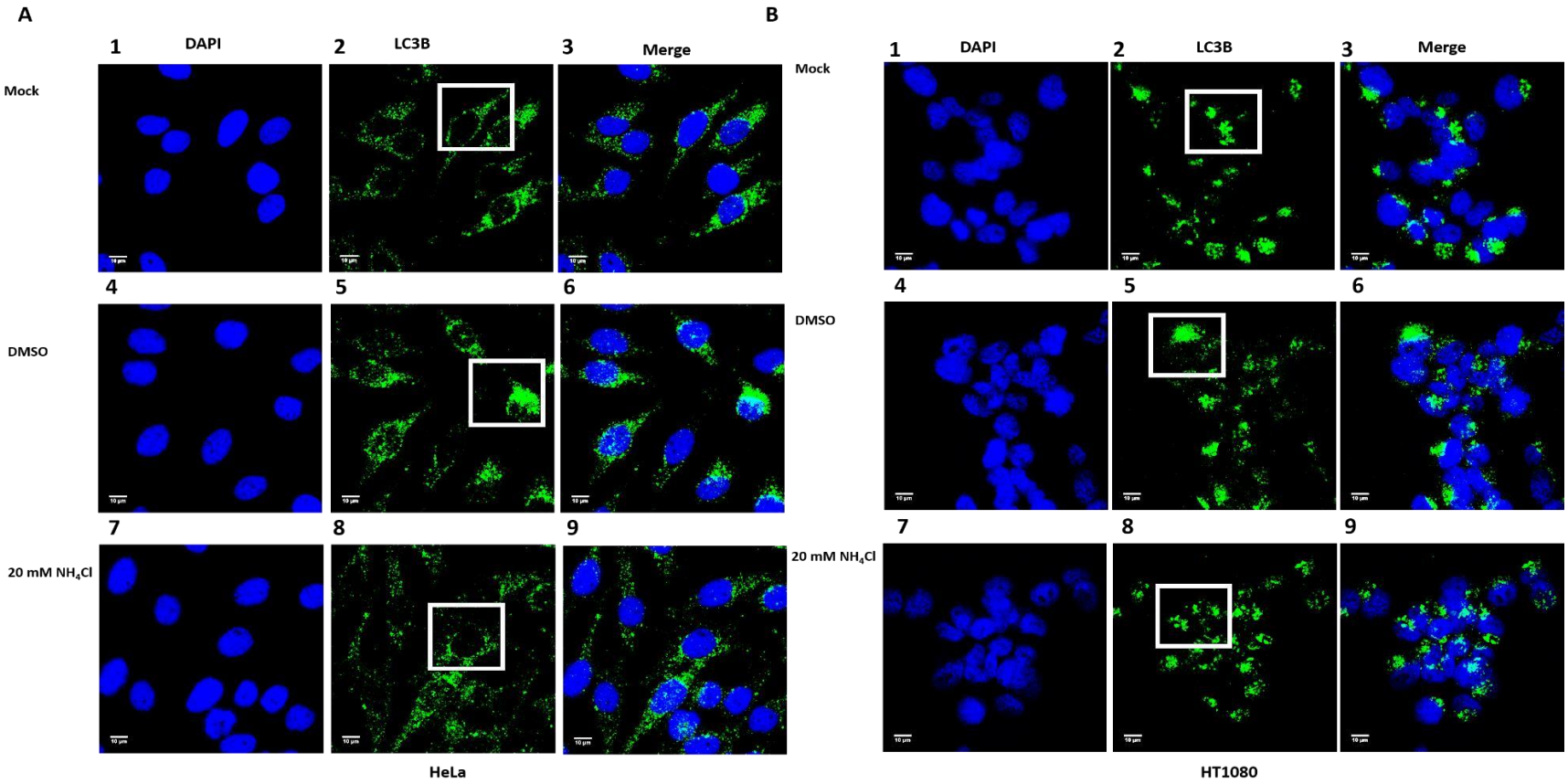

Figure 3.18: Increasing the concentration of anti-LC3B results in stronger staining

HeLa (A) and HT1080 (B) cells were grown on coverslips and treated with either mock treated (panels 1-3), DMSO (panels 4-6) or NH_4Cl (panels 7-9) prior to immunofluorescence analysis. Anti-LC3B antibody used to stain LC3B at 1:200 dilution (green) and DAPI was used to stain the nucleus (blue).
A. In HeLa cells, mock (panels 1-3) DMSO (panels 4-6) and NH_4Cl (panels 7-9) treated cells all showed comparable punctate staining (panels 2, 5 and 8, boxes).
B. In HT1080 cells, mock (panels 1-3), DMSO (panels 4-6) and NH_4Cl (panels 7-9) treated cells all showed diffuse and punctate staining which was comparable throughout all treatments (panels 2, 5, and 8, boxes).

With lysosomes being intrinsic components of autophagy, lysosome and autolysosome number and distribution were investigated in conjunction with the LC3B staining described above. In order to assess lysosome and ER behaviour concurrently, LysoTracker along with ERTracker dye uptake was optimised in
HeLa and HT1080 cells (Figure 3.19). Both cell types were initially incubated for 40 mins with the dyes and imaged every 20 minutes, using the Spinning Disk Confocal Laser microscope. In HeLa and HT1080 cells, the fluorescence intensity of Lysotracker stained cells was highest after ~ 60 mins and ~80 mins respectively. For ERTracker blue/white in HT1080 and HeLa cells, the fluorescence intensity was highest after ~120 mins, and ~80 mins, respectively (Figure 3.19B). Subsequent imaging experiments were undertaken under these conditions after chemical induction of ER stress.

HT1080 and HeLa cells were then incubated with ERTracker blue/white (120 mins HT1080 and 80 mins Hela) and Lysotracker (60 mins) dyes (as described in section 2.9) prior to treatment with tunicamycin. Live cells were then imaged for 18 hrs at 20 min intervals (Figure 3.20). In Hela cells, throughout the duration of imaging (excluding 18 hrs) punctae (red dots corresponding to lysosome and autolysosomes) remained localised to the ER region as evidenced by the overlapping of LysoTracker and ERTracker dyes (Figure 3.20A, panels 15-21, boxes). This was the same in HT1080 cells though in HT1080 cells punctae were clustered in a single region of the ER, in all cells as, opposed to random distribution as seen in HeLa cells (figure 3.20B, panels 15-21, boxes).

A

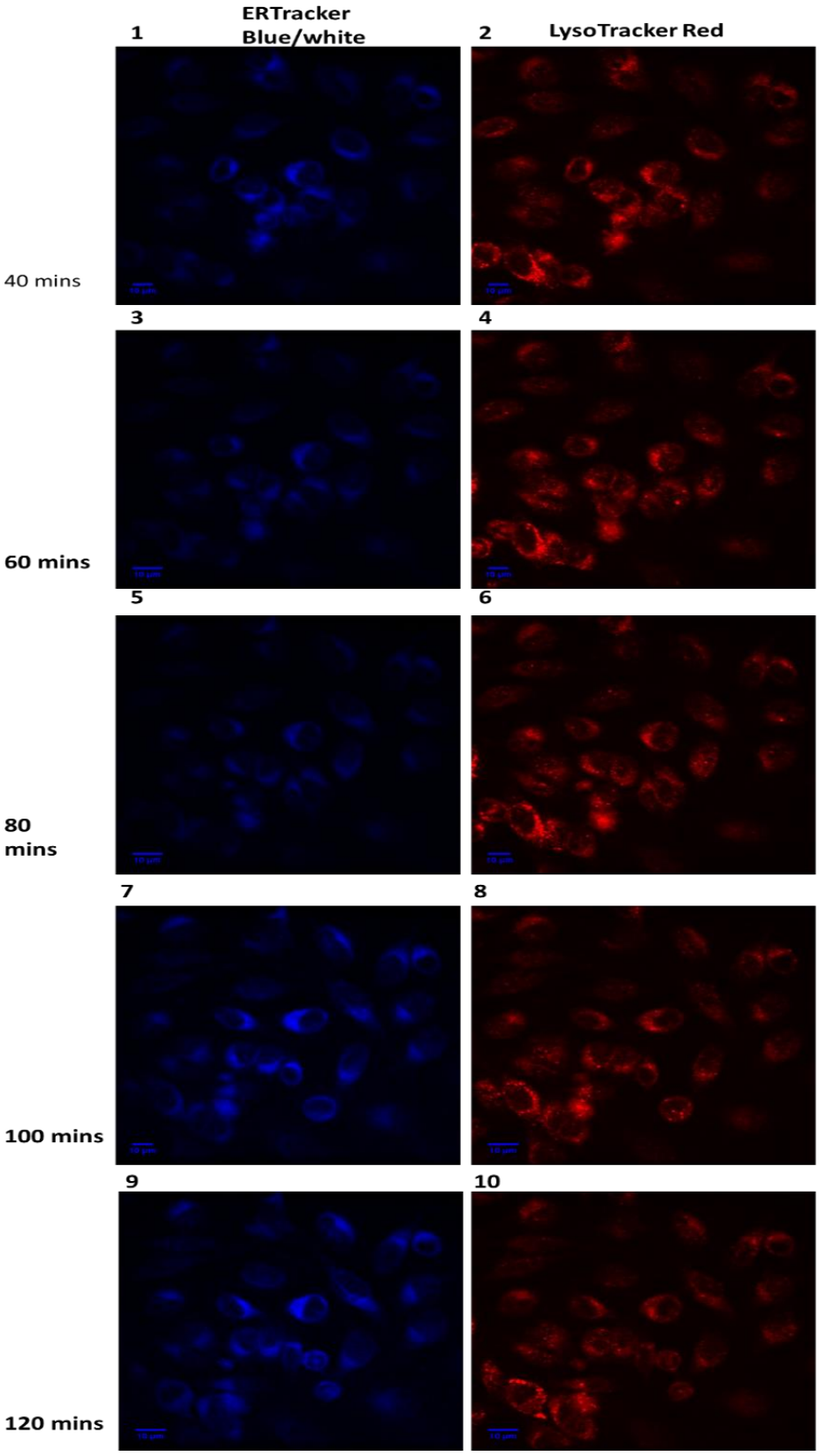
ERTracker
Blue/white
LysoTracker Red
1
2
40 mins
3
4
60 mins
5
6
80
mins
7
8
100 mins
9
10
120 mins

B

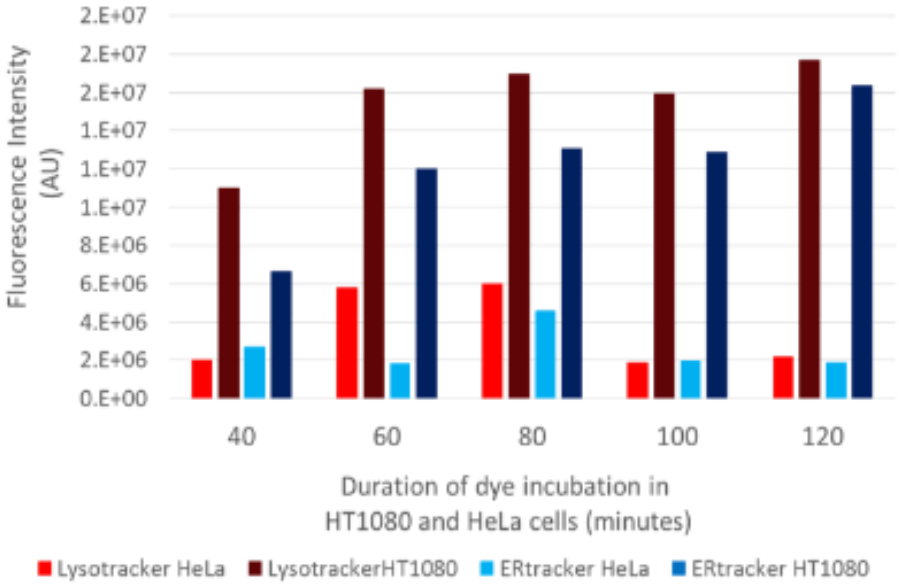

Figure 3.19: Optimisation of ER tracker and LysoTracker dyes

A. HeLa and HT1080 cells were incubated with ERTracker (1:1000) and LysoTracker (1:5000) dye for 40 mins prior to being imaged on Spinningdisk confocal under 5% $C0_2$ and 37^{o}C for 120 mins for 20 minute intervals.

B. Using ImageJ software, fluorescence intensity was measured in HeLa and HT1080 cells for ERTracker and LysoTracker. For HeLa cells intensity was highest at 80 mins and 60 mins for ERTracker blue/white and LysoTracker respectively and for HT1080 intensity was highest at 120 mins and around 80 mins respectively.

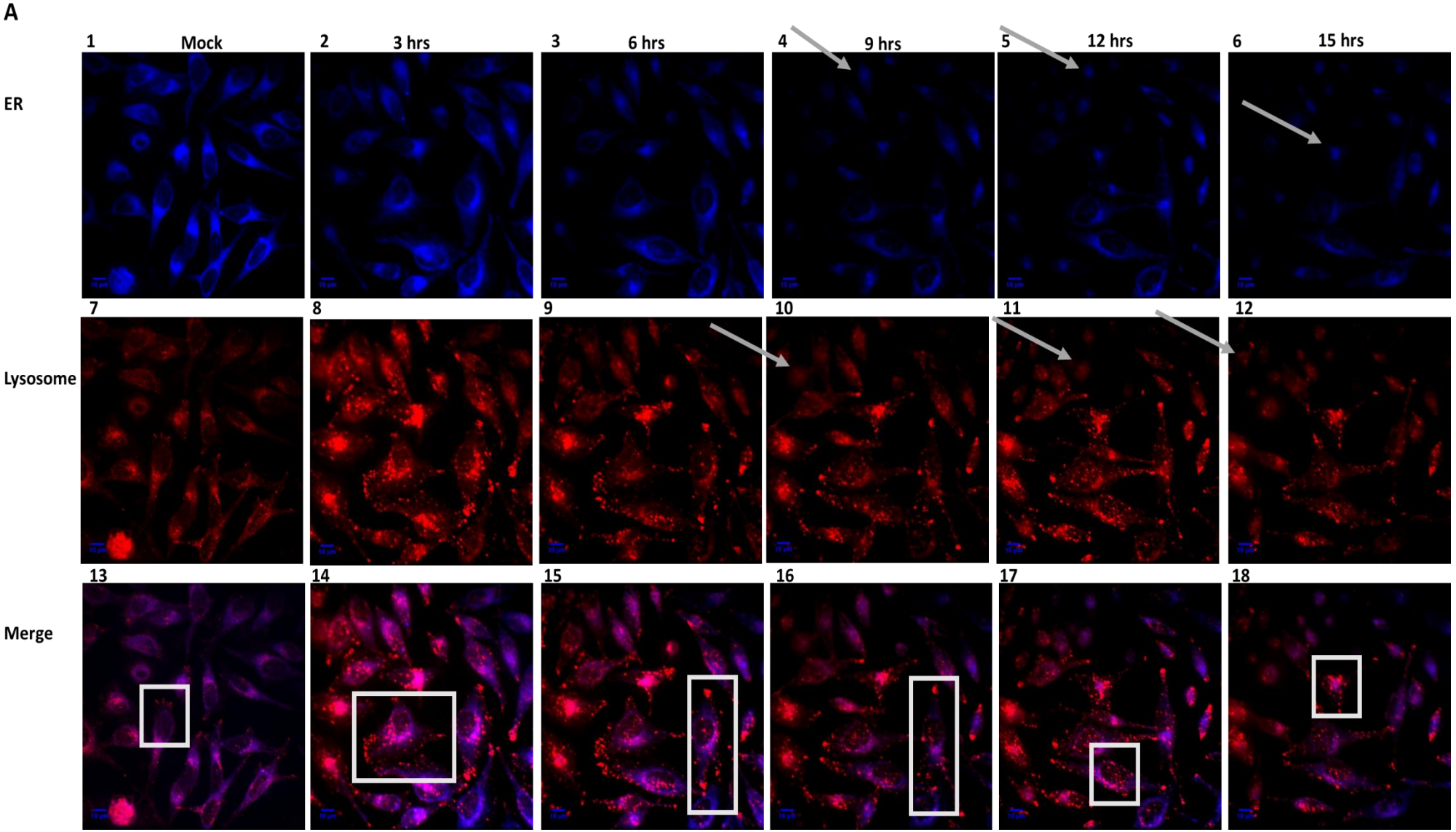
A
1
Mock
2
3 hrs
3
6 hrs
4
9 hrs
5
12 hrs
6
15 hrs
ER
7
8
9
10
11
12
Lysosome
13
14
15
16
17
18
Merge
HeLa

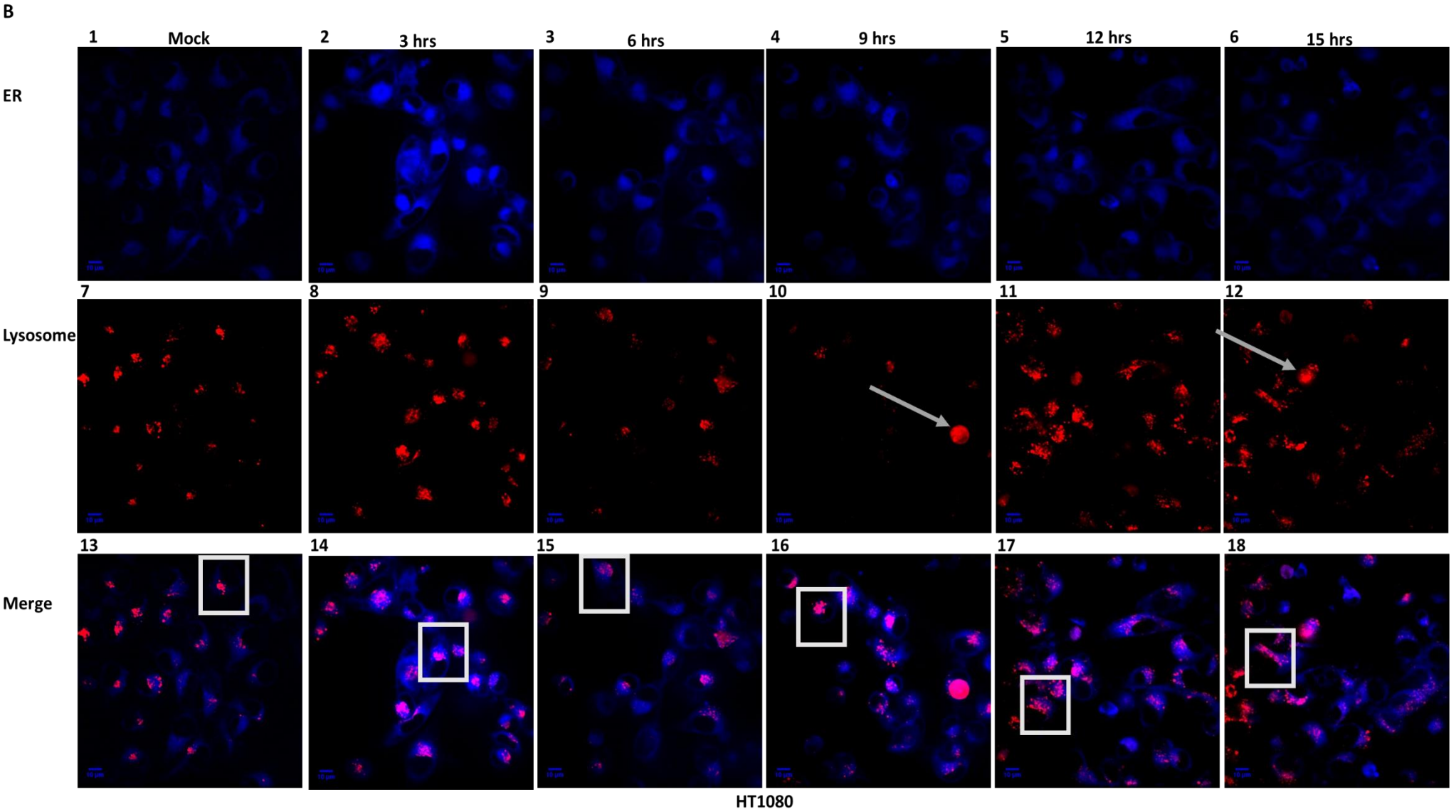
B
1
Mock
2
3 hrs
3
6 hrs
4
9 hrs
5
12 hrs
6
15 hrs
ER
7
8
9
10
11
12
Lysosome
13
14
15
16
17
18
Merge
HT1080

Figure 3.20: Lysosomal changes occur in HT1080 and Hela cells in response to tunicamycin induced ER stress

HeLa and HT1080 cells were incubated with ERTracker (1:1000) (blue) LysoTracker (red) dyes (1:5000) prior to imaging on spinningdisk confocal under 5% $C0_2$ and 37^{o}C for 18 hrs at 20 minute intervals. Right before imaging, cells were treated with tunicamycin.

A. In HeLa cells, with continued Tun treatment, punctate localisation remained throughout the ER region (panel 13-18, boxes). Cells began to round and detach from 6 hrs Tun treatment (panel 3-6, arrows).

B. In HT1080 cells, punctate localisation and distribution remained constant from 3 hrs to 15 hrs (panel 13-18, boxes).

The number of punctate structures in tunicamycin treated HeLa cells (figure 3.20A; panel 7-9, boxes and figure 3.21A) increased slightly from mock (which was considerably higher than HT1080 mock) to 3 hrs. From 6 hrs to 15 hrs Tun treatment, the number of punctate structures appeared to have decreased compared to mock treatment (figure 3.21A). In HT1080 cells, the number of punctate structures remained fairly constant up until 6hrs. From 12 hrs-15 hrs there was a spike in punctae number which then declined with extended tunicamycin treatment (figure 3.21A).

DTT was also used a positive control to see how lysosome number and distribution changed with ER stress. In HeLa cells, when compared to mock treated cells, punctae increased after 3 hrs DTT treatment (figure 3.21B). After 6 hrs, punctae number and distribution remained constant up until 12 hrs DTT treatment when the punctae structures began to cluster (figure 3.22A, panels 12-14, arrows). In HT1080 cells compared to mock treated cells, lysosomal number and distribution remained constant up until 15 hrs, when LysoTracker and ERTracker dyes began to fade. By 18 hrs no ERTracker fluorescence could be seen (figure 3.22B, panels 1-7).

Even though mock treated HT1080 and HeLa cells in figure 3.21B showed a higher number of punctate compared to mock treated cells in figure 3.21A (most probably due to slight differences in environmental stressors before ER stress treatments), these experiments suggested that lysosomal number and distribution were changing in response to tunicamycin and DTT treatments in both cell lines. As expected, in both HT1080 and HeLa cells, the number of punctae increased during early DTT treatment as seen in figure 3.21B. The punctate in both HeLa and HT1080 cells then clustered and cells detached following sustained DTT treatment (figure 3.22). In contrast, in tunicamycin treated HeLa cells, ER stained cells began to cluster and detach in a way that resembled cell death (figure 3.20A, panel 4-6, 10-12, arrows), this however was only evident in HeLa cells and not HT1080 cells, suggesting that in HeLa cells, there was an increase in autophagic pathway activation during early tunicamycin induced ER stress responses (figure 3.21A) compared to HT1080 cells where there was an increase in autophagic pathway activation during late tunicamycin ER stress responses (figure 3.21A).

A

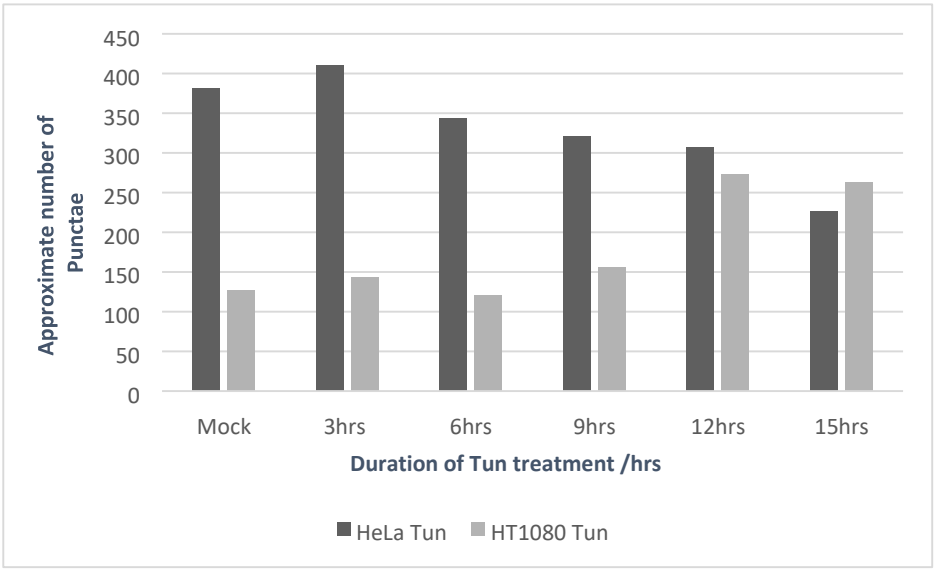

B

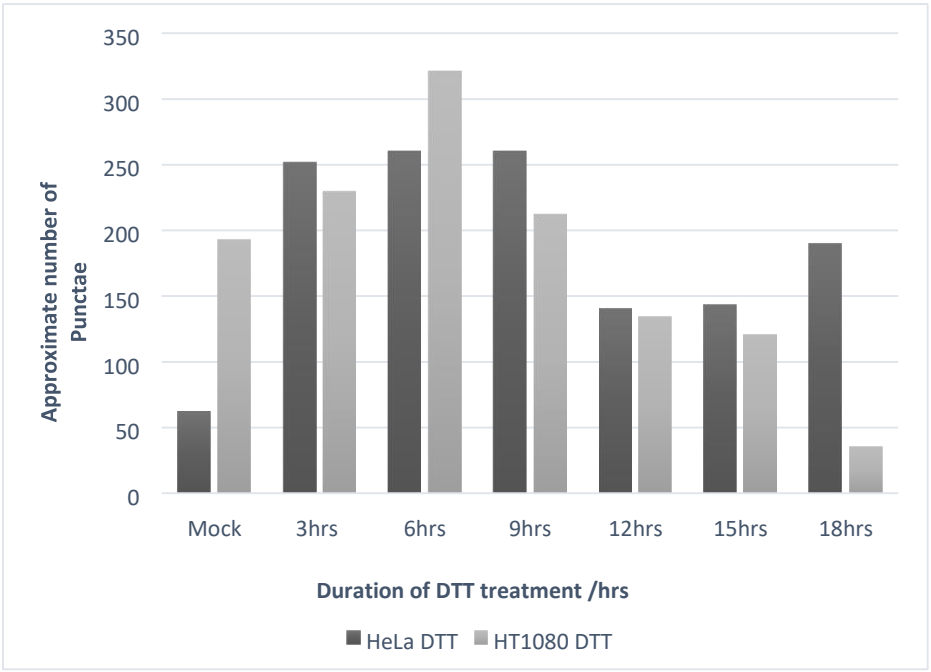

Figure 3.21: Changes to lysosomal punctae number during tunicamycin and DTT induced ER stress

A. Using ImageJ, the number of punctae were counted in HT1080 and HeLa cells treated with Tun for 15 hrs.

B. Using ImageJ, the number of punctae were counted in HT1080 and HeLa cells treated with DTT for 18 hrs.

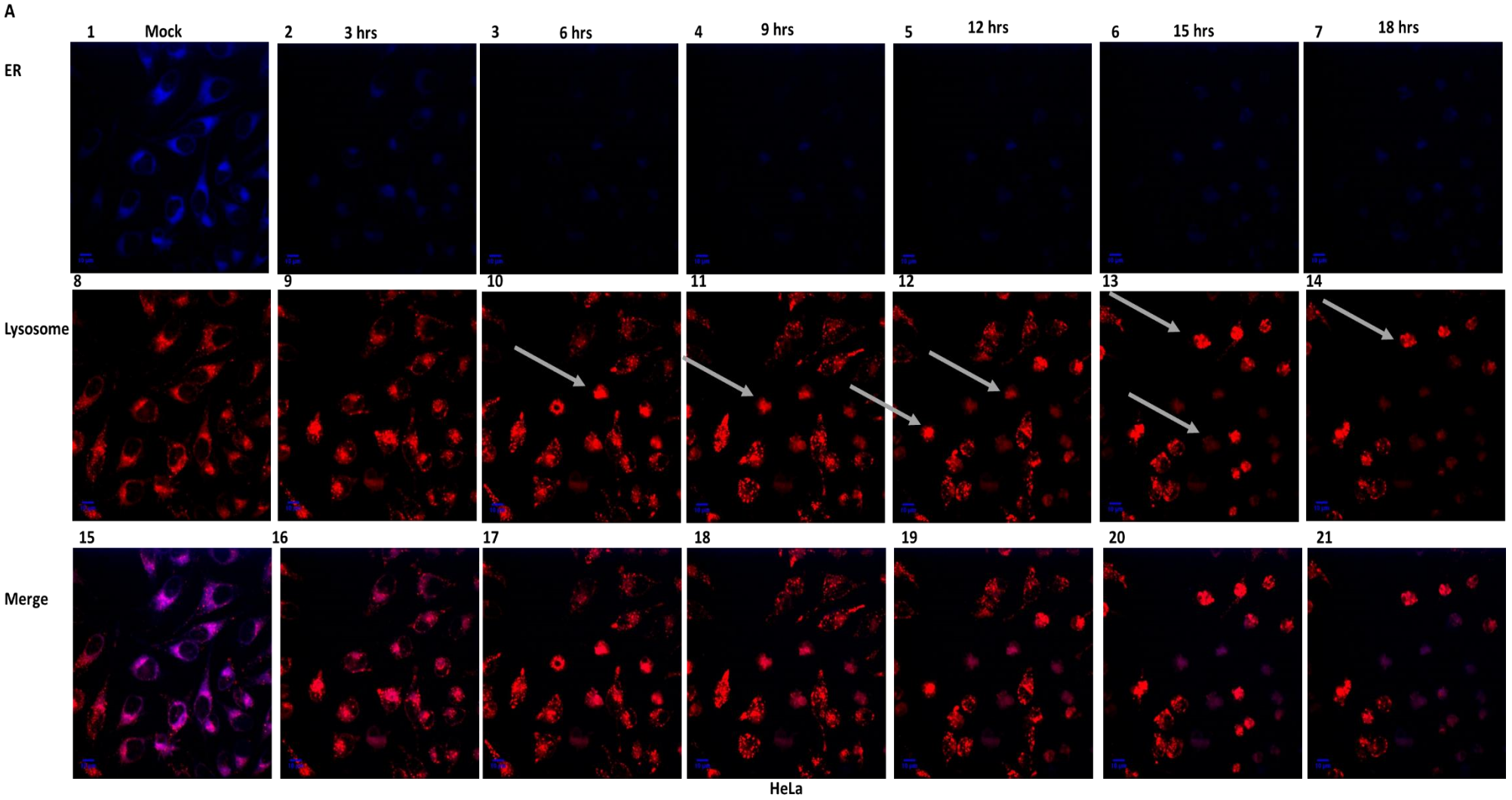
A
1 Mock
2 3 hrs
3 6 hrs
4 9 hrs
5 12 hrs
6 15 hrs
7 18 hrs
ER
8
9
10
11
12
13
14
Lysosome
15
16
17
18
19
20
21
Merge
HeLa

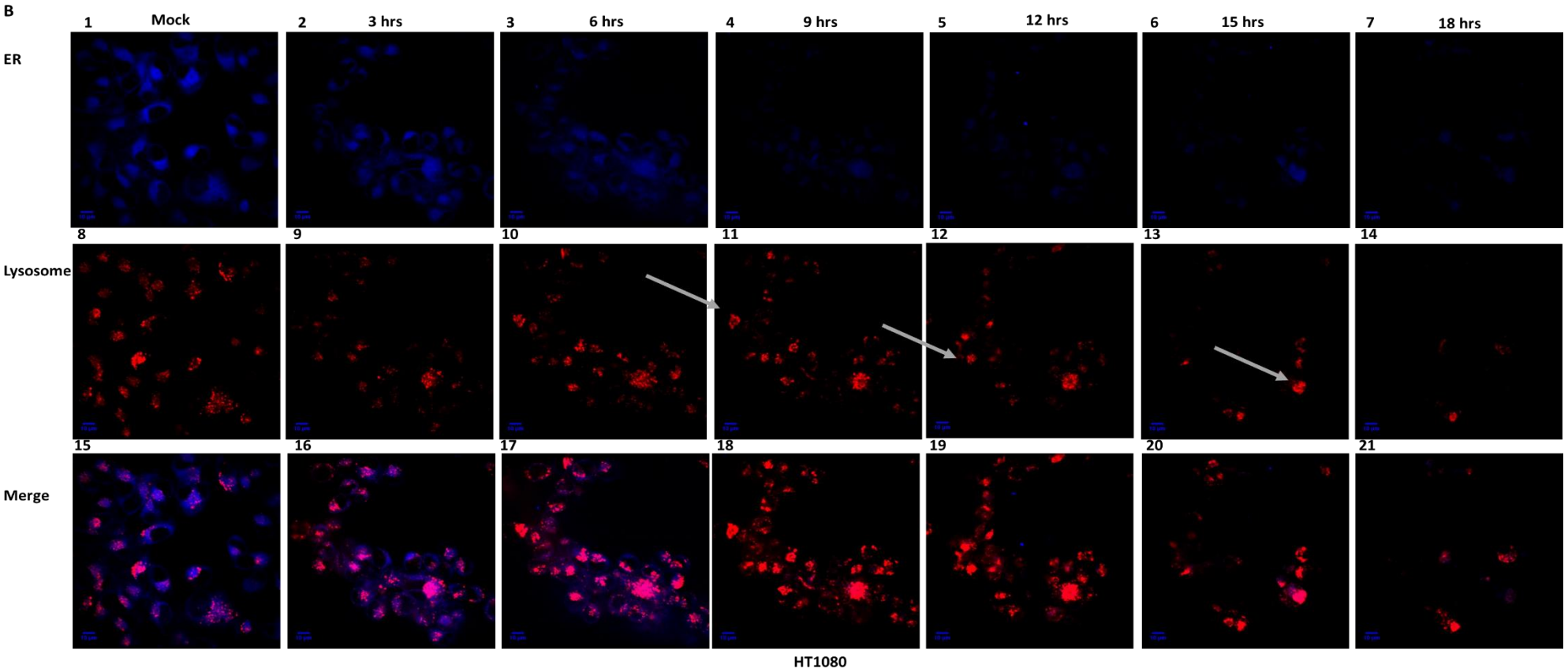

Figure 3.22: Lysosomal changes occur in HT1080 and Hela cells in response to DTT induced ER stress

HeLa (A) and HT1080 (B) cells were incubated with ERTracker (1:1000) (blue) and LysoTracker (1:5000) (red) dyes prior to imaging with the Spinningdisk confocal under 5% $C0_2$ and 37^{o}C for 18 hrs at 20 minute intervals. Right before imaging DTT was added.

A. In HeLa cells, punctae localization and distribution changed with treatment time. In mock treated cells, punctae were spread out in the cytoplasm whereas with DTT treatment from 6 hrs onwards, punctae began to cluster around the ER region (panels 10-14, arrows). ERTracker dye faded from 3 hrs onwards (panels 2-7).

B. In HT1080 cells, punctae localization and distribution did not change. Punctae localized to one region of the ER where they formed clusters (panels 11-13, arrows). ERTracker dye faded from 6 hrs onwards (panels 3-7).

3.2.3.3. Tunicamycin induced ER stress responses lead to the activation of cell death pathways.

Since signs of apoptosis were seen in previous experiments (figure 3.20A 4-6, 10-12 and figure 3.22). Caspase 9 (section 1.4) which is a component of the intrinsic cell death pathway and is involved in the activation of the caspase cascade leading to apoptosis (Li et. al. 1997) was investigated. Anti-Caspase 9 conditions were optimised using HeLa cells (figure 3.23). HeLa cells were treated with tunicamycin for 30 mins, 60 mins and 6 hrs and with DTT for 60 mins. Cells were lysed, and the lysates analysed by SDS-PAGE and western blotting. Initial investigations using 10 µg/µl protein and 1:1000 anti-caspase 9 resulted in the detection of a band at ~47kDa, likely corresponding to procaspase 9 (Figure 24, panel A). However, no bands representing the two catalytically active large cleavage products of procaspase 9 were detected, which were expected at 37kDa and 35kDa (Zou et. al. 2002). Following this experiment, the protein load was increased to 20 µg/µl and the anti-caspase 9 dilution kept constant. This modification to the protocol resulted in the detection of a band at 47kDa along with bands at 37kDa and ~30kDa (figure 3.23, panel B, arrows) so subsequent experiments were conducted using these conditions. Figure 3.23C shows a representative blot for β-actin which was used as a loading control and shows unequal loading.

A comparison of caspase 9 activation was then conducted in HT1080 and HeLa cells that were subjected to ER stress (figure 3.24). Although the β-actin control indicated that there was protein present in the HT1080 lysates, full length caspase 9 could be detected only weakly in HT1080 cells. Similarly the 37kDa cleaved caspase 9 product was also not detected in stressed HT1080 cells (Figure 3.24A, lanes 1-5, arrows). In HeLa cells, full length caspase 9 could be detected (Figure 3.24, lanes 6-10) and the band at 47kDa increased with tunicamycin and DTT treatment. A doublet band at approximately 37kDa was also seen at 6 hrs tunicamycin and a single band also at 37kDa (figure 3.24 panel A, lane 10, arrows). Although for HeLa cells, the β-actin control indicated that more protein was loaded for the 60 mins DTT and 6 hr tunicamycin treated samples, it was apparent from the ~30 kDa cleavage product of caspase 9 that apoptotic caspase activity was induced in the chronically ER stressed HeLa cells (figure 3.24A, lanes 9-10).

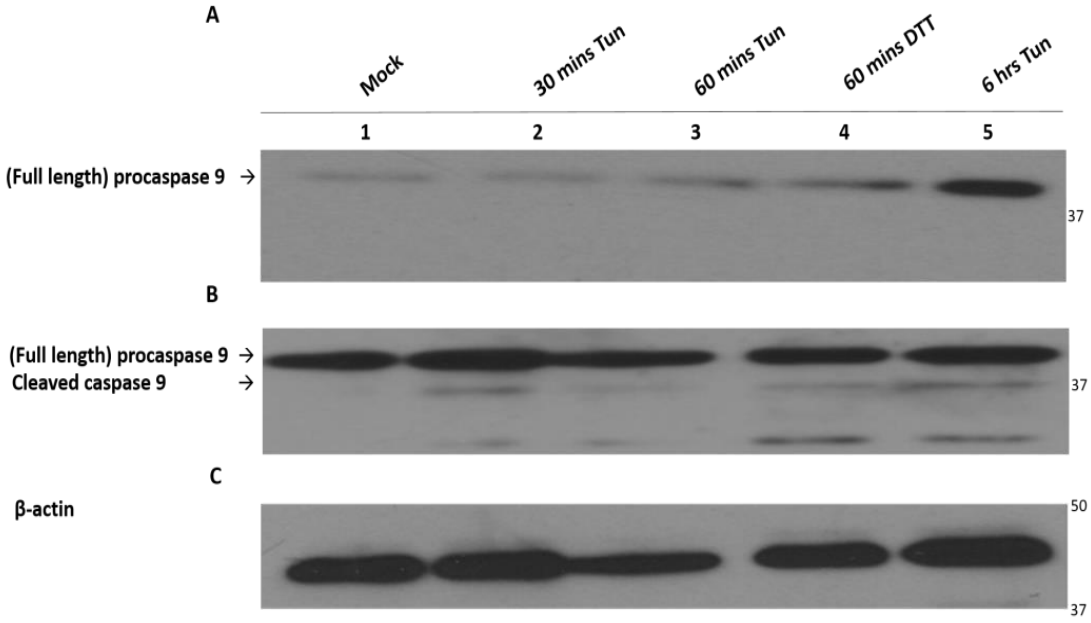

Figure 3.23: Optimisation of anti-Caspase 9 antibody conditions

HeLa cells were either mock treated or treated with Tun for 30 mins (lane 2), 60 mins (lane 3) and 6 hrs (lane 5) or with DTT for 60 mins (lane 4) prior to lysis in RIPA lysis buffer and subsequent analysis by SDS-PAGE and Western blotting. Anti-caspase 9 was used to probe for caspase 9 (panels A and B).

A. Blot of 10 µg of protein using 1:1000 anti-Caspase 9 dilution. 6 hrs treated procaspase 9 band showed higher intensity compared to others and no cleaved caspase 9 bands could be seen.

B. Blot of 20µg of protein using 1:1000 anti-Caspase 9 dilution. There was strong procaspase 9 expression and cleaved caspase 9 products detected at 37 kDa and 47kDa.

C. β- actin was used as a loading control which does not show equal loading.

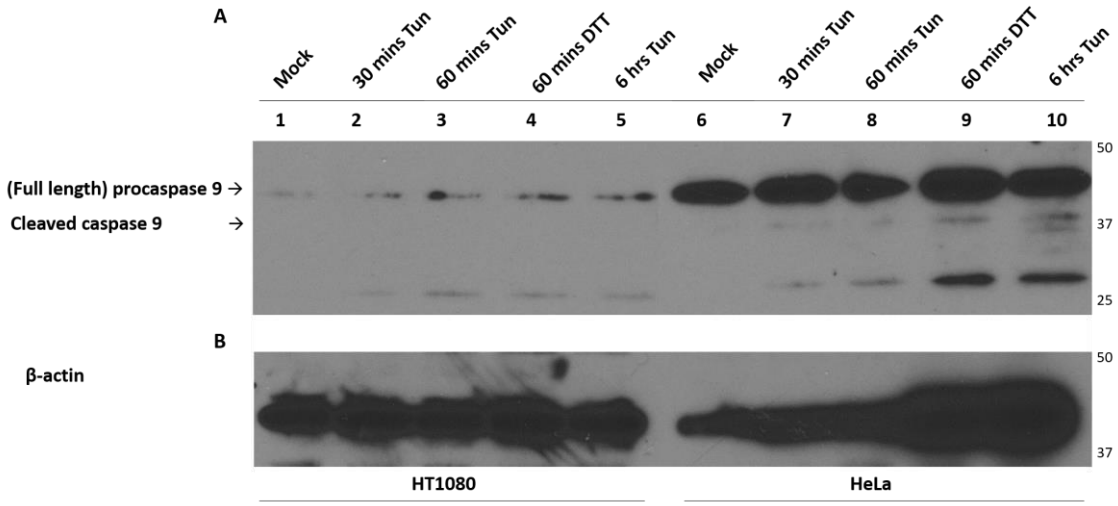

Figure 3.24: Comparison of Caspase 9 activation in HeLa and HT1080 cells

HeLa cells and HT1080 cells were either mock treated (lanes 1, 6) or treated with Tun for 30 mins (lane 2 and 7), 60 mins (lane 3 and 8) and 6 hrs (lane 5 and 10) or DTT for 60 mins (lane 4 and 9) prior to lysis and subsequent analysis by SDS-PAGE and Western blotting). Anti-caspase 9 was used to probe for caspase 9 (panel A).

A. HT1080 cells showed little procaspase 9 and no caspase 9 cleavage products were detected, even though procaspase 9 expression increased from 30 mins to 6 hrs Tun treatment (lanes 1-5). Procaspase 9 and caspase 9 (arrows) cleavage products could be detected in HeLa cells from 30 mins Tun treatment. The band density was very low but had increased by 6 hrs Tun treatment (lane 10). The band density was also increased with early DTT treatment (lane 9)

B. β-actin was used as a loading control and indicated that more protein was loaded for the 60 mins DTT and 6 Hr Tun treated HeLa samples (lanes 9-10).

3.3. Discussion

The experiments described in this chapter have shown that i) the dynamic nature of the ER, differs between HT10080 and HeLa cells (figure 3.5). ii) tunicamycin induced ER stress induces autophagic responses at different times in different cells (figure 3.20A, 3.21A) and iii) that HT1080 cells are better equipped to deal with tunicamycin induced ER stress as evidenced by late autophagy onset (figure 3.20B, 3.21B) and little apoptosis activation during early and late tunicamycin induced ER stress responses (figure 3.24A).

As reviewed in the introduction, the UPR has three branches the PERK, ATF6 and IRE1 branches (section 1.3) that when activated, have been shown to induce several different downstream events, including pro-survival pathways and apoptotic pathways that often lead to the same response. A comparative study using two different cell lines, HeLa and HT1080 cells was performed to elucidate if and when the UPR activates pro-survival (macroautophagy (section 1.4.1) and pro-apoptotic pathways (intrinsic pathway (section 1.4.2.) in response to ER stress and if there are any differences between UPR activation of said pathways and what these differences are.

Since ER morphology is linked with ER function during normal and stress responses (section 1.1), ER morphology was investigated to give an indication of whether ER membrane expansion could be visualised during ER stress responses for both HeLa and HT1080 cells. Even though prominent tubular/sheet like structures were seen in both cell lines (figure 3.5A-B, panels 14, 17, arrows) which suggested that there was an increase in ER remodelling and therefore ER membrane expansion, no significant differences in ER membrane expansion in both HeLa and HT1080 cells during early tunicamycin induced ER stress (figure 3.4). Similar studies that can be found in the literature include a study in yeast by Schuck et. al. which found that ER membranes expanded with both tunicamycin and DTT treatment during early stress responses (Schuck et.al. 2009). However, in mammalian cells, ER membrane remodelling triggered by apogossypol (a BCL2 antagonist) appeared to be largely independent of the UPR (Urra and Hetz 2012).

An observation that was of interest was that in HT1080 cells, there were clearly visible tubular/sheet structures seen in both control and tunicamycin treated cells as early as 0.5 hrs (figure 3.5A, panel 4, 5, arrows). A study by Lu et. al. has visualised the organization of ER cisternae during mitosis. They demonstrated that, tubular and cisternal networks were either extended and prominent (e.g. during interphase) or absent (e.g. during anaphase and telophase) which is in line with results seen in figure 3.5 and may explain the presence of distinct ER sheets/tubular structures in the DMSO control ER at specific points of the cell cycle (Lu et. al. 2009). It has also been demonstrated that the UPR inhibits cell cycle progression (Brewer et. al. 1999), which was also suggested by figure 3.5, (HT1080 DTT, 0.5 hrs onwards) where a cell appears to be frozen in telophase (figure 3.5, panel 6 and 12, T). So, taking the results in table 3.1 (specifically the number of cell divisions) into consideration, it can be postulated that the appearance of the tubular/sheet structures that were seen in tunicamycin treated HT1080 ER are a response to ER stress and not cell division. Note that cells which showed obvious signs of mitosis where not included when measuring ER membrane area (figure 3.5). However, a potential limitation to the dynamic imaging results presented in this thesis could be the imprecise identification of the different mitotic stages. For future experiments the precise identification of the mitotic stages could be helped by co-staining cells with ERTracker and a nontoxic cell permeable nuclear dye such as Hoechst 33342.

In the work presented in this thesis, steps were taken to ensure cell health throughout imaging; for example temperature was kept at 37^{o}C and fluctuations in temperature were prevented as the microscope was encased in a glass box. pH and humidity (approximately 95%) were kept constant by placing cells under a tightly sealed chamber. Oxygenation and osmolality were also kept constant. However, as evidenced by results shown in figure 3.1 and 3.3, problems were encountered with ERTracker green labelled control cells, where autofluorescence from the medium and exposure to the laser during imaging both presented problems. In some experiments, this resulted in the death of cells, so in future experiments, to avoid high background, ERTracker green can be used alongside a phenol red free medium to reduce autofluorescence.

Another potential limitation with regards to live cell imaging was the use of ERTracker blue/white, whose excitation is around 374nm. The dye can also be excited with a long

pass DAPI filter, which is relatively close to the UV light wavelength of 280-320 nm, which is known to induce DNA damage that can lead to cell death (Nakajima et. al. 2004). Thus both increased laser power and prolonged exposure to UV light have the potential to significantly affect cell health and therefore influence cellular events by potentially activating heat shock proteins and/or DNA damage response pathways. So decreasing the laser power and choosing alternative wavelengths for imaging would help in maintaining cell health and would also help to prevent photobleaching. The above limitations and complications of live cell imaging were taken into consideration in this thesis. ERTracker blue/white probed cells were i) imaged at a lower laser power and ii) exposed to the laser for shorter periods , which significantly improved cell health (data not shown).

Having established appropriate imaging parameters and controls, it was concluded that the drastic changes seen in ER morphology (figure 3.5 panels 20, 23, arrows) (which were suggestive of apoptosis) were due to tunicamycin treatment and that because HT1080 cells exhibited morphological changes earlier when compared to HeLa cells, it was concluded that HT1080 cells responded more rapidly to ER stress responses which suggested that HT1080 cells were more sensitive to tunicamycin. This was of interest because it showed that morphological changes occur even when changes to the glycosylation of MHC class I heavy chain pool cannot be observed (figure 3.5, figure 3.6).

Comparative investigations of cell survival and cell death at a molecular level yielded intriguing results. Although it was shown that JNK isoforms were constitutively expressed in both cell types (figure 3.9 and 3.10) the activation of upstream components of the UPR, specifically P-JNK and P-ASK in both cell types, were difficult to assess. Adding to this, there was also little to no PERK expression detectable in both cell types using the anti-PERK antibody, despite the fact that PERK has been shown to be expressed in both cell types (Dey et. al.2015, Mounir et. al. 2011 and Okada et. al. 2003). Thus antibody conditions may require further optimization, perhaps increasing the amount of protein loaded, including a tissue control or increasing antibody concentration, in order to facilitate further PERK analysis.

Next, the IRE1 branch, specifically the activation of the ASK-JNK pathway, was investigated. Though ASK1 activation itself was not detected, investigations into ASK expression yielded interesting results. There was a sharp band detected at approximately 60-75kDa which interestingly was only seen in HeLa cells (figure 3.8B lanes 6-10). Though the existence of this 60-75kDa band could not be confirmed from the published literature. Additional bands seen at 39kDa and 50kDa (data not shown) did corroborate findings by Stordal and Davey 2008 who also detected these endogenous ASK1 bands in several different human cell types (H69, U87-MG and HUVEC cells). Their data indicates that endogenous ASK1 is processed in a proteasome independent manner (Stordal and Davey 2008). However, they did not detect the approximately 60-75kDa band, suggesting that ASK1 processing may be different in HeLa and HT1080 cells and that this could result in different outcomes to some types of ER stress.

Since the anti-ASK1 antibody used in the work presented in this thesis is specific for amino acids surrounding amino acid 280, it was deduced that this truncated ASK1 seen in figure 3.8B may be part of the N-terminal region of full length ASK1. Several studies have observed the activities of N-terminal of AKS1; for example, Saitoh et. al. (1998) who observed that when thioredoxin associated with the constitutively expressed N-terminal fragment of ASK1, ASK1 kinase activity and ASK1 dependent apoptosis were inhibited. This study also found that some truncated forms of ASK1 had higher basal kinase activity compared to full length ASK1 (Saitoh et. al. 1998). These experiments suggest that under normal *in vivo* conditions, truncated ASK1 fragments, such as the 39 and 50 kDa fragments may have important biological functions. Taking this into consideration, many questions are raised by the detection of this 60-75kDa HeLa cell specific band in the experiments shown in this thesis. Although the truncation product is known to include the N-terminal domain, what other domains does it have? Are these domains regulatory or do they have catalytic activity? What are the possible roles (apoptosis, inflammation) and is it restricted to Hela cells? Mass spectrometry can be carried out to investigate this further.

Autophagy is a very dynamic and complex process with multiple steps that are regulated by various molecules including ATG14L and LC3B which mediate

autophagosome formation (section 1.4.1). For the experiments conducted in this thesis, activation of autophagic pathways rather than autophagic flux was investigated by monitoring the processing of LC3B. Many studies have also used LC3B as a measure of autophagy and have demonstrated that pro-LC3B and LC3B-I are in a diffuse state when not conjugated to PE, however when PE is conjugated onto LC3B-I to form LC3B-II and incorporated into the autophagosome membrane, LC3B staining is punctate (Gossner et. al. 2007, Liu et. al. 2015). However, though the activation of autophagy was seen in both cell types under tunicamycin induced ER stress (figure 3.15A panels 2 and 6 and figure 3.16B panels 2-15) in the experiments presented in this thesis, LC3B-I diffuse staining was difficult to visualise (figure 3.16A-3.18). Even investigations into autophagy activation by analysing lysosomal behaviour had its limitations. LysoTracker Red stains all acidic compartments which includes endosomes, lysosomes and autolysosomes meaning Lysotracker Red is not specific to autolysosomes making it difficult to quantify results for macroautophagy activation and the subsequent behaviour of lysosomes. However, interpretation of LysoTracker results in conjunction with the western blot data gives a clearer picture.

Taken together, the results gained from molecular studies and localisation and distribution studies suggested that HT1080 cells activated autophagic responses during late tunicamycin induced ER stress compared to HeLa cells which activated autophagic pathways during early tunicamycin induced ER stress responses (figures 3.14, 3.15, 3.16, 3.20 and 3.21A). HT1080 cells showed no cell death characteristics during early tunicamycin induced stress responses but instead showed sustained acidic compartment staining (figure 3.20B panels 7-12). However, this was inconsistent with results seen in figure 3.5 panels 23, 29 and 34 which showed apoptotic features during late tunicamycin induced ER stress responses in HT1080 cells. Since the only difference was an increased exposure to laser power, it was concluded that tunicamycin sensitizes cells to apoptosis when they are exposed to high laser powers for long durations. However the same was not true for HeLa cells treated with tunicamycin in figures 3.5 and figure 3.20. Compared to HT1080 cells, HeLa cells showed apoptotic characteristics during late tunicamycin treatment (figure 3.5), even when exposed to laser power for a shorter period of time (figure 3.20) suggesting that perhaps HeLa cells are not as well equipped to deal with tunicamycin induced ER stress when compared to HT1080 cells. The resilience of HT1080 cells to stress can be

corroborated by a recent study by Dey et. al. 2015. This study demonstrated that HT1080 which are highly metastatic cells, are able to survive the harsh circulatory system environment and evade anoikis (a form of cell death which results from a cell losing contact with the extracellular matrix) by activating autophagic responses which were sustained for as long as 48 hrs with no significant amount of apoptosis (Dey et. al. 2015). Moving forward with the data presented in this thesis, a more detailed comparison of HT080 and HeLa cell death pathway activation is required.

The experiments in Figure 3.24 suggested that HT1080 cells did not show caspase 9 cleavage during late tunicamycin induced ER stress responses, whereas HeLa cells showed caspase 9 cleavage during early tunicamycin induced ER stress responses, adding weight to previous suggestions that HT1080 cells have a high capacity to dealing with ER stress. Studies by Malladi et. al. have shown that once procaspase 9 has been processed to the active caspase 9 form, caspase 9 quickly losses its affinity for the apoptosome and pro-caspase 9 binds instead (Malladi et. al. 2009), so studying downstream components of the apoptotic pathway such as caspase 3 would give a better indication of significant apoptosis initiation.

4. Tyrosine Phosphorylation in Responses to Tunicamycin Induced ER Stress in Different Human Cell Lines

4.1. Introduction

Tyrosine kinase signalling, which involves the addition of a phosphate group onto tyrosine residues of target proteins, regulates numerous cellular events ranging from cell proliferation, differentiation, metabolism, apoptosis (Schlessinger and Ullrich 1992) and also inflammatory responses through the regulation and activation of immune cells such as B cells (de Lavallade et. al. 2013) T cells (Cooke et. al. 1991) and macrophages (Chen et. al. 2012). Tyrosine kinase signalling has also been shown by multiple studies to be involved in UPR stress responses, for example, endothelial growth factor receptor tyrosine kinase is involved in BiP induction (Cao et. al. 1995) and PERK tyrosine kinase activity in response to ER stress (Su et. al. 2007).

Recent studies have indicated that Th17 immune responses may contribute to disease progression in AS, with a recent study by Wright et. al. demonstrating that the plasma and spinal fluid of AS patients had extremely elevated levels of Th17 cell associated cytokines IL-6 and IL-23 (Wright et. al. 2015). These cytokines had previously been shown to promote the differentiation of Th17 cells through the signal transducer and activator of transcription 3 (STAT3) (Mathur et. al. 2007, Yang et. al. 2007), which is essential for Th17 cell differentiation and function (Asakawa et. al. 2015). STAT3, a transcription factor that is partly tyrosine phosphorylated in response to numerous molecules including IL-6 and EGF (Asakana et. al. 2015, Zhong et. al. 1994) has recently been linked to the UPR and inflammation by Meares et. al. (Meares et. al. 2014). These authors demonstrated that through PERK dependent pathways, the JAK1-dependent activation of STAT3 corresponded with ER stress responses in a variety of cell lines and that STAT3 activation was required for a robust ER stress induced inflammatory response, even though NFkB responses were also elicited. All this together suggests a possible role for STAT3 in AS pathogenesis.

Interestingly, studies have shown that genistein, a tyrosine kinase inhibiter (Akiyama et.al. 1987) is not only able to inhibit cell-mediated inflammatory responses (Verdrengh et. al. 2003) but is also able to inhibit the phosphorylation of STAT3 (Yu et. al. 2003). Altogether,

the studies presented here suggest that the targeting of tyrosine kinases may be a potential therapeutic avenue for intervening in inflammatory diseases such as AS.

An extensive comparative study of tyrosine kinase signalling has not been undertaken, so the work in this chapter endeavoured to identify global tyrosine kinases activity during ER stress responses, determine if there are differences between cell types and what these differences are, with the aim of discovering potential therapeutic targets.

4.2. Results

4.2.1. Tyrosine phosphorylation mediated responses in tunicamycin induced ER stress responses

To investigate the effects of tyrosine kinase activity (i.e. identify tyrosine phosphorylated proteins) during early and late tunicamycin induced stress responses, the anti-phosphotyrosine p-Tyr 100 antibody was used to i) observe differences between tyrosine kinase signalling between cells and ii) identify possible targets for future in depth characterisation. Both HT1080 and HeLa cells were treated with tunicamycin for 30 mins, 60 mins and 6 hrs and with DTT for 60 mins and processed as described in section 2.4-2.7. In both HT1080 and HeLa cells, tunicamycin induced ER stress resulted in tyrosine phosphorylation on multiple proteins in both early and late responses.

In HT1080 cells, changes in tyrosine phosphorylation were visible at approximately 48kDa, 40kDa, 38kDa, 30kDa and 22kDa (figure 4.1, panel A, lanes 1-5). At approximately 48kDa, band intensity fluctuated throughout tunicamycin treatment. At 30 mins the intensity of the ~48kDa band increased however by 60 mins the band had decreased and finally at 6 hrs tunicamycin treatment, the band intensity had increased again (figure 4.1, panel A, lanes 2, 3, 5). The 60 mins DTT control sample also showed increased band intensity compared to mock treated cells (figure 4.1, panel A, lane 1, 4).

The doublet bands at approximately 38kDa and 40kDa showed an increased band intensity at 30 mins and at 6 hrs tunicamycin treatment had increased further (figure 4.1, panel A, lanes 2, 5, arrows). DTT control band intensity also increased compared to mock treated cells and was comparable to 6 hrs tunicamycin treated band (figure 4.1, panel A,

lanes 1, 3, 5, arrows). At ~30kDa, no band was seen with mock treatment (figure 4.1, panel A, lane 1), however at 30 mins, 60 mins and 6 hrs tunicamycin treatment increased this 30kDa band (figure 4.1, panel A, lanes 2, 3, 5, arrows). At ~ 22kDa, band intensity increased at 30 mins compared to mock (figure 4.1, panel A, lanes 1, 2) with the highest band density seen at 60 mins (Figure 4.1 panel A, lane 3), however this then decreased at 6 hrs tunicamycin treatment (figure 4.1 panel A, lane 5). The DTT control band intensity also increased compared to mock treated cells (figure.4.1A, lane 4), with the β-actin loading control demonstrating equal loading (figure. 4.1A). This suggested that in HT1080 cells, tyrosine phosphorylation was involved in both early and late ER stress responses and together (figure.4.1, panels A, B), this data suggested that the phosphotyrosine proteome differed between HT1080 and HeLa cells in response to ER stress.

In HeLa cells, as indicated by various arrows, band intensity increased at ~ 80kDa, 75kDa, 50kDa, 37kDa, 30kDa and 10kDa corresponding to phosphorylation of proteins by tyrosine kinases (figure 4.1B). For the band at approximately 80kDa, density peaked at 30 mins (figure 4.1, panel B, lane 2, arrows) but then decreased from 60 mins until 6 hrs (figure 4.1, panel A, lanes 3 and 5). This observation suggested that this specific protein was phosphorylated during the early stress response and then dephosphorylated during late ER stress responses.

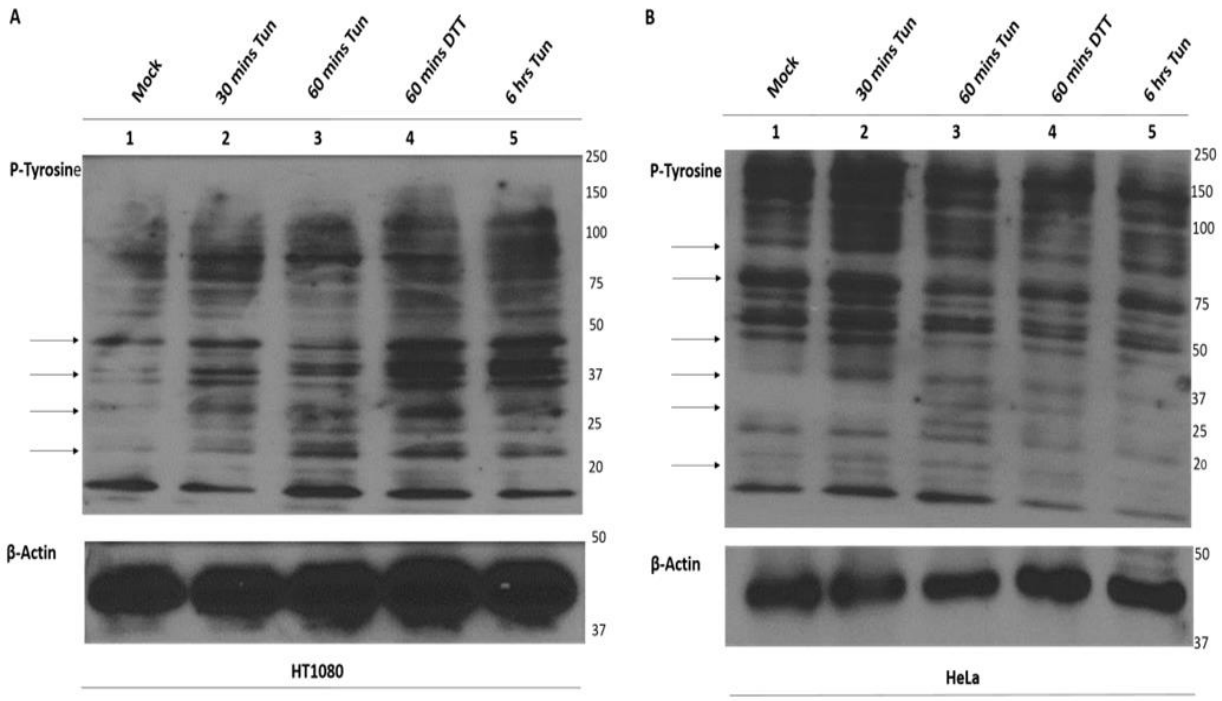

Figure 4.1 Tunicamycin induces changes in tyrosine phosphorylation in HT1080 and HeLa cells

HT1080 (panel A) and HeLa (panel B) cells were either mock (lanes 1) or treated with Tun for 30 mins (lanes 2), 60 mins (lanes 3) and 6 hrs (lanes 5) or 60 mins with DTT (lanes 4) prior to cell lysis and subsequent analysis by SDS-PAGE and Western blotting. Anti-phospho-tyrosine was used to detect tyrosine phosphorylated proteins.

A.HT1080 cells had proteins at approximately 48kDa, 40kDa, 38kDa, 30kDa and 22kDa (arrows) whose tyrosine phosphorylation was differentially regulated during both early and late Tun induced ER stress responses. β-actin was used as a loading control.

B. HeLa cells had proteins at approximately 80kDa, 75kDa, 50kDa, 37kDa, 30kDa and 10k (arrows) whose tyrosine phosphorylated was differentially regulated during both early and late Tun induced ER stress responses. β-actin was used as a loading control.

At 75kDa, there was a decrease in the intensity of a band at 60 mins (figure 4.1, panel B, lane 3, arrow) and 6 hrs (figure 4.1, panel B, lane 5) tunicamycin treatment compared to mock. For the 50kDa band, intensity decreased from 60 mins (figure 4.1, panel B, lane 3, arrows) tunicamycin treatment. The 37kDa band density increased from 30 mins (figure 4.1, panel B, lane 2, arrow), but then decreased at 60 mins (figure 4.1, panel B, lane 3 arrow) and 6 hrs tunicamycin (figure 4.1, panel B, lane 5, arrow) and at 30kDa, a band appeared at 30 mins (figure 4.1, panel B, lane 2, arrow) but by 6 hrs (figure 4.1, panel B, lane 5, arrow) tunicamycin treatment had become less prominent. In DTT treated cells, the 30kDa band also increased in intensity when compared to mock treated cells, though to a lesser extent when compared to 60 mins tunicamycin treated cell lysates (figure 4.1, panel B, lanes 1 and 4). Finally at approximately 10kDa, a band decreased at 60 mins DTT and 6 hrs tunicamycin treatment, suggesting another dephosphorylation event (figure 4.1, panel B, lanes 4 and 5). This data suggested that tyrosine phosphorylation is involved in both early and late ER stress responses and that though the expression levels of the majority of tyrosine phosphorylated proteins remained constant throughout the duration of ER stress, the expression levels of many tyrosine phosphorylation proteins also changed in response to ER stress.

Because most changes in tyrosine kinase activity were seen during early ER stress responses (30 mins to 60 mins), ER morphology during early ER stress responses was investigated in the presence of the tyrosine kinase inhibitor genistein (Gen), to get an indication of the downstream cellular consequences of ER stress. HT1080 cells were treated with either DMSO, tunicamycin, genistein or tunicamycin/genistein and imaged using ERTracker Blue/white as in section 2.9 to observe ER morphology (figures 4.2 and 4.3).

The peripheral ER membrane area was measured using ImageJ software (figure 4.2, panel B, box (yellow outline)). As seen in figure 4.2A tunicamycin treatment did not significantly change ER membrane area at the times seen in protein expression studies. Significant ($p<0.05$) change in ER membrane area was only seen at 10 mins tunicamycin treatment where ER membrane area increased in response to tunicamycin treatment when compared to DMSO control. Genistein only treatment did significantly ($p <0.05$) change ER membrane area, with increases to ER membrane area seen at 10 mins, 40 mins, 50 mins

and 60 mins compared to DMSO control. However, tunicamycin/genistein only treatment showed a significant change in ER membrane area at 10 mins post treatment (Figure 4.2A).

The morphology of HT1080 ER following DMSO treatment was varied but was mostly oval. This remained constant with tunicamycin and genistein treatments. However in tunicamycin/genistein treated HT1080 cells, the ER in some cells became elongated with time, particularly those treated with genistein (figure 4.3, panels 4, 7, 8, 11, 12, e). All treatments resulted in sheet/tubule structures at the periphery of the ER with tunicamycin/genistein treatment resulting in the most prominent sheet/ tubule structures (figure 4.3, panels 1-12, arrows). This data suggests that, immediately following ER stress induction, ER membrane expands to deal with acute ER stress but that this is a transient response that resolves over a 60 minute time course with the stressor. The ER may use different mechanisms to deal with unabated stress. However, whether the decrease in ER size in HT1080 cells is a pro-survival adaptation to chronic ER stress and whether HeLa cells have the same response remains an open question.

A

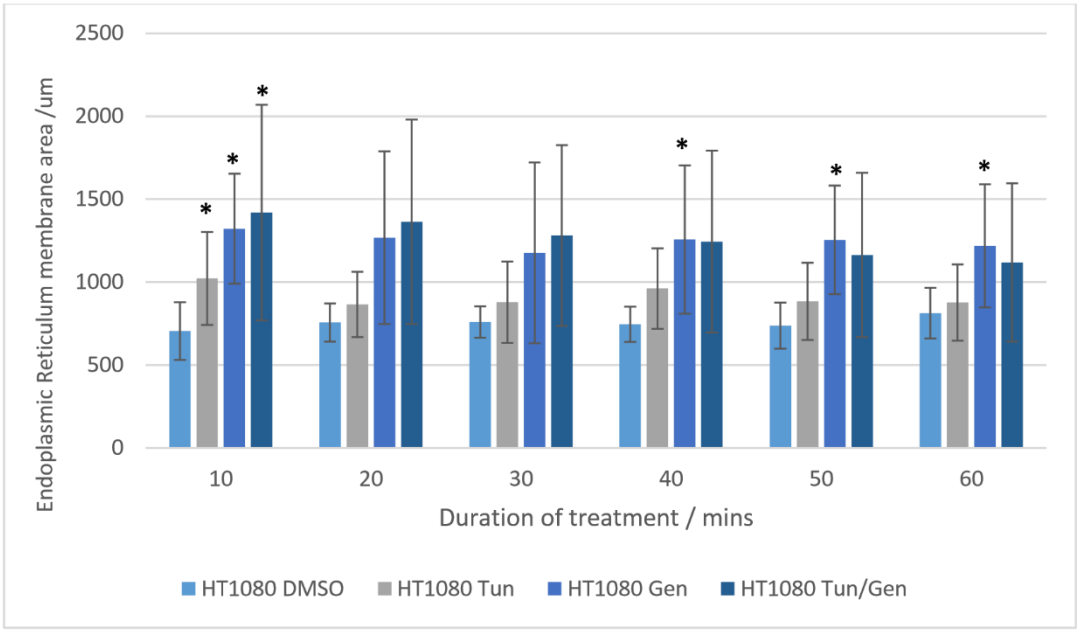

B

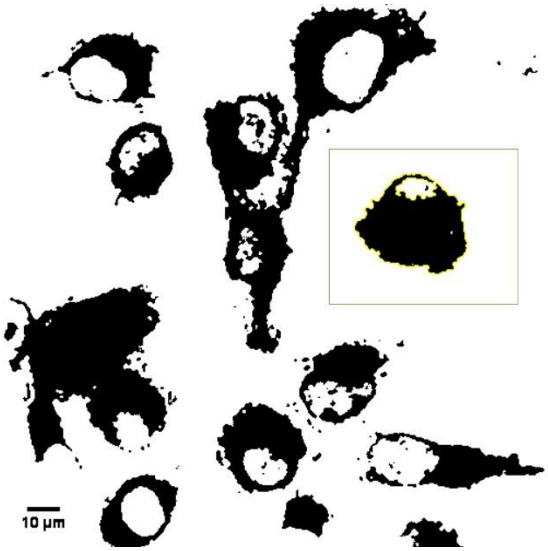

Figure 4.2: Quantification of ER membrane expansion shows ER membrane expansion during immediate ER stress responses.

HT1080 cells were incubated with medium containing ERTracker Blue/white (1:1000) dye prior to imaging on Spinning disk confocal under 5% $C0_2$ and 37^{o}C for 18 hrs. Right before imaging Tun and/or Genistein was added.

A. Quantification of ER membrane expansion from images in figure 4.3. At 10 mins Tun (grey), Gen (blue) and Tun/Gen (dark blue) treatment, ER membrane area was significantly increased. Tun and Tun/Gen treatment did not significantly increase ER membrane area from 20-60 mins. Gen treatment significantly increased ER membrane area from 40 to 60 mins. B. ImageJ was used to quantify ER membrane area. ER periphery was measured (yellow outline, box).

n=6, *= $p<0.05$

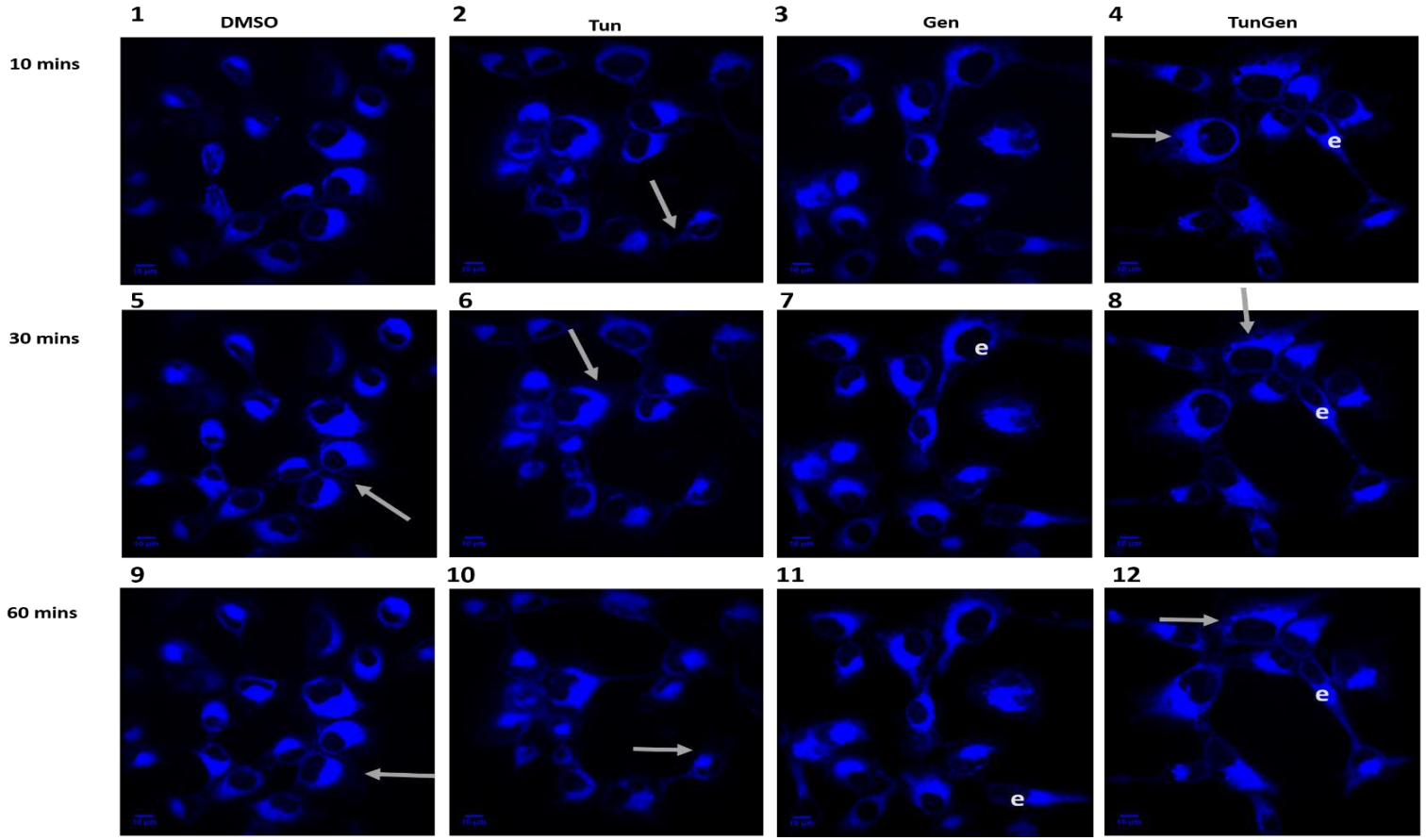

Figure 4.3: Early tunicamycin and genistein responses induce ER membrane expansion

HT1080 and HeLa cells were incubated with 1 mM ERTracker blue/white (1:1000) dye for 120 mins then immediately before imaging the cells were treated with DMSO (panels, 1, 5 and 9), 1 µg/ml Tun (panels, 2, 6 and 10) 140 mM Gen (panels, 3, 7, 11) and Tun/Gen (panels 4, 8, 12) for 18 hours on Spinningdisk confocal under 5% $C0_2$ and 37^{o}C.

No changes seen to tubular/sheet structures with the Tun treatments with time (arrows). With Gen (panels 4, 8, 12) treatment, some cells elongated (e) from 10 mins to 60 mins (panels 3, 7, 11). All ER showed peripheral membrane tubular/sheets structures.

4.2.2. The effects of STAT3 activation in tunicamycin induced stress responses

With STAT3 having been shown to link UPR stress responses and inflammation (Meares et. al. 2014), STAT3 was investigated as a potential target of the tunicamycin induced ER stress response. STAT3 can be alternatively spliced into a STAT3α full length form and STAT3β, the truncated form. Shown in figure 4.4 and indicated by the arrow is major STAT3 86kDa form. In HeLa cells, STAT3 expression was seen at all treatments and at all times (figure 4.4, panel A, lanes 8-14, arrows). Notably STAT3 was more strongly expressed in HT1080 cells compared to HeLa cells. In HT1080 cells, the STAT3 bands were also seen with all treatments and at all times (figure 4.4, panel A, lanes 1-7, arrows). However, though the expression of STAT3 could be demonstrated in both HT1080 and HeLa cells, it was not possible to detect to phospho-STAT3 after treatment of the cells with tunicamycin of DTT (figure 4.4C). However, the difference in expression levels of STAT3 between the two cell lines is worthy of further investigation.

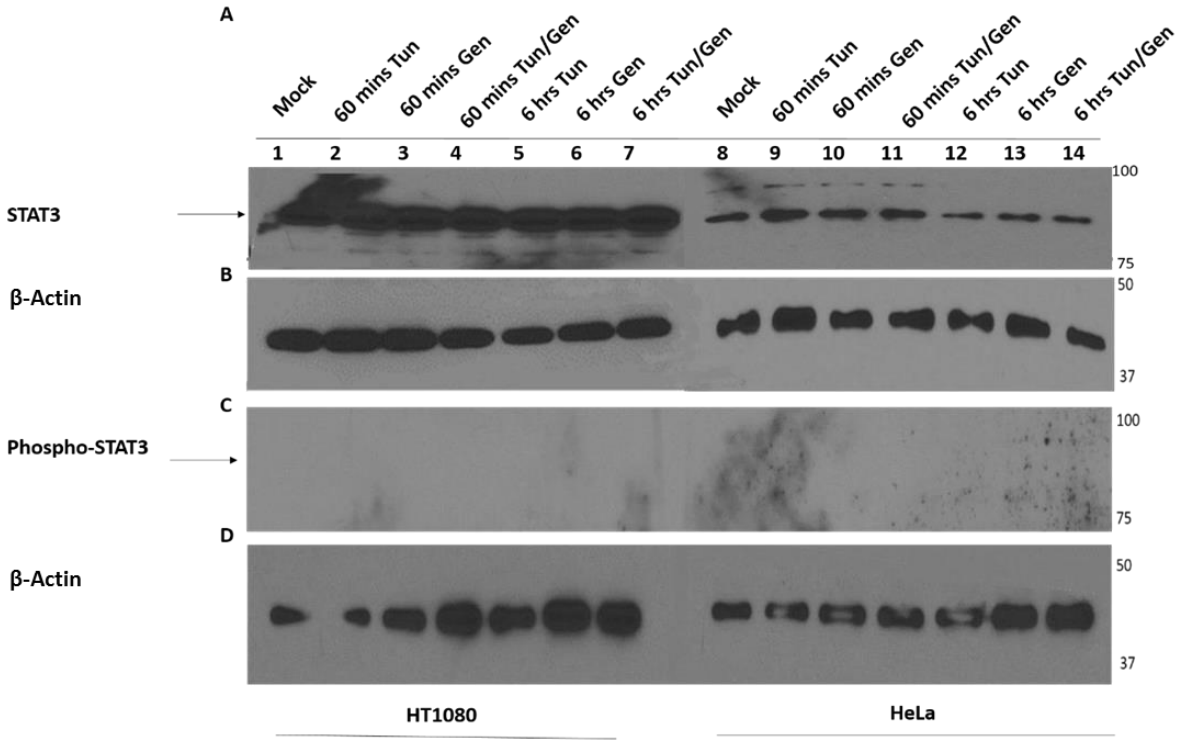

4.4 Expression of STAT3 in HT1080 and HeLa cells

HeLa and HT1080 cells were either mock treated or treated with 1 µg/ml Tun and/or 140 µM Gen, for 60 mins and 6 hrs prior to cell lysis and subsequent analysis with SDS-PAGE and Western blotting. Anti-STAT3 and anti-phospho-STAT3 were used to detect STAT3 and Phospho- STAT3 respectively (panels A and C).

A. STAT3 expression was seen in both HT1080 and HeLa cells with all treatments and at all times, however, STAT3 was expressed in HT1080 cells strongly (lanes 1-7) and in HeLa cells more weakly (lanes 8-14).

B. B-actin loading control for STAT3.

C. No phospho-STAT3 expression was detected after ER stress induction in either HT1080 (lanes 1-7) or HeLa cells (lanes 8-14).

D. β- actin loading control phospho-STAT3.

4.3. Discussion

With tyrosine kinases being involved in numerous different activities within cells including mainly inflammatory responses as well as survival and apoptotic responses (Schlessinger and Ullrich 1992), the aims of this chapter investigations (figure 4.1-4.4) were to identify changes in tyrosine phosphorylation expression during tunicamycin induced ER stress responses and identify possible therapeutic targets using the tyrosine kinase inhibitor genistein, which also has other roles including an agonist response via β- oestrogen receptors (Patisaul et. al. 2002), apoptosis initiation (Gossner et. al. 2007) and inhibition of telomerase activity (Ouchi et. al. 2005).

Initial investigations of tyrosine kinase activity during tunicamycin induced ER stress responses showed that numerous proteins are tyrosine phosphorylated during both early and late tunicamycin induced ER stress responses (figure 4.1). Many proteins that were Tyr-phosphorylated in HT1080 and HeLa cells were of different molecular weights except for the proteins identified at approximately 37kDa, 38kDa and 30kDa in HeLa and HT1080 cells respectively. Though these Tyr-phosphorylated proteins shared a similar molecular weight, the time of phosphorylation differed, which could either indicate differences in their regulation or that they are different proteins. These results were consistent with other reports that have noted Tyr phosphorylation during ER stress responses (Meares et. al. 2014, Hong et. al. 2005, Yu et. al. 2003). Further investigations will be required to identify the differentially regulated phospho-tyrosine proteins through 2D gel electrophoresis proteomics and mass spectrometry analysis.

Interestingly with the membrane labelling studies all ER stress induced treatments (tunicamycin, genistein and tunicamycin/genistein) gave rise to a significant increase in membrane expansion in the first 10 mins of imaging but not with prolonged exposure to ER stress (figure 4.2). With particular reference to tunicamycin treated cells, this was consistent with results seen by Schuck et. al. who saw ER membrane expansion in yeast cells after 90 mins of 1 μg/ml tunicamycin treatment. Taking this into consideration, the data presented suggests that HT1080 cells may undergo membrane expansion during immediate ER stress responses but then later induce different responses to deal with the prolonged stress. However, it is worth noting that after 10

mins of tunicamycin and tunicamycin/genistein treatment, although there was no significant difference in ER membrane area compared to DMSO control; the average membrane area still remained greater when compared to DMSO control (figure 4.2). The standard deviations for treatment groups were 2-3x higher than control standard deviation so an increased sample size may improve the chance of detecting small significant differences. Repeat experiments could also further clarify whether membrane expansion responses are only optimally elicited during immediate ER stress responses. 3D imaging techniques and z stacking could also be utilised during further experimentation to minimise variation from normal cellular movement. Surprisingly, Gen treatment alone induced ER membrane expansion in HT1080 cells, although it did not induce an ER stress response at the concentrations used (Lemin and Benham, unpublished data). It will be interesting to determine whether HeLa cells have a similar response to genistein.

Investigations into STAT3 showed that STAT3 was expressed in both HeLa and HT1080 cells but that STAT3 was more strongly expressed in HT1080 cells.
However, phosphorylated STAT3 could not be detected after tunicamycin induced ER stress (Figure 4.4 panel C). This was unexpected, as studies have observed STAT3 activation (as early as 30 mins after ER stress induction in some cells) in different cell types including astrocytes, neural precursor cells and in INS832/13 a pancreatic β-cell (Meares et. al. 2014). Thus further controls are required to confirm whether the anti-P-STAT3 antibody is capable of detecting phosphorylated STAT3 by western blotting.

It was expected from our groups previous findings that HT1080 cells (which were observed to have a reduced response to tunicamycin induced ER stress) would behave similarly to astrocytes which were relatively resistant to thapsigargin or tunicamycin induced ER stress responses and instead activated inflammatory responses through STAT3 (Meares et. al. 2014). It was anticipated that HT1080 cells would signal through STAT3 in response to tunicamycin however, no STAT3 activation was observed. Thus further investigations into STAT3 activation in both HT1080 and HeLa cells should be conducted with a positive control for STAT3 activation.

Further investigations of STAT3 are warranted due to the breadth of JAK/STAT3 signalling which has been shown to mediate a range of very diverse functions in

different tissues. For example, STAT3 signalling has been shown to prevent apoptosis in T cells thus promoting their proliferation (Takeda et. al. 1998) and to promote the formation of bone osteoblasts in response to many different stimuli including cytokines produced by monocytes/macrophages (Nicolaidou et. al. 2012) and Oncostatin M (Kakutani et. al. 2015). This is particularly interesting for inflammatory disease like AS which mainly effects the axial skeleton, but often with involvement of the eye and bowel. However further work will need to be carried out to determine if and when STAT3 is activated in AS associated tissues, what the different effects of STAT3 signalling are and if STAT3 can be a potential therapeutic target.

5. Final Discussion

The pathogenesis of the chronic inflammatory disease ankylosing spondylitis (AS) has been linked to the misfolding of HLA-B27 MHC class I heavy chains (Turner et. al. 2005). AS primarily affects the axial skeleton but can also affect several different organs including the heart (Ehrenfeld, 2012), lungs (Hsieh et. al. 2014) and eyes (Zambrano-Zaragoza et. al. 2013). A study by Turner et. al. 2007 conducted in mouse macrophages and splenocytes revealed that some cell types are more susceptible to the activation of HLA-B27 misfolding associated ER stress responses compared to others: which may have implications in AS disease pathogenesis (Turner et. al 2007). With limited evidence to show how HLA-B27 misfolding leads to differing responses in different human cell types; and with the molecular mechanisms of AS pathogenesis not fully elucidated, this study sought to investigate the activation of downstream UPR stress pathways. The autophagy, apoptosis and inflammatory signalling associated pathways were investigated in HT1080 and HeLa cells in the hope of translating the data into an AS disease model.

It was found that as a response to immediate ER stress induction, the ER membrane of in HT1080 cells expanded to cope with protein misfolding induced by tunicamycin and genistein associated responses. However, with continued ER stress induction, the ER may employ different mechanisms to cope with unabated stress (figure 3.4, 4.2 and 4.3). One such mechanism is autophagy.

In both HeLa and HT1080 cells, autophagy was differentially activated. In HT1080 cells, autophagy pathways were activated during late tunicamycin induced ER stress responses as the activation of LC3B and an increase in the number of acidic compartments (i.e autolysosomes and lysosomes) was seen only after chronic tunicamycin induced ER stress responses (6 and 12 hrs respectively) (figure 3. 14 and 3. 20A). In HeLa cells, even though western blot and dynamic imaging data suggested that autophagy pathways were activated in untreated cells, albeit at low levels, increases to autophagy activation were observed during early tunicamycin induced ER stress responses (figures 3.13 panel C, 3.14 and 3.20A).

Another coping mechanism that these cells may employ when ER stress cannot be overcome is apoptosis. In HT1080 cells no apoptosis activation was seen. No caspase 9

was seen in both early and late responses even though procaspase 9 expression increased from early ER stress responses into late ER stress responses, albeit these expression levels of procaspase 9 were very low and may not have been enough to cause significant, detectable caspase 9 expression. This was consistent with a study by Dey et. al. which showed that the highly metastatic HT1080 cells were resistant to apoptosis during chronic stress conditions (Dey et. al 2015). In contrast, apoptosis was activated in HeLa cells during late tunicamycin induced stress responses (figure 3.20A, 3.23B and 3.24A). Moreover, further investigations into the identity and function of the HeLa cell specific truncated N-terminal domain ASK1 fragment may provide more insight into the different outcomes to tunicamycin induced ER stress responses, especially seeing as ASK1 is involved in both apoptotic and autophagic pathways.

Finally, it was also found that HT1080 and HeLa cells have different phospho-proteomes as a result of differential tyrosine kinase signalling, with each of the phospho-proteomes having been found to be differentially regulated between early and late tunicamycin induced ER stress responses (figure 4.1). Interestingly, in HT1080 cells, (in the context of ER morphology) during continued suppression of tyrosine kinase signalling by genistein during tunicamycin induced ER stress responses, sheet/tubule structures became less prominent. This suggests that ER remodelling may be an immediate response to stress and that genistein treatment may exacerbate this response (figure 3.4, panels 4, 8 and 12).

Bringing these findings together, the following hypothesis has been put forward. The induction of ER stress responses as a result of protein misfolding, may have different consequences in different human cell types. It is proposed that immediately following ER stress induction, the ER membranes of HT1080 cells expand, thereby increasing ER lumen volume. This increase in ER lumen volume may act to reduce stress by preventing the aggregation of misfolded proteins thereby promoting the folding of misfolded proteins (However, it is yet to be confirmed whether the same response occurs in HeLa cells). If this acute response does not abate stress and restore ER homeostasis, unabated ER stress in HT1080 cells and also in HeLa cells may then lead to increased ER remodelling (e.g. as sheets/tubules become more prominent with continued stress even in the absence of ER membrane expansion (figure 3.4A, 3.5, arrows, 4.2 and 4.3)).

Following this, autophagy pathways are then activated to degrade misfolded proteins and if this too fails to restore ER homeostasis, then apoptosis is activated.

It is important to note that the duration, level and activation time of each of these phases will differ between cell types. It is also likely that all these pathways may be dynamically activated since HT1080 and HeLa cells showed both sheet/tubule structures and expression of caspase 9 and LC3B at low levels in un-stressed cells and during early stress responses and late responses. What's more, tyrosine kinase signalling which was also shown to be differentially regulated between HT1080 and HeLa cells would also dynamically mediate the activation of other pathways which may include inflammatory responses. However, the identity of these ER stress mediated Tyr-phosphorylated proteins would need to be elucidated to get a clearer indication of what pathways are occurring downstream of the UPR.

This differential regulation of UPR responses may be important when it comes to AS pathogenesis. This is because the sustained activation of autophagy (as seen in HT1080 cells) may result in the prolonged survival of proinflammatory cells thereby exacerbating inflammation and disease progression. This is also in line with previous laboratory findings which showed that HT1080 cells to not induce CHOP expression in response to tunicamycin induced ER stress (Lemin and Benham, unpublished data). Thus further investigations into the differential activation of downstream UPR pathways in the AS disease models i.e. macrophages and/or osteoclasts, may have implications in elucidating the pathogenesis of AS and in the development of more effective therapies. Consequently, it follows that this activation of ER stress pathways during early tunicamycin induced stress responses is promising with regards to the AS disease model. This is because when compared to tunicamycin, HLA-B27 would be a much weaker activator of the UPR so with responses seen even when changes to the glycosylation of MHC class I heavy chain pool cannot be observed (figure 3.6A), weaker HLA-B27 misfolding may also induce the similar responses to tunicamycin induced protein misfolding.

To conclude, with approximately 5-10% of AS patients not being HLA-B27 positive, it comes that although HLA-B27 has the highest susceptibility to AS, other factors may contribute to AS pathogenesis. For example, several additional AS susceptibility loci

including IL-23R, ERAP1 and IL-1R2 have been revealed (Reveille et. al. 2010), and with current AS studies linking AS pathogenesis to Th17 cells and IL-23/Th17 responses (Sherlock et. al. 2012, Zhang et. al. 2012, Milanez et. al. 2016 and Shen et. al. 2009 and Wright et. al. 2015) which are known to be dependent upon STAT3 for activation (Mathur et. al. 2007, Yang et. al 2007 and Asakawa et. al. 2015), further investigation into STAT3/Th17 cell responses in the context of the AS disease model are warranted as they may help elucidate the pathogenesis of AS and help further the development of more effective therapies.

6. References

Akiyama, T., Ishida J., Nakagawa S., Ogawara H., Watanabe S., Itoh N., Shibuya M., Fukami Y. Genistein, a specific inhibitor of tyrosine-specific protein kinases. 1987. *The Journal of Biological Chemistry.* 262 (12), pp.5592-5595

Appel, H., Maier, R., Bleil, J., Hempfing, A., Loddenkemper, C., Schlichting, U., Syrbe, U. and Sieper, J. (2013). In Situ Analysis of Interleukin-23- and Interleukin-12-Positive Cells in the Spine of Patients With Ankylosing Spondylitis. *Arthritis & Rheumatism*, 65(6), pp.1522-1529.

Arensdorf, A. and Rutkowski, T.D. (2013). Endoplasmic reticulum stress impairs IL-4/IL13 signaling through C/EBP -mediated transcriptional suppression. *Journal of Cell Science*, 126(17), pp.4026-4036.

Asakawa, M., Yoshida, H., Sakai, R., Saeki, K., Okada, M., Kanamori, M., Kotani, H., Wei, X. and Yoshimura, A. (2015). A novel JAK-STAT inhibitor, 2-[(3-Carbamoyl-2thienyl)amino]-2-oxoethyl(2,6-dichlorophenyl)acetate, suppresses helper T cell differentiation in vitro and collagen-induced arthritis in vivo. *Biochemical and Biophysical Research Communications*, 468(4), pp.766-773.

Averous, J., Bruhat, A., Jousse, C., Carraro, V., Thiel, G. and Fafournoux, P. (2003). Induction of CHOP Expression by Amino Acid Limitation Requires Both ATF4 Expression and ATF2 Phosphorylation. *Journal of Biological Chemistry*, 279(7), pp.5288-5297.

Barbosa, J. Santos-Aguado, J., Mentzer, S.J., Stromeinger, .J.L Burakoff, S.J and Biro, P.A. (1987). Site-directed mutagenesis of class I HLA genes. Role of glycosylation in surface expression and functional recognition. *Journal of Experimental Medicine*, 166(5), pp.1329-1350.

Barth, S., Glick, D. and Macleod, K. (2010). Autophagy: assays and artifacts. *The Journal of Pathology.*, 221(2), pp.117-124.

B'chir, W., Maurin, A., Carraro, V., Averous, J., Jousse, C., Muranishi, Y., Parry, L., Stepien, G., Fafournoux, P. and Bruhat, A. (2013). The eIF2 /ATF4 pathway is essential for stress-induced autophagy gene expression. *Nucleic Acids Research*, 41(16), pp.7683-7699.

Becker, T., Bhushan, S., Jarasch, A., Armache, J., Funes, S., Jossinet, F., Gumbart, J., Mielke, T., Berninghausen, O., Schulten, K., Westhof, E., Gilmore, R., Mandon, E. and Beckmann, R. (2009). Structure of Monomeric Yeast and Mammalian Sec61 Complexes Interacting with the Translating Ribosome. *Science*, 326(5958), pp.1369-1373.

Bertolotti A, Zhang Y, Hendershot LM, Harding HP & Ron D. (2000) Dynamic interaction of BiP and ER stress transducers in the unfolded-protein response. *Nature Cell Biology,* 2 (6) pp. 326−332

Bertolotti, A., Wang, X., Novoa, I., Jungreis, R., Schlessinger, K., Cho, J., West, A. and Ron, D. (2001). Increased sensitivity to dextran sodium sulfate colitis in IRE1β-deficient mice. *Journal of Clinical Investigation*, 107(5), pp.585-593.

Boldin, M., Goncharov, T., Goltseve, Y. and Wallach, D. (1996). Involvement of MACH, a Novel MORT1/FADD-Interacting Protease, in Fas/APO-1- and TNF Receptor–Induced Cell Death. *Cell*, 85(6), pp.803-815.

Brattain M.G., Fine W.D., Khaled F.M, Thompson J and Brattain D.E. (1981). Heterogeneity of malignant cells from a human colonic carcinoma. *Cancer Research*. 41(5) pp. 1751-1756.

Bratton, S Walker, G., Srinivasula, S.M., Sun, XM., Butterworth, M. (2001). Recruitment, activation and retention of caspases-9 and -3 by Apaf-1 apoptosome and associated XIAP complexes. *The EMBO Journal*, 20(5), pp.998-1009.

Bratton, S. and Salvesen, G. (2010). Regulation of the Apaf-1-caspase-9 apoptosome. *Journal of Cell Science*, 123(19), pp.3209-3214.

Brewer, J., Hendershot, L., Sherr, C. and Diehl, J. (1999). Mammalian unfolded protein response inhibits cyclin D1 translation and cell-cycle progression. *Proceedings of the National Academy of Sciences*, 96(15), pp.8505-8510.

Brodsky, J. and Skach, W. (2011). Protein Folding and Quality Control in the Endoplasmic Reticulum: Recent lessons from Yeast and Mammalian Cell Systems. *Current Opinion in Cell Biology*, 23(4), pp.464-475.

Brooks S.C., Locke E.R and Soule, H.D. Estrogen receptor in a human cell line (MCF-7) from breast carcinoma. (1973).*The Journal of biological chemistry*. 248. (17) pp. 6251 – 6253

Brown, C. (2014). Live-cell techniques—Advances and challenges. *Cell Adhesion & Migration*, 8(5), pp.429-429.

C Scaffidi, S Fulda, A Srinivasan, C Friesen, F Li, K J Tomaselli, K M Debatin, P H Krammer, and M E Peter

Calfon, M., Zeng, H., Urano, F., Till, J., Hubbard, S., Harding, H., Clark, S. and Ron, D. (2002).IRE1 couples endoplasmic reticulum load to secretory capacity by processing the XBP-1 mRNA. *Nature*, 420(6912), pp.202-202.

Cao, X., Zhou, Y. and Lee, A. (1995). Requirement of Tyrosine- and Serine/Threonine Kinases in the Transcriptional Activation of the Mammalian grp78/BiP Promoter by Thapsigargin. *Journal of Biological Chemistry*, 270(1), pp.494-502.

Chang, S., Momburg, F., Bhutani, N. and Goldberg, A. (2005). The ER aminopeptidase, ERAP1, trims precursors to lengths of MHC class I peptides by a "molecular ruler" mechanism. *Proceedings of the National Academy of Sciences*, 102(47), pp.1710717112.

Chen C, Zhang X. (2015).ERAP1 variants are associated with ankylosing spondylitis in East Asian population: a new Chinese case-control study and meta-analysis of published series. *International Journal Immunogenetics*. 42(3) pp.168-173.

Chen L, Wei X, Evans B, Jiang W, Aeschlimann D. (2008). IL-23 promotes osteoclast formation by up-regulation of receptor activator of NF-κB (RANK) expression in myeloid precursor cells. *European Journal of Immunology*. 38(10) pp.2845-2854.

Chen, Y., Hsieh, M., Chang, M., Chen, H., Jan, M., Maa, M. and Leu, T. (2012). Eps8 Protein Facilitates Phagocytosis by Increasing TLR4-MyD88 Protein Interaction in Lipopolysaccharide-stimulated Macrophages. *Journal of Biological Chemistry*, 287(22), pp.18806-18819.

Cole, L., Davies, D., Hyde, G and Ashford, A. (2000). ER-Tracker dye and BODIPYbrefeldin A differentiate the endoplasmic reticulum and Golgi bodies from the tubularvacuole system in living hyphae of Pisolithus tinctorius. *Journal of Microscopy*, 197(3), pp.239-249.

Cooke M, Abraham K, Forbush K, Perimutter R. (1991) Regulation of T cell receptor signaling by a src family protein-tyrosine kinase (p59fyn). *Cell*. 65(2) pp.281-291.

Crowley, K., Liao, S., Worrell, V., Reinhart, G. and Johnson, A. (1994). Secretory Proteins Move through the Endoplasmic Reticulum Membrane via an Aqueous, Gated Pore. *Cell*, 78(3), pp.461-471.

Cui X, Rouhani F, Hawari F, Levine S. (2003). Shedding of the Type II IL-1 Decoy Receptor Requires a Multifunctional Aminopeptidase, Aminopeptidase Regulator of TNF Receptor Type 1 Shedding. The *Journal of Immunology*. 171(12) pp.6814-6819.

de Lavallade, H., Khoder, A., Hart, M., Sarvaria, A., Sekine, T., Alsuliman, A., Mielke, S., Bazeos, A., Stringaris, K., Ali, S., Milojkovic, D., Foroni, L., Chaidos, A., Cooper, N., Gabriel, I., Apperley, J., Belsey, S., Flanagan, R., Goldman, J., Shpall, E., Kelleher, P., Marin, D. and Rezvani, K. (2013). Tyrosine kinase inhibitors impair B-cell immune responses in CML through off-target inhibition of kinases important for cell signaling. *Blood*, 122(2), pp.227-238.

Dean, N and Pelham, H. R.B. (1990). Recycling of proteins from the Golgi compartment to the ER in yeast. *The Journal of Cell Biology*, 111(2), pp.369-377.

DeLay, M., Turner, M., Klenk E., Smith J., Sowders D., Colbert R. (2009).HLA-B27 misfolding and the unfolded protein response augment interleukin-23 production and are associated with Th17 activation in transgenic rats.*Arthritis & Rheumatism*. 65(8) pp.2123-2131.

Deng, J., Lu, P., Zhang, Y., Scheuner, D., Kaufman, R., Sonenberg, N., Harding, H. and Ron, D. (2004). Translational Repression Mediates Activation of Nuclear Factor Kappa B by Phosphorylated Translation Initiation Factor 2. *Molecular and Cellular Biology*, 24(23), pp.10161-10168.

Dey, S., Sayers, C., Verginadis, I., Lehman, S., Cheng, Y., Cerniglia, G., Tuttle, S., Feldman, M., Zhang, P., Fuchs, S., Diehl, J. and Koumenis, C. (2015). ATF4-dependent induction of heme oxygenase 1 prevents anoikis and promotes metastasis. *Journal of Clinical Investigation*, 125(7), pp.2592-2608.

Dowdle, W., Nyfeler, B., Nagel, J., Elling, R., Liu, S., Triantafellow, E., Menon, S., Wang,

Z., Honda, A., Pardee, G., Cantwell, J., Luu, C., Cornella-Taracido, I., Harrington, E., Fekkes, P., Lei, H., Fang, Q., Digan, M., Burdick, D., Powers, A., Helliwell, S., D'Aquin, S., Bastien, J., Wang, H., Wiederschain, D., Kuerth, J., Bergman, P., Schwalb, D., Thomas, J., Ugwonali, S., Harbinski, F., Tallarico, J., Wilson, C., Myer, V., Porter, J., Bussiere, D., Finan, P., Labow, M., Mao, X., Hamann, L., Manning, B., Valdez, R., Nicholson, T., Schirle, M., Knapp, M., Keaney, E. and Murphy, L. (2014). Selective VPS34 inhibitor blocks autophagy and uncovers a role for NCOA4 in ferritin degradation and iron homeostasis in vivo. Nature Cell Biology, 16(11), pp.1069-1079.

Duskin D, Mahoney WC. (1982).Relationship of the Structure and Biological Activity of the Natural Homologues of Tunicamycin. Journal of Biological Chemistry. 257 (6) pp.3105-9.

Ehrenfeld, M. (2012). Spondyloarthropathies. *Best Practise and Research Clinical Rheumatology*. 26 (1) pp.135-145

Eken A, Singh A, Treuting P, Oukka M. (2013).IL-23R+ innate lymphoid cells induce colitis via interleukin-22-dependent mechanism. *Mucosal Immunology*. 7(1) pp.143154.

Enari, M., Talanian, R., Wrong, W. and Nagata, S. (1996). Sequential activation of ICElike and CPP32-like proteases during Fas-mediated apoptosis. *Nature*, 380(6576), pp.723-726.

Fernandes-Alnemri, T., Armstrong, R., Krebs, J., Srinivasula, S., Wang, L., (1995). In vitro activation of CPP32 and Mch3 by Mch4, a novel human apoptotic cysteine protease containing two FADD-like domains. *Proceedings of the National Academy of Sciences*, 93(15), pp.7464-7469.

Ganley, I., Lam, D., Wang, J., Ding, X., Chen, S. and Jiang, X. (2009). ULK1-ATG13-FIP200 Complex Mediates mTOR Signaling and Is Essential for Autophagy. *Journal of Biological Chemistry*, 284(18), pp.12297-12305.

Gilchrist, A., Au, C., Hiding, J., Bell, A., Fernandez-Rodriguez, J., Lesimple, S., Nagaya, H., Roy, L., Gosline, S., Hallett, M., Paiement, J., Kearney, R., Nilsson, T. and Bergeron, J. (2006). Quantitative Proteomics Analysis of the Secretory Pathway. Cell, 127(6), pp.1265-1281.

Glick, D., Barth, S. and Macleod, K. (2010). Autophagy: cellular and molecular mechanisms. *Journal of Pathology.*, 221(1), pp.3-12.

Gossner, G., Choi, M., Tan, L., Fogoros, S., Griffith, K., Kuenker, M. and Liu, J. (2007). Genistein-induced apoptosis and autophagocytosis in ovarian cancer cells. *Gynecologic Oncology*, 105(1), pp.23-30.

Gross, A., Yin, X., Wang, K., Wei, M., Jockel, J., Milliman, C., Erdjument-Bromage, H., Tempst, P. and Korsmeyer, S. (1999). Caspase Cleaved BID Targets Mitochondria and Is Required for Cytochrome c Release, while BCL-XL Prevents This Release but Not Tumor Necrosis Factor-R1/Fas Death. *Journal of Biological Chemistry*, 274(2), pp.1156-1163.

Hambrock, A., Löffler-Walz, C. and Quast, U. (2002). Glibenclamide binding to sulphonylurea receptor subtypes: dependence on adenine nucleotides. *British Journal of Pharmacology*, 136(7), pp.995-1004.

Harding, H., Zhang,Y., Ron, D. (1999). Protein Translation and Folding are Coupled by an Endoplasmic Reticulum-reticulum-resident kinase. Nature. 397(6716),pp271-274.

Harding, H., Zhang, Y., Bertolotti, A., Zeng, H. and Ron, D. (2000). Perk Is Essential for Translational Regulation and Cell Survival during the Unfolded Protein Response. *Molecular Cell*, 5(5), pp.897-904.

Harding, H., Zhang, Y., Zeng, H., Novoa, I., Lu, P., Calfon, M., Sadri, N., Yun, C., Popko, B., Paules, R., Stojdl, D., Bell, J., Hettmann, T., Leiden, J. and Ron, D. (2003). An Integrated Stress Response Regulates Amino Acid Metabolism and Resistance to Oxidative Stress. *Molecular Cell*, 11(3), pp.619-633.

Hatai, T., Matsuzawa, A., Inoshita, S., Mochida, Y., Kuroda, T., Sakamaki, K., Kuida, K., Yonehara, S., Ichijo, H and Takeda, K. (2000). Execution of Apoptosis Signal-regulating Kinase 1 (ASK1)-induced Apoptosis by the Mitochondria-dependent Caspase Activation. *Journal of Biological Chemistry*, 275(34), pp.26576-26581.

Haze, K., Yoshida, H., Yanagi, H., Yura, T. and Mori, K. (1999). Mammalian Transcription Factor ATF6 Is Synthesized as a Transmembrane Protein and Activated by Proteolysis in Response to Endoplasmic Reticulum Stress. *Molecular Biology of the Cell*, 10(11), pp.3787-3799.

Henderson, B. and Pockley, A. (2005). *Molecular chaperones and cell signalling*. Cambridge, UK: Cambridge University Press.

Hong, M., Lin, M., Huang, J., Baumeister, P., Hakre, S., Roy, A. and Lee, A. (2005). Transcriptional Regulation of the Grp78 Promoter by Endoplasmic Reticulum Stress: ROLE OF TFII-I AND ITS TYROSINE PHOSPHORYLATION. *Journal of Biological Chemistry*. 280(17), pp.16821-16828.

Hsieh L, Wei J, Lee H, Chuang C, Jiang J, Chang K. (2014). Aerobic capacity and its correlates in patients with ankylosing spondylitis. *International Journal of Rheumatic Diseases*. doi: 10.1111/1756-185X.12347.

Huang, W., Tso, T., Kuo, Y., Tsay ,G. (2011). Distinct impacts of syndesmophyte formation on male and female patients with ankylosing spondylitis. *International Journal of Rheumatic Diseases*. 15(2):163-168.

Ikawa, T., Ikeda, M., Yamaguchi, A., Tsai, W., Tamura, N., Seta, N., Trucksess, M., Raybourne, R. and Yu, D. (1998). Expression of arthritis-causing HLA-B27 on Hela cells promotes induction of c-fos in response to in vitro invasion by Salmonella typhimurium. *Journal of Clinical Investigation*. 101(1), pp.263-272.

Imagawa, Y., Hosoda, A., Sasaka, S., Tsuru, A. and Kohno, K. (2008). RNase domains determine the functional difference between IRE1α and IRE1β. *FEBS Letters.* 582(5), pp.656-660.

Inesi, G. and Sagara, Y. (1992). Thapsigargin, a high affinity and global inhibitor of intracellular Ca2+ transport ATPases. *Archives of Biochemistry and Biophysics*. 298(2), pp.313-317.

Itakura, E., Kishi, C., Inoue, K. and Mizushima, N. (2008). Beclin 1 Forms Two Distinct Phosphatidylinositol 3-Kinase Complexes with Mammalian Atg14 and UVRAG. *Molecular Biology of the Cell*, 19(12), pp.5360-5372.

Janssens S, Pulendran B, Lambrecht B. (2014) Emerging functions of the unfolded protein response in immunity. *Nature Immunology*. 15(10):910-919.

Kabeya Y., Mizushima, N., Ueno ,T., Yamamoto, A., Kirisako, T., Noda, T., Kominami ,E., Ohsumi, Y and Yoshimori T (2000).LC3, a mammalian homologue of yeast Apg8p, is localized in autophagosome membranes after processing. *The EMBO Journal*. 19(21):5720-5728.

Kakutani, Y., Shioi, A., Shoji, T., Okazaki, H., Koyama, H., Emoto, M. and Inaba, M. (2015). Oncostatin M Promotes Osteoblastic Differentiation of Human Vascular Smooth Muscle Cells Through JAK3-STAT3 Pathway. *Journal of Cellular Biochemistry*, 116(7), pp.1325-1333.

Kaur, J. and Debnath, J. (2015). Autophagy at the crossroads of catabolism and anabolism. *Nature Reviews Molecular Cell Biology*, 16(8), pp.461-472.

Kim, S., Joe, Y., Kim, H., Kim, Y., Jeong, S., Pae, H., Ryter, S., Surh, Y. and Chung, H. (2015). Endoplasmic Reticulum Stress-Induced IRE1 Activation Mediates Cross-Talk of GSK-3 and XBP-1 To Regulate Inflammatory Cytokine Production. *The Journal of Immunology*, 194(9), pp.4498-4506.

Kischkel, F.C., Hellbardt, S., Behrmann, I., Germer, M. Pawlita, M., Krammer, P.H and Peter, M.E. (1995).Cytotoxicity-dependent APO-1 (Fas/CD95)-associated proteins form a death-inducing signaling complex (DISC) with the receptor. *The EMBO Journal*. 14(22): pp. 5579–5588.

Kowarik, M., Küng, S., Martoglio, B. and Helenius, A. (2002). Protein Folding during Cotranslational Translocation in the Endoplasmic Reticulum. *Molecular Cell*, 10(4), pp.769-778.

Kozlov, G., Pocanschi, C., Rosenauer, A., Bastos-Aristizabal, S., Gorelik, A., Williams, D. and Gehring, K. (2010). Structural Basis of Carbohydrate Recognition by Calreticulin. *Journal of Biological Chemistry*, 285(49), pp.38612-38620.

Laval, S., Timms, A., Edwards, S., Bradbury, L., Brophy, S., Milicic, A., Rubin, L., Siminovitch, K., Weeks, D., Calin, A., Wordsworth, B. and Brown, M. (2001). WholeGenome Screening in Ankylosing Spondylitis: Evidence of Non-MHC GeneticSusceptibility Loci. *The American Journal of Human Genetics*, 68(4), pp.918-926.

Layh-Schmitt, G., Yang, E., Kwon, G. and Colbert, R. (2013). HLA-B27 Alters the Response to Tumor Necrosis Factor α and Promotes Osteoclastogenesis in Bone Marrow Monocytes From HLA-B27-Transgenic Rats. *Arthritis & Rheumatism*, 65(8), pp.2123-2131.

Lee, A., Iwakoshi, N. and Glimcher, L. (2003). XBP-1 Regulates a Subset of Endoplasmic Reticulum Resident Chaperone Genes in the Unfolded Protein Response. *Molecular and Cellular Biology*, 23(21), pp.7448-7459.

Li, P., Nijhawan, D., Budihardjo, I., Srinivasula, S., Ahmad, M., Alnemri, E. and Wang, X. (1997). Cytochrome c and dATP-Dependent Formation of Apaf-1/Caspase-9 Complex Initiates an Apoptotic Protease Cascade. Cell, 91(4), pp.479-489.

Liao, S., Lin, J., Do, H. and Johnson, A. (1997). Both Lumenal and Cytosolic Gating of the Aqueous ER Translocon Pore Are Regulated from Inside the Ribosome during Membrane Protein Integration. *Cell*, 90(1), pp.31-41.

Lin, Z., Bei, J., Shen, M., Li, Q., Liao, Z., Zhang, Y., Lv, Q., Wei, Q., Low, H., Guo, Y., Cao, S., Yang, M., Hu, Z., Xu, M., Wang, X., Wei, Y., Li, L., Li, C., Li, T., Huang, J., Pan, Y., Jin, O., Wu, Y., Wu, J., Guo, Z., He, P., Hu, S., Wu, H., Song, H., Zhan, F., Liu, S., Gao, G., Liu, Z., Li, Y., Xiao, C., Li, J., Ye, Z., He, W., Liu, D., Shen, L., Huang, A., Wu, H., Tao, Y., Pan, X., Yu, B., Tai, E., Zeng, Y., Ren, E., Shen, Y., Liu, J. and Gu, J. (2012). A genome-wide association study in Han Chinese identifies new susceptibility loci for ankylosing spondylitis. Nature Genetics, 44(1), pp.73-77.

Liu, Y., Wang, M., Wang, D., Li, X., Wang, W., Lou, H. and Yuan, H. (2015). Malformin A1 promotes cell death through induction of apoptosis, necrosis and autophagy in prostate cancer cells. *Cancer Chemotherapy and Pharmacology*, 77(1), pp.63-75.

Lu, L., Ladinsky, M. and Kirchhausen, T. (2009). Cisternal Organization of the Endoplasmic Reticulum during Mitosis. *Molecular Biology of the Cell*, 20(15), pp.34713480.

Malladi, S., Challa-Malladi, M., Fearnhead, H. and Bratton, S. (2009). *The Apaf1•procaspase-9 apoptosome complex functions as a proteolytic-based molecular timer.* EMBO J, 28(13), pp.1916-1925.

Martino, M., Jones, L., Brighton, B., Ehre, C., Abdulah, L., Davis, C., Ron, D., O'Neal, W. and Ribeiro, C. (2012). The ER stress transducer IRE1β is required for airway epithelial mucin production. *Mucosal Immunol*, 6(3), pp.639-654.

Mathur, A., Chang, H., Zisoulis, D., Stritesky, G., Yu, Q., O'Malley, J., Kapur, R., Levy, D., Kansas, G. and Kaplan, M. (2007). Stat3 and Stat4 Direct Development of IL-17Secreting Th Cells. The Journal of Immunology, 178(8), pp.4901-4907.

Matsunaga, K., Morita, E., Saitoh, T., Akira, S., Ktistakis, N., Izumi, T., Noda, T. and Yoshimori, T. (2010). Autophagy requires endoplasmic reticulum targeting of the PI3kinase complex via Atg14L. J Cell Biol, 190(4), pp.511-521.

McCullough, K., Martindale, J., Klotz, L., Aw, T. and Holbrook, N. (2001). Gadd153 Sensitizes Cells to Endoplasmic Reticulum Stress by Down-Regulating Bcl2 and Perturbing the Cellular Redox State. *Molecular and Cellular Biology*, 21(4), pp.12491259.

Meares, G., Liu, Y., Rajbhandari, R., Qin, H., Nozell, S., Mobley, J., Corbett, J. and Benveniste, E. (2014). PERK-Dependent Activation of JAK1 and STAT3 Contributes to Endoplasmic Reticulum Stress-Induced Inflammation. *Molecular and Cellular Biology*, 34(20), pp.3911-3925.

Merksamer P, Trusina A, Papa F. (2008). Real-Time Redox Measurements during Endoplasmic Reticulum Stress Reveal Interlinked Protein Folding Functions. Cell. 135(5) pp.933-947.

Meunier, L., Usherwood, Y.,Chung, K.T. and Hendershoot, L.M. (2002). A Subset of Chaperones and Folding Enzymes Form Multiprotein Complexes in Endoplasmic Reticulum to Bind Nascent Proteins. *Molecular Biology of the Cell*, 13(12), pp.44564469.

Milanez, F., Saad, C., Viana, V., Moraes, J., Périco, G. (2016). IL-23/Th17 axis is not influenced by TNF-blocking agents in ankylosing spondylitis patients. *Arthritis Research Therapy*, 18(52). DOI**:** 10.1186/s13075-016-0949-6

Milani, M., Rzymski, T., Mellor, H., Pike, L., Bottini, A., Generali, D. and Harris, A. (2009). The Role of ATF4 Stabilization and Autophagy in Resistance of Breast Cancer Cells Treated with Bortezomib. *Cancer Research*, 69(10), pp.4415-4423.

Mizushima, N., Yoshimori, T. and Ohsumi, Y. (2003). Role of the Apg12 conjugation system in mammalian autophagy. *The International Journal of Biochemistry & Cell Biology*, 35(5), pp.553-561.

Mounir, Z., Krishnamoorthy, J., Wang, S., Papadopoulou, B., Campbell, S., Muller, W., Hatzoglou, M. and Koromilas, A. (2011). Akt Determines Cell Fate Through Inhibition of the PERK-eIF2 Phosphorylation Pathway. Science Signaling, 4(192), pp.ra62-ra62.

Nakajima, S., Lan, L., Kanno, S., Takao, M., Yamamoto, K., Eker, A. and Yasui, A. (2004). UV Light-induced DNA Damage and Tolerance for the Survival of Nucleotide Excision Repair-deficient Human Cells. *Journal of Biological Chemistry*, 279(45), pp.4667446677.

Nakanishi, K., Sudo, T. and Morishima, N. (2005). Endoplasmic reticulum stress signaling transmitted by ATF6 mediates apoptosis during muscle development. *Journal of Cell Biology*. 169(4), pp.555-560.

Nicolaidou, V., Wong, M., Redpath, A., Ersek, A., Baban, D., Williams, L., Cope, A. and Horwood, N. (2012). Monocytes Induce STAT3 Activation in Human Mesenchymal Stem Cells to Promote Osteoblast Formation. PLoS ONE, 7(7), p.e39871.

Nilsson, I., Kelleher, D., Miao, Y., Shao, Y., Kreibich, G., Gilmore, R., von Heijne, G. and Johnson, A. (2003). Photocross-linking of nascent chains to the STT3 subunit of the oligosaccharyltransferase complex. *The Journal of Cell Biology*, 161(4), pp.715-725.

Nishitoh, H., Saitoh, M., Mochida, Y., Takeda, K., Nakano, H., Rothe, M., Miyazono, K. and Ichijo, H. (1998). ASK1 Is Essential for JNK/SAPK Activation by TRAF2. *Molecular Cell*, 2(3), pp.389-395.

Ogata, M., Hino, S., Saito, A., Morikawa, K., Kondo, S. (2006). Autophagy Is Activated for Cell Survival after Endoplasmic Reticulum Stress. *Molecular and Cellular Biology*, 26(24), pp.9220-9231.

Okada, T., Haze, K., Nadanaka, S., Yoshida, H., Seidah, N., Hirano, Y., Sato, R., Negishi, M. and Mori, K. (2003). A Serine Protease Inhibitor Prevents Endoplasmic Reticulum Stress-induced Cleavage but Not Transport of the Membrane-bound Transcription Factor ATF6. *Journal of Biological Chemistry*, 278(33), pp.31024-31032.

Oltmanns, U., Issa, R., Sukkar, M., John, M. and Chung, K. (2003).Role of c-jun Nterminal kinase in the induced release of GM-CSF, RANTES and IL-8 from human airway smooth muscle cells. *British Journal of Pharmacology*, 139(6), pp.1228-1234

Oslowski, C.M and Urano, F. (2011). Measuring ER stress and the unfolded protein response using mammalian tissue culture system. 490 (1), pp.71-92.

Ouchi, H., Ishiguro, H., Ikeda, N., Hori, M., Kubota, Y. and Uemura, H. (2005). Genistein induces cell growth inhibition in prostate cancer through the suppression of telomerase activity. *International Journal of Urology*, 12(1), pp.73-80.

Oyadomari, S. and Mori, M. (2003). Roles of CHOP/GADD153 in endoplasmic reticulum stress. *Cell Death and Differentiation*, 11(4), pp.381-389.

Palade, G. (1955a). Studies on the Endoplasmic Reticulum: II. Simple Dispositions in Cells in Situ. *The Journal of Cell Biology*, 1(6), pp.567-582.

Palade, G. (1955b). A Small Particulate Component of the Cytoplasm. *The Journal of Cell Biology*, 1(1), pp.59-68.

Palade, G. (1956).The Endoplasmic Reticulum. *Journal of Cell Biology*. 2(4) pp. 85-98

Pankiv, S., Clausen, T., Lamark, T., Brech, A., Bruun, J., Outzen, H., Øvervatn, A., Bjørkøy, G. and Johansen, T. (2007). p62/SQSTM1 Binds Directly to Atg8/LC3 to Facilitate Degradation of Ubiquitinated Protein Aggregates by Autophagy. *Journal of Biological Chemistry*, 282(33), pp.24131-24145.

Patisaul, H., Melby, M., Whitten, P. and Young, L. (2002). Genistein Affects ERβ- But Not ERα-Dependent Gene Expression in the Hypothalamus. *Endocrinology*, 143(6), pp.2189-2197.

Peng J, Yang X, Chang S, Yang J, Dong C. (2010).IL-23 signaling enhances Th2 polarization and regulates allergic airway inflammation. *Cell Research*. 20(1) pp.62-71.

Petiot, A., Ogier-Denis, E., Blommaart, E., Meijer, A. and Codogno, P. (2000). Distinct Classes of Phosphatidylinositol 3'-Kinases Are Involved in Signaling Pathways That Control Macroautophagy in HT-29 Cells. *Journal of Biological Chemistry*, 275(2), pp.992-998.

Raciti M, Lotti L, Valia S, Pulcinelli F, Di Renzo L. (2012) JNK2 is activated during ER stress and promotes cell survival. *Cell Death and Disease*, 3(11):e429.

Read, M., Whitley, M., Gupta, S., Pierce, J., Best, J., Davis, R. and Collins, T. (1997). Tumor Necrosis Factor -Induced E-selectin Expression Is Activated by the Nuclear Factor-B and c-JUN N-terminal Kinase/p38 Mitogen-activated Protein Kinase Pathways. *Journal of Biological Chemistry*, 272(5), pp.2753-2761.

Reveille, J., Sims, A., Danoy, P., Evans, D., Leo, P., Pointon, J., Jin, R., Zhou, X., Bradbury, L., Appleton, L., Davis, J., Diekman, L., Doan, T., Dowling, A., Duan, R., Duncan, E., Farrar, C., Hadler, J., Harvey, D., Karaderi, T., Mogg, R., Pomeroy, E., Pryce, K., Taylor, J., Savage, L., Deloukas, P., Kumanduri, V., Peltonen, L., Ring, S., Whittaker, P., Glazov, E., Thomas, G., Maksymowych, W., Inman, R., Ward, M., Stone, M., Weisman, M., Wordsworth, B. and Brown, M. (2010). Genome-wide association study of ankylosing spondylitis identifies non-MHC susceptibility loci. Nature Genetics, 42(2), pp.123-127.

Rutkevich, L., Cohen-Doyle, M., Brockmeier, U. and Williams, D. (2010). Functional Relationship between Protein Disulfide Isomerase Family Members during the Oxidative Folding of Human Secretory Proteins. *Molecular Biology of the Cell*, 21(18), pp.3093-3105.

Rzymski, T., Milani, M., Pike, L., Buffa, F., Mellor, H. (2010). Regulation of autophagy by ATF4 in response to severe hypoxia. *Oncogene*, 29(31), pp.4424-4435.

Saitoh, M., Nishitoh, H., Fujii, M., Takeda, K., Tobiume, K., Sawada, Y., Kawabata, M., Miyazono, K and Ichijo H. (1998). Mammalian thioredoxin is a direct inhibitor of apoptosis signal-regulating kinase (ASK) 1. *The EMBO Journal*, 17(9), pp.2596-2606.

Salipalli, S., Singh, P. and Borlak, J. (2014). Recent advances in live cell imaging of hepatoma cells. *BMC Cell Biol*, 15(1), p.26.

Scaffidi, C. Fulda, S., C Friesen, C., F Li,F., K J Tomaselli, K.J., Debatin, K.M., Krammer, P.H and Peter M.E. (1998). Two CD95 (APO-1/Fas) signaling pathways. *The EMBO Journal*, 17(6), pp.1675-1687.

Schindler, A. and Schekman, R. (2009). In vitro reconstitution of ER-stress induced ATF6 transport in COPII vesicles. *Proceedings of the National Academy of Sciences*, 106(42), pp.17775-17780.

Schlessinger J and Ullrich A. (1992).Growth factor signaling by receptor tyrosine kinases. *Neuron*. 9(3) pp.383-391.

Schuck, S., Prinz, W., Thorn, K., Voss, C. and Walter, P. (2009). Membrane expansion alleviates endoplasmic reticulum stress independently of the unfolded protein response. *Journal of Cell Biology*, 187(4), pp.525-536.

Shen H, Goodall J, Hill Gaston J. (2009) Frequency and phenotype of peripheral blood Th17 cells in ankylosing spondylitis and rheumatoid arthritis. *Arthritis Rheum*. 60(6):1647-1656.

Shen, J., Chen, X., Hendershot, L. and Prywes, R. (2002). ER Stress Regulation of ATF6 Localization by Dissociation of BiP/GRP78 Binding and Unmasking of Golgi Localization Signals. *Developmental Cell*, 3(1), pp.99-111.

Sheridan, C., Kishimoto, H., Fuchs, R.K., Mehrotra, S., Bhat-Nakshatri, P., Turner, C.H., Goulet, R Jr., Badve, S., Nakshatri, H. (2006) CD44+/CD24- breast cancer cells exhibit enhanced invasive properties: an early step necessary for metastasis. *BREAST CANCER RESEARCH*. 8 (5) Article Number: R59

Sherlock, J., Joyce-Shaikh, B., Turner, S., Chao, C., Sathe, M., Grein, J., Gorman, D., Bowman, E., McClanahan, T., Yearley, J., Eberl, G., Buckley, C., Kastelein, R., Pierce, R., LaFace, D. and Cua, D. (2012). IL-23 induces spondyloarthropathy by acting on ROR-γt+ CD3+CD4−CD8− entheseal resident T cells. *Nature Medicine*, 18(7), pp.1069-1076.

Shi, Y., Vattem, K., Sood, R., An, J., Liang, J., Stramm, L. and Wek, R. (1998). Identification and Characterization of Pancreatic Eukaryotic Initiation Factor 2 αSubunit Kinase, PEK, Involved in Translational Control. *Molecular and Cellular Biology*, 18(12), pp.7499-7509.

Shibata, Y., Voeltz, G. and Rapoport, T. (2006). Rough Sheets and Smooth Tubules. *Cell*, 126(3), pp.435-439.

Shibatani, T., David, L.L., McCormack, A.L, Frueh, K and Skach WR. (2005). Proteomic analysis of mammalian oligosaccharyltransferase reveals multiple subcomplexes that contain Sec61, TRAP, and two potential new subunits. *Biochemistry*. 44 pp.5982–5992

Stordal, B. and Davey, R. (2008). A 39 kDa fragment of endogenous ASK1 suggests specific cleavage not degradation by the proteasome. *International Union of Biochemistry and Molecular Biology Life*, 60(3), pp.180-184.

Su, Q., Wang, S., Gao, H., Kazemi, S., Harding, H., Ron, D. and Koromilas, A. (2007). Modulation of the Eukaryotic Initiation Factor 2 -Subunit Kinase PERK by Tyrosine Phosphorylation. *Journal of Biological Chemistry*, 283(1), pp.469-475.

Szegezdi, E., Logue, S., Gorman, A. and Samali, A. (2006). Mediators of endoplasmic reticulum stress-induced apoptosis. *EMBO Reports*, 7(9), pp.880-885.

Takahashi, A., Hirata, H., Yonehara, S., Imai, Y., Lee, K. (1997). Affinity labeling displays the stepwise activation of ICE-related proteases by Fas, staurosporine, and CrmAsensitive caspase-8. *Oncogene*, 14(23), pp.2741-2752.

Takeda, K., Kaisho, T., Yoshida, N., Takeda, J., Kishimoto, T. and Akira, S. (1998). Correction: Stat3 Activation Is Responsible for IL-6-Dependent T Cell Proliferation through Preventing Apoptosis: Generation and Characterization of T Cell-Specific Stat3Deficient Mice. *The Journal of Immunology*, 194(7), pp.3526-3526.

Tanaka, A., Jin, Y., Lee, S., Zhang, M., Kim, H., Stolz, D., Ryter, S. and Choi, A. (2012). Hyperoxia-Induced LC3B Interacts with the Fas Apoptotic Pathway in Epithelial Cell Death. American Journal of Respiratory Cell and Molecular Biology, 46(4), pp.507-514.

Tanida I, Sou Y, Ezaki J, Minematsu-Ikeguchi N, Ueno T, Kominami E. (2004) HsAtg4B/HsApg4B/Autophagin-1 Cleaves the Carboxyl Termini of Three Human Atg8 Homologues and Delipidates Microtubule-associated Protein Light Chain 3- and GABAA Receptor-associated Protein-Phospholipid Conjugates. *Journal of Biological Chemistry*. 279(35):36268-36276.

Tanida, I., Tanida-Miyake, E., Ueno, T. and Kominami, E. (2000). The Human Homolog of Saccharomyces cerevisiae Apg7p Is a Protein-activating Enzyme for Multiple Substrates

Including Human Apg12p, GATE-16, GABARAP, and MAP-LC3. *Journal of Biological Chemistry*, 276(3), pp.1701-1706.

Thermofisher.com, (2016). LysoTracker Red DND-99 - Special Packaging - Thermo Fisher Scientific. [online] Available at: https://www.thermofisher.com/order/catalog/product/L7528 [Accessed 20 Jan. 2016].

Tirasophon, W., Welihinda, A. and Kaufman, R. (1998). A stress response pathway from the endoplasmic reticulum to the nucleus requires a novel bifunctional protein kinase/endoribonuclease (Ire1p) in mammalian cells. Genes & Development, 12(12), pp.1812-1824.

Tom, B., Rutzky, L., Jakstys, M., Oyasu, R., Kaye, C. and Kahan, B. (1976). Human colonic adenocarcinoma cells. *In Vitro*, 12(3), pp.180-191.

Turner, M., DeLay, M., Bai, S., Klenk, E. and Colbert, R. (2007). HLA–B27 up-regulation causes accumulation of misfolded heavy chains and correlates with the magnitude of the unfolded protein response in transgenic rats: Implications for the pathogenesis of spondylarthritis-like disease. Arthritis Rheum, 56(1), pp.215-223.

Turner, M., Sowders, D., DeLay, M., Mohapatra, R., Bai, S., Smith, J., Brandewie, J., Taurog, J. and Colbert, R. (2005). HLA-B27 Misfolding in Transgenic Rats Is Associated with Activation of the Unfolded Protein Response. The Journal of Immunology, 175(4), pp.2438-2448.

Urano, F. Wang, X., Bertolotti, A., Zhang, Y., Chung, P., Harding, P and Ron, D. (2000). Coupling of Stress in the ER to Activation of JNK Protein Kinases by Transmembrane Protein Kinase IRE1. *Science*, 287(5453), pp.664-666.

Van Gaalen , F. (2011). Does HLA-B*2706 protect against ankylosing spondylitis? A meta-analysis. International Journal of Rheumatic Diseases, 15(1), pp.8-12.

Vattem, K. and Wek, R. (2004). Reinitiation involving upstream ORFs regulates ATF4 mRNA translation in mammalian cells. Proceedings of the National Academy of Sciences, 101(31), pp.11269-11274.

Verdrengh M, Jonsson IM, Holmdahl R and Tarkowski A.(2003) Genistein As an AntiInflammatory Agent. *Inflammatory Research*, 52(8) pp.341-346

Voeltz G, Rolls M, Rapoport T. (2002) Structural organization of the endoplasmic reticulum. *EMBO reports*. 3 (10) pp.944-950.

Wang, X Harding, H.P., Zhang, Y., Jolicoeur, E.M, Kuroda M and Ron D (1998). Cloning of mammalian Ire1 reveals diversity in the ER stress responses. *The EMBO Journal*, 17(19), pp.5708-5717.

Wei, M. Zong, W., Cheng, E.H.Y., Lindsten, T. Panoutsakopoulou, V., Ross, A.J., Roth, K.A. MacGregor, G.R., Thompson, C.B and Korsmeyer, S.J. (2001). Proapoptotic BAX and BAK: A Requisite Gateway to Mitochondrial Dysfunction and Death. *Science*, 292(5517), pp.727-730.

West, M., Zurek, N., Hoenger, A. and Voeltz, G. (2011). A 3D analysis of yeast ER structure reveals how ER domains are organized by membrane curvature. *The Journal of Cell Biology*, 193(2), pp.333-346.

Westrate, L., Lee, J., Prinz, W. and Voeltz, G. (2015). Form Follows Function: The Importance of Endoplasmic Reticulum Shape. *Annual Reviews of Biochemistry,* 84(1), pp.791-811.

Wright, P., McEntegart, A., McCarey, D., McInnes, I., Siebert, S. and Milling, S. (2015). Ankylosing spondylitis patients display altered dendritic cell and T cell populations that implicate pathogenic roles for the IL-23 cytokine axis and intestinal inflammation. *Rheumatology, 55(1), pp.120-132.*

Xuhong, S., Diener, K., Jannuzzi, D., Trollinger, D., Tse-Hua, T., Lichenstein, H., Zukowski, M. and Yao, Z. (1996). Molecular Cloning and Characterization of a Novel Protein Kinase with a Catalytic Domain Homologous to Mitogen-activated Protein Kinase Kinase Kinase*. Journal of Biological Chemistry, 271(49), pp.31607-31611.*

Yan, W., Frank, C., Korth, M., Sopher, B., Novoa, I., Ron, D. and Katze, M. (2002). Control of PERK eIF2 kinase activity by the endoplasmic reticulum stress-induced molecular chaperone P58IPK. *Proceedings of the National Academy of Sciences*, 99(25), pp.15920-15925.

Yang, X., Panopoulos, A., Nurieva, R., Chang, S., Wang, D., Watowich, S. and Dong, C. (2007). STAT3 Regulates Cytokine-mediated Generation of Inflammatory Helper T Cells. *Journal of Biological Chemistry*, 282(13), pp.9358-9363.

Ye, J., Rawson, R., Komuro, R., Chen, X., Davé, U., Prywes, R., Brown, M. and Goldstein, J. (2000). ER Stress Induces Cleavage of Membrane-Bound ATF6 by the Same Proteases that Process SREBPs.*Molecular Cell*, 6(6), pp.1355-1364.

Yoshida, H. Haze, K., Yanagi, H., Yura, T and Mori, K. (1998). Identification of the cis-Acting Endoplasmic Reticulum Stress Response Element Responsible for Transcriptional Induction of Mammalian Glucose-regulated Proteins. INVOLVEMENT OF BASIC LEUCINE ZIPPER TRANSCRIPTION FACTORS. *Journal of Biological Chemistry*, 273(50), pp.33741-33749.

Yoshida, H., Matsui, T., Yamamoto, A., Okada, T. and Mori, K. (2001). XBP1 mRNA Is Induced by ATF6 and Spliced by IRE1 in Response to ER Stress to Produce a Highly Active Transcription Factor. *Cell*, 107(7), pp.881-891.

Yu, X., Kennedy, R. and Liu, S. (2003). JAK2/STAT3, Not ERK1/2, Mediates Interleukin-6induced Activation of Inducible Nitric-oxide Synthase and Decrease in Contractility of Adult Ventricular Myocytes. *Journal of Biological Chemistry*, 278(18), pp.16304-16309.

Zambrano-Zaragoza J, Agraz-Cibrian J, González-Reyes C, Durán-Avelar M, VibancoPérez N. (2013) Ankylosing Spondylitis: From Cells to Genes. *International Journal of Inflammation*. 2013: pp. 1-16.

Zha, X., Yue, Y., Dong, N. and Xiong, S. (2015). Endoplasmic Reticulum Stress Aggravates Viral Myocarditis by Raising Inflammation Through the IRE1-Associated NFκB Pathway. *Canadian Journal of Cardiology*, 31(8), pp.1032-1040.

Zhang, L., Li, Y., Li, Y., Qi, L., Liu, X., Yuan, C., Hu, N., Ma, D., Li, Z., Yang, Q., Li, W. and Li, J. (2012). Increased Frequencies of Th22 Cells as well as Th17 Cells in the Peripheral Blood of Patients with Ankylosing Spondylitis and Rheumatoid Arthritis. PLoS ONE, 7(4), p.e31000.

Zhong, Z., Wen, Z. and Darnell, J. (1994). Stat3: a STAT family member activated by tyrosine phosphorylation in response to epidermal growth factor and interleukin6. *Science*, 264(5155), pp.95-98.

Zhu, X., Zhang, J., Sun, H., Jiang, C., Dong, Y., (2014). Ubiquitination of Inositolrequiring Enzyme 1 (IRE1) by the E3 Ligase CHIP Mediates the IRE1/TRAF2/JNK Pathway. *Journal of Biological Chemistry*, 289(44), pp.30567-30577.

Zinszner, H., Kuroda, M., Wang, X., Batchvarova, N., Lightfoot, R. (1998). CHOP is implicated in programmed cell death in response to impaired function of the endoplasmic reticulum. *Genes & Development*, 12(7), pp.982-995.

Zou, H., Henzel, W., Liu, X., Lutschg, A. and Wang, X. (1997). Apaf-1, a Human Protein Homologous to C. elegans CED-4, Participates in Cytochrome c–Dependent Activation of Caspase-3. *Cell*, 90(3), pp.405-413.

Zou, H., Yang, R., Hao, J., Wang, J., Sun, C., Fesik, S.W., Wu, J.C, Tomaselli, K.J, Armstrong, R.C (2002).Regulation of the Apaf-1/Caspase-9 Apoptosome by Caspase-3 and XIAP. *Journal of Biological Chemistry.* 278(10), pp.8091-8098.